Environmental & Water Quality Operational Studies

TECHNICAL REPORT E-81-2

A REVIEW OF NUMERICAL RESERVOIR HYDRODYNAMIC MODELING

By Billy H. Johnson

Hydraulics Laboratory
U. S. Army Engineer Waterways Experiment Station
P. O. Box 631, Vicksburg, Miss. 39180

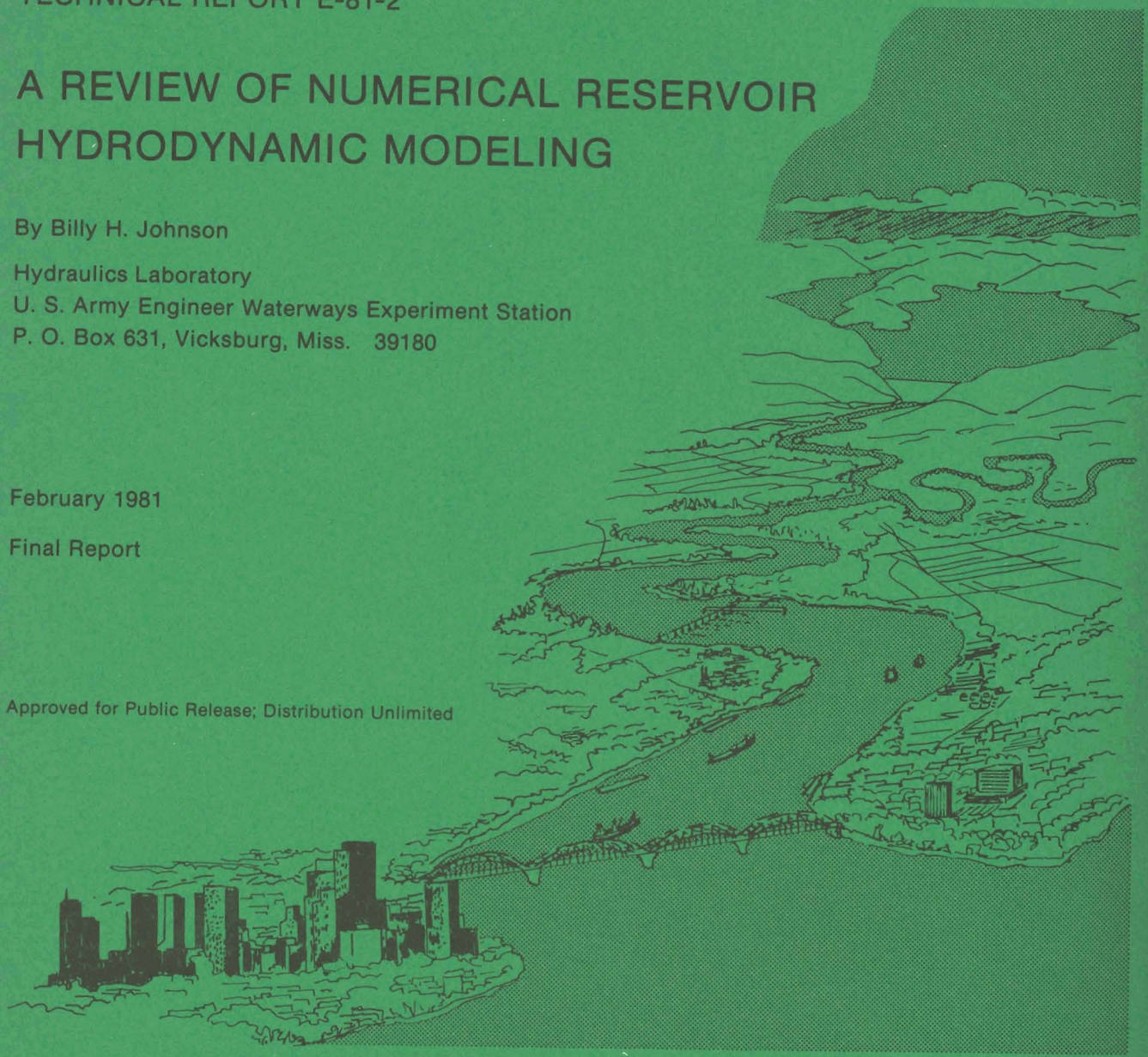

February 1981

Final Report

Approved for Public Release; Distribution Unlimited

Prepared for Office, Chief of Engineers, U. S. Army
Washington, D. C. 20314

Under EWQOS Work Unit No. IA.4

Monitored by Environmental Laboratory
U. S. Army Engineer Waterways Experiment Station
P. O. Box 631, Vicksburg, Miss. 39180

Unclassified

SECURITY CLASSIFICATION OF THIS PAGE *(When Data Entered)*

REPORT DOCUMENTATION PAGE

READ INSTRUCTIONS BEFORE COMPLETING FORM

1. REPORT NUMBER: Technical Report E-81-2	2. GOVT ACCESSION NO.
3. RECIPIENT'S CATALOG NUMBER	
4. TITLE *(and Subtitle)*: A REVIEW OF NUMERICAL RESERVOIR HYDRODYNAMIC MODELING	5. TYPE OF REPORT & PERIOD COVERED: Final report
	6. PERFORMING ORG. REPORT NUMBER
7. AUTHOR(s): Billy H. Johnson	8. CONTRACT OR GRANT NUMBER(s)
9. PERFORMING ORGANIZATION NAME AND ADDRESS: U. S. Army Engineer Waterways Experiment Station, Hydraulics Laboratory, P. O. Box 631, Vicksburg, Miss. 39180	10. PROGRAM ELEMENT, PROJECT, TASK AREA & WORK UNIT NUMBERS: EWQOS Work Unit No. IA.4
11. CONTROLLING OFFICE NAME AND ADDRESS: Office, Chief of Engineers, U. S. Army, Washington, D. C. 20314	12. REPORT DATE: February 1981
	13. NUMBER OF PAGES: 182
14. MONITORING AGENCY NAME & ADDRESS *(if different from Controlling Office)*: U. S. Army Engineer Waterways Experiment Station, Environmental Laboratory, P. O. Box 631, Vicksburg, Miss. 39180	15. SECURITY CLASS. *(of this report)*: Unclassified
	15a. DECLASSIFICATION/DOWNGRADING SCHEDULE

16. DISTRIBUTION STATEMENT *(of this Report)*

Approved for public release; distribution unlimited.

17. DISTRIBUTION STATEMENT *(of the abstract entered in Block 20, if different from Report)*

18. SUPPLEMENTARY NOTES

19. KEY WORDS *(Continue on reverse side if necessary and identify by block number)*

Hydrodynamics
Mathematical models
Reservoir stratification
Stratified flow
Water quality models

20. ABSTRACT *(Continue on reverse side if necessary and identify by block number)*

Stratification, i.e., density variations in a reservoir, occurs due to temperature variations as a result of surface heat exchange and plays an important role in determining the water quality of a reservoir. This role is determined through the influence of density variations on the movement of water in the reservoir. Therefore, the primary objective of a prediction of stratified flow hydrodynamics in reservoirs is to enable scientists to compute temperature

(Continued)

DD FORM 1 JAN 73 1473 EDITION OF 1 NOV 65 IS OBSOLETE

Unclassified

SECURITY CLASSIFICATION OF THIS PAGE *(When Data Entered)*

20. ABSTRACT (Continued).

distributions and water transports insofar as they affect various water quality parameters.

One objective of the Environmental & Water Quality Operational Study (EWQOS) program of the U. S. Army Corps of Engineers is to provide District and Division offices with a tool for predicting reservoir hydrodynamics over periods of time extending from the initial setup of thermal stratification in the spring through its breakup in the fall. Such a predictive technique will subsequently be used in the prediction of water quality parameters. An important tool that provides a relatively low cost highly flexible model of the hydrodynamics of a water body is a numerical model.

Under an EWQOS work unit, both two- and three-dimensional, unsteady, variable density, heat-conducting models have been investigated during the past year. This investigation has centered around an analysis of both the mathematical and numerical bases of individual models as well as their ability to simulate a density underflow in the Generalized Reservoir Hydrodynamics (GRH) flume located at the U. S. Army Engineer Waterways Experiment Station (WES). A discussion of the limitations and relative advantages of the various models is presented along with results of the GRH flume applications.

The general conclusion is that a two-dimensional laterally averaged model developed by Edinger and Buchak offers the most promise of providing the Corps with a computationally efficient and accurate multidimensional reservoir hydrodynamic model. It does not appear that any three-dimensional models that allow for economical long-term simulations have been developed.

PREFACE

The study reported herein was conducted by the Hydraulics Laboratory (HL) of the U. S. Army Engineer Waterways Experiment Station (WES) during the period January 1978-December 1979. The work was conducted under the Environmental & Water Quality Operational Study (EWQOS) Work Unit No. IA.4, "Improve and Verify Multi-Dimensional Hydrodynamic Mathematical Models." The EWQOS is sponsored by the Office, Chief of Engineers, U. S. Army, and is monitored by the Environmental Laboratory (EL) of the WES.

Dr. Billy H. Johnson, Hydraulic Analysis Division (HAD), HL, conducted the study and prepared this report under the general supervision of Messrs. Henry B. Simmons, Chief, HL; John L. Grace, Jr., Chief, Hydraulic Structures Division (HSD), HL; and Marden B. Boyd, Chief, HAD. Dr. Jerome L. Mahloch managed the project for the EWQOS under the general supervision of Dr. John Harrison, Chief, EL. Special thanks are extended to Mr. Mark S. Dortch and Dr. Dennis R. Smith of the Reservoir Water Quality Branch of HSD for their assistance in guiding the study to completion. In addition, appreciation is expressed to Drs. John Edinger, Frank Tatom, Bill Waldrop, Lynn Spraggs, Bob MacArthur, and Arsev Eraslan for the model applications they made, as well as the many fruitful discussions they have provided over the past year and a half. Review comments by Dr. Joe Thompson as well as the consultation he has provided are gratefully acknowledged.

Commanders and Directors of WES during the conduct of this study and the preparation and publication of this report were COL John L. Cannon, CE, and COL Nelson P. Conover, CE. Technical Director was Mr. Fred R. Brown.

CONTENTS

CONVERSION FACTORS, U. S. CUSTOMARY TO METRIC (SI)
UNITS OF MEASUREMENT

U. S. customary units of measurement can be converted to metric (SI) units as follows:

Multiply	By	To Obtain
cubic feet per second	0.02831685	cubic metres per second
Fahrenheit degrees	5/9	Celsius degrees or Kelvins*
feet	0.3048	metres
feet per second	0.3048	metres per second
pounds (mass) per cubic foot	0.01601846	grams per cubic centimetre
square feet	0.09290304	square metres
square feet per second	0.09290304	square metres per second

* To obtain Celsius (C) temperature readings from Fahrenheit (F) readings, use the following formula: $C = (5/9)(F - 32)$. To obtain Kelvin (K) readings, use: $K = (5/9)(F - 32) + 273.15$.

A REVIEW OF NUMERICAL RESERVOIR HYDRODYNAMIC MODELING

PART I: INTRODUCTION

Reservoir Stratification and Its Importance

1. As the population of the United States has increased over the past few decades, there has been a corresponding increase in the demand on water supplies. To help meet this demand, numerous impounding reservoirs have been constructed. The impoundment or damming of a flowing stream can significantly affect the quality of the water. This can happen as a result of the direct increase in travel time required for water to traverse the distance from the headwater of the stream to the dam as well as the effect that stratification plays in determining the quality of the water released from the reservoir. The relationship between density variations and quality parameters in the reservoir is a direct result of the influence of stratification on the movement and mixing of water.

2. Stratification or density variations in a reservoir can occur as a result of solute concentrations, suspended solids concentrations, or temperature variations as a result of surface heat exchange. Surface heat exchange is a function of both short- and longwave radiation as well as surface conduction, evaporation, and precipitation. In the remainder of this report, the term "stratification" will refer to density variations due to thermal effects.

3. At the beginning of spring, a reservoir is essentially homogeneous. However, as the weather warms, the water near the surface also warms due to an exchange of heat from the atmosphere to the water surface. The warmer water near the surface is then mixed downward, primarily by wind action and diurnal cooling. By late summer, the reservoir will attain maximum stratification (Figure 1). A warm upper layer (epilimnion) of water resides over the cold deeper layer (hypolimnion) with a zone

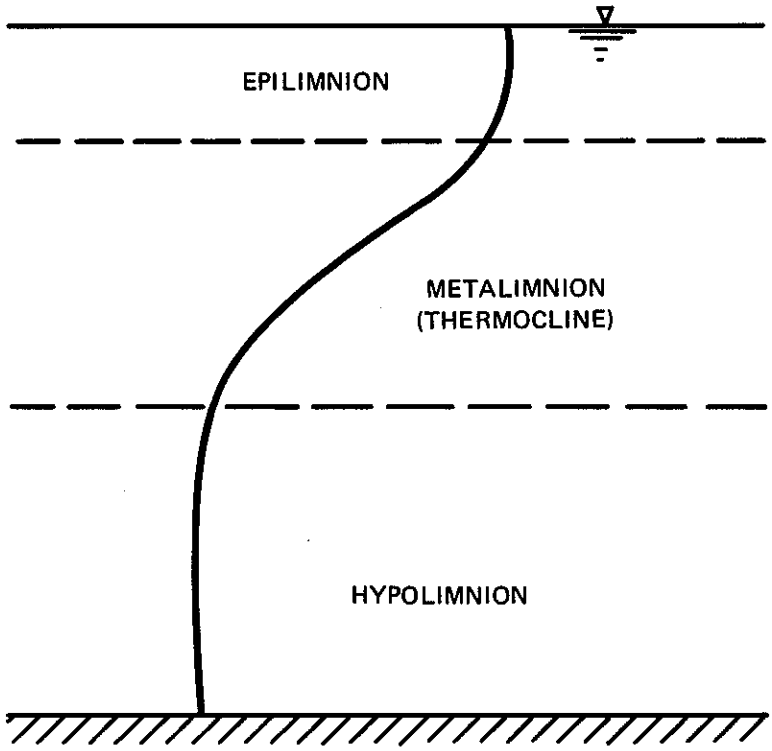

Figure 1. Regions associated with thermal stratification

between the two (metalimnion) in which a large density gradient exists. As the weather cools during the fall, the surface temperature decreases, resulting in denser water at the surface and a corresponding convective overturning. This mixing eventually results in an isothermal water body that remains isothermal through the winter, except during periods of ice cover. Such a cyclic variation of temperature is demonstrated by the seasonal temperature profiles presented in Figure 2.

Density Currents

4. The variation of the fluid density in a stratified reservoir gives rise to what are known as internal density currents or stratified flow. Such flow refers to motions involving fluid masses of the same phase. A heavier liquid flowing beneath a lighter liquid or a heavier

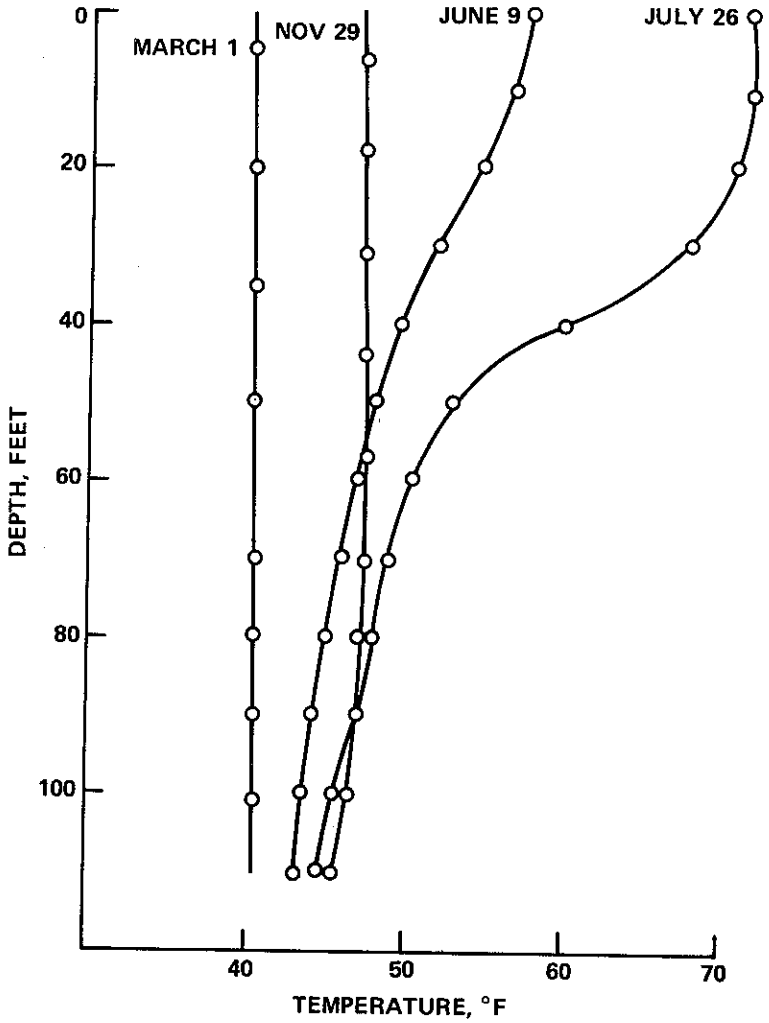

Figure 2. Temperature profiles of the west basin of Horn Lake, B. C., during 1960 (taken from Slotta et al. 1969)

gas moving under a lighter gas will be subject to gravitational effects that depend upon the differences between the two densities. Such flows can be extremely important. Slotta et al. (1969) discusses an example of a density current in the Watts Bar reservoir of the Tennessee Valley Authority (TVA) system in which a coldwater density flow moves over 13 miles* upstream into the warmer waters of one of the arms of the

* A table of factors for converting U. S. customary units of measurement to metric (SI) units is presented on page 4.

reservoir. This bottom density current flows past a sewer outlet as well as the outfall from a large paper mill. At one time, sewage and mill waste were discharged into the coldwater current and carried upstream to the intake of a water plant. The situation has since been corrected by use of a variable level outfall for the sewage and mill waste. The internal motions in reservoirs due to temperature variations or perhaps due to the inflow of sediment-laden streams plus the understanding and control of salinity intrusion in tidal estuaries are among the most challenging of present-day problems dealing with stratified flow.

Relationship of Water Quality to Hydrodynamics

5. The primary objective of a prediction of stratified flow in reservoirs is to enable scientists to compute temperature distributions and water transports insofar as they affect various water quality parameters. While the process of heat transfer in bodies of water is nothing new, the prediction of the resulting multidimensional flow phenomena in a reservoir for varying stream inputs as well as dam discharges from varying levels is extremely difficult.

6. A substance (either chemical or biological) disperses through a reservoir by convection and turbulent diffusion. In addition, the substance is also acted upon by various chemical, biological, and physical processes. An understanding of both the dispersion and the chemical and biological processes is essential in any prediction of water quality, which is the ultimate goal to be sought, although not the goal of this study. It should be clear then that a problem of such scope calls for a cooperative effort of a wide variety of scientific disciplines ranging from meteorology, hydrology, and hydrodynamics to chemistry and biology.

Hydrodynamic Predictive Techniques

7. In an attempt to predict the hydrodynamics of a reservoir, one

or perhaps a combination of three approaches may be taken--field investigations, physical models, and mathematical or numerical models. Field investigations may reveal what presently occurs in a water system, but cannot predict what will result from changes due to new inputs to the system. In addition, field investigations are usually relatively expensive. Depending upon their complexity, e.g., large models of river basins, estuaries, and bays, physical models can require significant investments of capital, long construction times, and long test periods. However, physical models of reservoirs to address problems such as near-field inflow selective withdrawal and pumpback characteristics of specific outlet structures and geometries are far less expensive to construct and operate. Depending upon approximations made to the governing equations of motion and the solution technique employed to solve the equations, numerical models can often provide relatively low cost and highly flexible models. However, it should be remembered that, as with many physical models, numerical models must be calibrated and verified before confidence can be placed in results obtained from them. Data from both field studies and physical model tests are used to assess the reasonableness of numerical predictions and to aid in the further development of mathematical descriptions of observed physical processes. However, the steady advances in computer technology over the past two decades (Table 1) indicate the potential for even greater economical use of more widely applicable numerical models in the future. In a practical sense, a combination of the most desirable features of both physical and numerical models will probably continue to provide the best approach for solving most hydrodynamic problems.

Types of Numerical Models

8. Numerical hydrodynamic models can differ widely, depending upon such things as the solution technique applied to the governing differential equations representing the physical processes, the assumptions made in the derivation of the governing equations, whether the phenomena are steady or time-varying, and the spatial dimensionality

Table 1

Conventional Computer Characteristics*

Computer	First Delivered month/yr	Add Time** μs	Memory Cycle Time μs	Memory Capacity† words
Univac I	3/51	282	242	1000
IBM 704	12/55	24	12	32K
Univac LARC	5/60	4	4	30000
IBM Stretch	5/61	1.5	2.2	96K
CDC 6600	9/64	0.3	1.0	128K
IBM 360/90	2/67	0.18	0.75	512K
CDC 7600	1/69	0.0275	0.275 1.760	64K 512K
IBM 360/195	2/71	0.054	0.054 0.810 8	32K 256K 16M
CYBER 203	-/79	0.10	0.10	Real - 1 million Virtual - 4 trillion

* Data from Charles W. Adams Associates (1967) and Keydata Corporation (1971). Taken from Leith (1975).

** In recent computers some concurrence has been used to decrease both add time and memory time.

† K = 1024 = 2^{10}; M = 1048576 = 2^{20}.

considered, with perhaps the spatial dimensionality being the most commonly used delineator.

9. One-, two-, and fully three-dimensional numerical models that provide for the simultaneous solution of the coupled turbulent velocity field and the temperature field, subject to varying boundary conditions, exist and are applicable in varying degrees to the problem of predicting stratified reservoir hydrodynamics for use in developing water quality predictions. Perhaps the earliest work in which computations for the fluid density and the flow were coupled was the work of Welch et al. (1966) in the development of the two-dimensional Marker and Cell code commonly referred to as MAC. Paralleling the development of MAC and the MAC-related codes, e.g., Chan and Street's (1970) SUMMAC, Slotta et al.'s (1969) NUMAC, etc., have been a host of models that might be described as control volume models. With this method, a reservoir is divided into a number of horizontal layers extending over its breadth and length. Homogeneity is then assumed in each layer. The result is a one-dimensional model with variations allowed only in the vertical. Governing differential equations are obtained by applying mass, momentum, and heat balances for the control layers. Inflow and outflow boundaries can be included quite easily in such models. Parker et al. (1975) reviewed such one-dimensional reservoir models and concluded that such models could be applied to larger, deep reservoirs where horizontal flow has minimal impact on the vertical density structure. The primary advantage of such a model is its ability to resolve long-term or seasonal temperature profiles economically. However, it must be noted that such one-dimensional models are not applicable to the problem with which this study is concerned--predicting multidimensional flow fields within stratified reservoirs for quality predictions.

10. Both two- and three-dimensional hydrodynamic models are discussed in detail in succeeding sections. Some of the models investigated, such as the two-dimensional models of Edinger and Buchak (1979), Waldrop and Farmer (1976), and Roberts and Street (1975), are directly applicable to reservoirs, although in varying degrees; while others, such as the two-dimensional depth-averaged models of Leendertse (1967),

Masch et al. (1969), and Reid and Bodine (1968), have no applicability to the modeling of internal flows in stratified reservoirs other than perhaps in the numerical techniques employed.

11. Three-dimensional hydrodynamic models have only recently been developed to the state where application to complex geometries with reasonable resolution for short simulation periods appears possible; however, the cost is still prohibitive for simulations over long periods of time. Thus, it appears that if one is only interested in the steady-state flow and temperature field resulting from situations such as a discharge of warm water from a power plant, three-dimensional modeling appears feasible. However, if the interest lies in computing reservoir hydrodynamics over a stratification cycle, i.e., several months, new developments in solution techniques and the availability of larger and faster computers must be realized before such modeling becomes practical.

Purpose and Scope

12. The need for a predictive capability--numerical models in the area of stratified reservoir hydrodynamics--has been firmly established. The purpose of the study described herein then is to select the most applicable existing models and to provide recommendations for additional developmental work needed to meet that need. Because of the nature of the problem to be addressed, selected models must have the capability of handling free surface variable density flows that are time-dependent. PARTS II and III present a detailed discussion of the theoretical basis and corresponding numerical techniques that are common to all numerical hydrodynamic models. Three-dimensional hydrodynamic models are discussed in PART IV, and two-dimensional hydrodynamic models are discussed in PART V. In addition to an investigation of the theoretical limitations of various models, a limited attempt at analyzing the actual performance of several models has been made. This was accomplished through model applications to a coldwater underflow in the U. S. Army Engineer Waterways Experiment Station (WES) Hydraulics Laboratory's General Reservoir Hydrodynamics (GRH) flume. These results are presented

in PART VI. Finally, conclusions of this study and recommendations for additional developmental work needed to provide the Corps of Engineers with computer models with the potential to provide a predictive capability in the area of reservoir hydrodynamics in an accurate and economical fashion are presented in PART VII.

PART II: MATHEMATICAL DISCUSSIONS

Basic Equations and Approximations

13. The Navier-Stokes equations express the conservation of mass and momentum of a flow field and are the basic governing equations for the solution of any fluid dynamics problem. These equations written in tensor notation are*

$$\underline{\text{Continuity}}: \quad \frac{\partial \rho}{\partial t} + \frac{\partial \rho u_i}{\partial x_i} = 0 \tag{1}$$

$$\underline{\text{Momentum}}: \quad \frac{\partial \rho u_i}{\partial t} + \frac{\partial (\rho u_i u_j)}{\partial x_j} = \frac{-\partial P}{\partial x_i} + \rho g_i - 2\varepsilon_{ijk}\Omega_j \rho u_k + \frac{\partial T_{ij}}{\partial x_j} \tag{2}$$

where

ρ = water density

t = time

u_i = tensor notation for velocity

x_i = tensor notation of spatial coordinate

g_i = acceleration of gravity

ε_{ijk} = cyclic tensor

Ω_j = Coriolis parameter

T_{ij} = laminar stress tensor

μ = molecular eddy viscosity

δ_{ij} = Kronecker delta

and where

$$T_{ij} = \mu\left(\frac{\partial u_i}{\partial x_j} + \frac{\partial u_j}{\partial x_i}\right) - \frac{2}{3}\mu \frac{\partial u_i}{\partial x_j} \delta_{ij}$$

represents the viscous molecular stress arising as a result of the continuum approach. It will be recalled from tensor theory that repeated

---

* For convenience, symbols are listed and defined in the Notation (Appendix C).

indices imply a summation and also that ε_{ijk} in the Coriolis term is the cyclic tensor defined as

$$\begin{aligned} \varepsilon_{ijk} &= 1 \text{ , for an even permutation of } ijk \\ &= -1 \text{ , for an odd permutation of } ijk \\ &= 0 \text{ , otherwise} \end{aligned}$$

For example, $\varepsilon_{123} = \varepsilon_{231} = \varepsilon_{312} = 1$; whereas, $\varepsilon_{321} = \varepsilon_{213} = \varepsilon_{132} = -1$; and the Kronecker delta δ_{ij} is defined as

$$\begin{aligned} \delta_{ij} &= 1 \text{ , if } i = j \\ &= 0 \text{ , otherwise} \end{aligned}$$

In addition to the above equations, a conservation of energy equation must also be written for fluid flow problems with thermal effects. With the assumption of a constant specific heat and with the neglection of viscous dissipative effects, one can write the energy equation as the following transport equation for temperature T :

$$\underline{\text{Energy}}: \quad \frac{\partial T}{\partial t} + \frac{\partial (T u_i)}{\partial x_i} = \frac{\partial \left(D_{ij} \frac{\partial T}{\partial x_j} \right)}{\partial x_i} + \sum \text{sources} - \sum \text{sinks} \qquad (3)$$

where D_{ij} is equal to the diffusivity coefficient. This equation states that the temperature can change as a result of advection by the flow field, molecular diffusion, and the actions of any sources and sinks of heat. As a matter of fact, this same equation applies to the transport of any constituent ϕ , where ϕ would replace T in the equation and appropriate sources and sinks and boundary conditions would be prescribed. For example, in the numerical modeling of the hydrodynamics of an estuary, a similar transport equation for the salinity would be required.

14. One additional equation remains to be written in order to close the system. An equation of state expressing the density as a

function of the temperature and pressure (and salinity in estuarine modeling) must be employed:

$$\underline{\text{Equation of State}}: \quad \rho = \rho(T,P) \tag{4}$$

With the closure of the system, there exist six equations to be solved for the six unknowns--density ρ ; three velocity components u , v , w ; pressure P ; and temperature T .

Time averaging for turbulent flow

15. The above equations written with molecular values of viscosity and diffusivity are only applicable in a practical sense to laminar flow fields where the flow and thermodynamic variables do not exhibit random irregular fluctuations in time. However, most fluids in motion exhibit such fluctuations and are referred to as "turbulent flows."

16. Following Reynolds, the approach normally taken to make the equations applicable to turbulent flows is to assume that the dependent variables are composed of an average time-varying component plus a small randomly varying component about the average value. This is illustrated below.

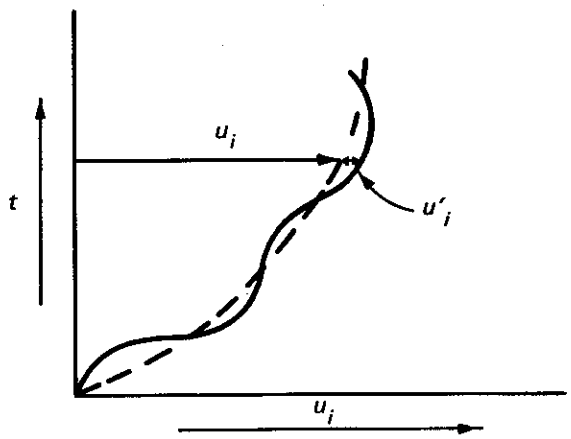

Thus, one writes

$$u_i(x,y,z,t) = \overline{u}_i(x,y,z,t) + u_i'(x,y,z,t)$$

where

$$\bar{u}_i = \frac{1}{\Delta t} \int_{t-\Delta t/2}^{t+\Delta t/2} u_i(x,y,z,t)\, dt$$

and

$$\frac{1}{\Delta t} \int_{t-\Delta t/2}^{t+\Delta t/2} u_i'(x,y,z,t)\, dt = 0$$

u_i' = deviation between instantaneous velocity and time-averaged velocity

$\bar{u}_i$ = time-averaged velocity

Δt = time step

With all the dependent variables written in the form above, substitution into Equations 1, 2, and 3 and then integration over the time increment Δt produces the same form of the previous equations, but now written with the time-averaged components as the dependent variables, plus the additional terms

$$\frac{1}{\Delta t} \int_{t-\Delta t/2}^{t+\Delta t/2} u_i' u_j'\, dt$$

and

$$\frac{1}{\Delta t} \int_{t-\Delta t/2}^{t+\Delta t/2} T'u'\, dt$$

where T' = deviation between instantaneous and time-averaged temperature .

17. The first term is referred to as the turbulent Reynolds stress, since the high frequency turbulent fluctuations manifest themselves as viscous stresses acting on the average component of flow. Using Boussinesq's concept of eddy viscosity, the first term is written as

$$\frac{1}{\Delta t} \int_{t-\Delta t/2}^{t+\Delta t/2} u_i' u_j'\, dt = \varepsilon_{ij}\left(\frac{\partial \bar{u}_i}{\partial x_j} + \frac{\partial \bar{u}_j}{\partial x_i}\right) \text{(no summation over } i\text{)}$$

In analogy with the laminar flow case, ε_{ij} is referred to as the turbulent or eddy viscosity tensor.

18. In a similar fashion, the second term above, which arises from the time averaging of the temperature equation, is commonly written as

$$\frac{1}{\Delta t}\int_{t-\Delta t/2}^{t+\Delta t/2} T'u_i' \, dt = A_{ij}\frac{\partial \overline{T}}{\partial x_j}$$

where A_{ij} is called the "eddy diffusivity tensor" and $\overline{T}$ is the time-averaged temperature.

19. The equations commonly applied to turbulent flow problems can now be written as

$$\underline{\text{Continuity}}: \quad \frac{\partial \overline{\rho}}{\partial t} + \frac{\partial \overline{\rho u_i}}{\partial x_i} = 0 \tag{5}$$

$$\underline{\text{Momentum}}: \quad \frac{\partial \overline{\rho u_i}}{\partial t} + \frac{\partial(\overline{\rho u_i}\,\overline{u_j})}{\partial x_j} = -\frac{\partial \overline{P}}{\partial x_i} + \overline{\rho} g_i - 2\varepsilon_{ijk}\Omega_j \overline{\rho u_k} + \frac{\partial}{\partial x_j}\left[\varepsilon_{ij}\left(\frac{\partial \overline{u_i}}{\partial x_j} + \frac{\partial \overline{u_j}}{\partial x_i}\right)\right] \tag{6}$$

$$\underline{\text{Energy}}: \quad \frac{\partial \overline{T}}{\partial t} + \frac{\partial \overline{T u_i}}{\partial x_i} = \frac{\partial}{\partial x_i}\left(A_{ij}\frac{\partial \overline{T}}{\partial x_j}\right) + \sum \text{sources} - \sum \text{sinks} \tag{7}$$

$$\underline{\text{Equation of State}}: \quad \overline{\rho} = \overline{\rho}(\overline{T}, \overline{P}) \tag{8}$$

where

$\overline{\rho}$ = time-averaged water density

$\overline{P}$ = time-averaged pressure

and where the assumption has been made that the eddy coefficients are much larger than the molecular values; i.e.,

$$\varepsilon_{ij} >> \mu$$

$$A_{ij} >> D_{ij}$$

Boussinesq approximation

20. Subject to the assumptions made in their derivation, the time-averaged governing equations (Equations 5-8) are applicable to any turbulent fluid dynamics problem. An approximation usually made when applying the equations to hydrodynamic problems was first pointed out by Boussinesq. When variations of temperature are small ($\Delta t \leq \pm 10°C$), variations in density will be less than one percent. For example, Edinger and Buchak's expression relating the density of water to the water's temperature results in only a 0.15 percent increase in the density when decreasing the temperature from 20°C to 10°C. These small variations can be ignored in general with one exception. The variability of density in the gravitational term cannot be ignored. Hence, ρ is treated as a constant in all places except the body force term.

21. With the Boussinesq approximation, the continuity and momentum equations become

$$\underline{\text{Continuity}}: \quad \frac{\partial \bar{u}_i}{\partial x_i} = 0 \tag{9}$$

$$\underline{\text{Momentum}}: \quad \frac{\partial \bar{u}_i}{\partial t} + \frac{\partial (\bar{u}_i \bar{u}_j)}{\partial x_j} = -\frac{1}{\rho_o}\frac{\partial \bar{P}}{\partial x_i} + \frac{\bar{\rho}}{\rho_o} g_i$$

$$- 2\varepsilon_{ijk}\Omega_j \bar{u}_k + \frac{1}{\rho_o}\frac{\partial}{\partial x_j}\left[\varepsilon_{ij}\left(\frac{\partial \bar{u}_i}{\partial x_j} + \frac{\partial \bar{u}_j}{\partial x_i}\right)\right] \tag{10}$$

where ρ_o is a reference water density. The energy equation and the equation of state are not affected.

Conservative versus nonconservative

22. When the momentum equations are written as Equation 10, they are known as the conservative form of the equations. If the convective

term is expanded and Equation 9 is substituted, Equation 10 reduces to

$$\frac{\partial \bar{u}_i}{\partial t} + \bar{u}_j \frac{\partial \bar{u}_i}{\partial x_j} = -\frac{1}{\rho_o}\frac{\partial \bar{P}}{\partial x_i} + \left(\frac{\bar{\rho}}{\rho_o}\right) g_i - 2\varepsilon_{ijk}\Omega_j \bar{u}_k + \frac{1}{\rho_o}\frac{\partial}{\partial x_j}\left[\varepsilon_{ij}\left(\frac{\partial \bar{u}_i}{\partial x_j} + \frac{\partial \bar{u}_j}{\partial x_i}\right)\right] \tag{11}$$

which is referred to as the nonconservative form. Analytically, the two forms are equivalent. However, in numerical solutions of flow problems, they are not. As discussed by Leendertse (1967), a finite difference representation of Equation 11 does not conserve momentum of the flow field; whereas, the identical numerical representation of Equation 10 does. As a result, most of the more recent numerical hydrodynamic models use the conservative form as opposed to the nonconservative form employed in many of the earlier models.

23. An interesting point is that in the laminar form of the momentum equations, i.e., Equation 2, when the assumption of incompressibility is made, researchers have historically neglected that portion of the viscous term that contains the condition of incompressibility, i.e., $\frac{2}{3}\mu\frac{\partial u_i}{\partial x_j}\delta_{ij}$, even though they may have retained the conservative form of the convective terms. In the turbulent form of the equations, there is no such inconsistency, since all molecular viscous terms are neglected due to the assumption that the eddy viscosity is much larger than the molecular viscosity. Therefore, the condition of incompressibility is not invoked in dropping the $\frac{2}{3}\mu\frac{\partial u_i}{\partial x_j}\delta_{ij}$ term in the turbulent form of the equations.

Convective versus quasi-static

24. An assumption that is usually made in hydrodynamic models is that vertical accelerations are negligible when compared to the gravitational acceleration. Neglecting viscous terms also, the vertical momentum equation reduces to

$$\frac{\partial \overline{P}}{\partial z} = \overline{\rho} g \qquad (12)$$

where z is the vertical spatial coordinate and is positive downward. Equation 12, of course, states that the pressure is hydrostatic.

25. When considering the coupling of the thermodynamics and the hydrodynamics of a water body, a distinction must be made between convective and, as labeled by Simons (1973), "quasi-static" models. Convective models retain the complete vertical momentum equation and can simulate in full detail the convective overturning of unstable water masses, such as the upwelling of cells of warm water or perhaps the plunging of a coldwater inflow. Quasi-static models where the pressure is hydrostatic eliminate vertical accelerations due to buoyancy effects, which precludes the explicit treatment of free convection associated with unstable stratification. Convective overturnings can only be handled as mixing along the vertical axis.

26. A commonly used technique is that of invoking a large vertical diffusion of heat to counteract such instabilities. This results in the removal of any unstable stratification the moment it occurs. Such a technique is implemented by checking the vertical temperature profile at each horizontal location after each computation. If at any point lighter water lies below denser water, the profile is adjusted without affecting the total heat content of the column.

27. As will be discussed in more detail in connection with the numerical solution of the governing equations, models with the hydrostatic assumption require far less computer time than the fully convective models.

Spatial averaging

28. A solution of Equations 7, 8, 9, and either 10 or 11 constitutes a fully time-varying, three-dimensional model with the only assumption being the Boussinesq approximation. Such models do currently exist and will be discussed in a later section. However, most hydrodynamic modelers employ a spatial-averaging technique similar to the turbulent time-averaging technique to yield either one- or two-dimensional models.

As previously noted, the present state of the art is such that three-dimensional models are not practical for long-term simulations of the hydrodynamics of a reservoir.

29. The basic assumption in the spatial averaging of the three-dimensional equations is that the dependent variables can be represented by an average value over one or more of the spatial coordinates plus some small random deviation; e.g., the velocity would be written as

$$\bar{u}_i = \tilde{\bar{u}}_i + \bar{u}_i' \tag{13}$$

where

$$\tilde{\bar{u}}_i = \frac{1}{\Delta x_i} \int_{x_i - \Delta x_i/2}^{x_i + \Delta x_i/2} \bar{u}_i \, dx_i$$

$$\frac{1}{\Delta x_i} \int_{x_i - \Delta x_i/2}^{x_i + \Delta x_i/2} \bar{u}_i' \, dx_i = 0$$

and

$\tilde{\bar{u}}_i$ = time- and space-averaged velocity

Δx_i = spatial step

$\bar{u}_i'$ = deviation between time-averaged velocity and time- and space-averaged velocity

In an x, y, z coordinate system (with x referring to the longitudinal; y, the lateral; and z, the vertical), if $i = 2$, the integration is over the width and a width-averaged model results. However, if $i = 3$, the integration is taken over the depth and a depth-averaged model will result. Many depth-averaged models have been developed since Leendertse's (1967) work; whereas, laterally averaged models have only been developed over the past five years or so. If the integration is performed over the complete cross section, a one-dimensional model with variations allowed only in the longitudinal direction results. Such models are not considered in this study.

30. As was done in the time-averaging of the instantaneous

equations, expressions such as Equation 13 are substituted into the turbulent time-averaged equations to yield a set of equations with the time-averaged and spatially averaged components of the flow and thermodynamic variables as dependent variables plus the additional terms

$$\frac{1}{\Delta x_i} \int_{x_i - \Delta x_i/2}^{x_i + \Delta x_i/2} \overline{u}_i' \overline{u}_j' \, dx_i$$

and

$$\frac{1}{\Delta x_i} \int_{x_i - \Delta x_i/2}^{x_i + \Delta x_i/2} \overline{T}' \overline{u}_i' \, dx_i$$

As in the time-averaging case, these terms are normally approximated by

$$\frac{1}{\Delta x_i} \int_{x_i - \Delta x_i/2}^{x_i + \Delta x_i/2} \overline{u}_i' \overline{u}_j' \, dx_i = \varepsilon_{ij}' \left(\frac{\partial \tilde{\tilde{u}}_i}{\partial x_j} + \frac{\partial \tilde{\tilde{u}}_j}{\partial x_i} \right)$$

and

$$\frac{1}{\Delta x_i} \int_{x_i - \Delta x_i/2}^{x_i + \Delta x_i/2} \overline{T}' \overline{u}_i' \, dx_i = A_{ij}' \frac{\partial \tilde{\tilde{T}}}{\partial x_i}$$

where ε_{ij}' and A_{ij}' are referred to as "eddy dispersion coefficients" by Holley (1969) to distinguish them from the turbulent eddy diffusion coefficients arising from the time averaging, and $\tilde{\tilde{T}}$ is the time-averaged and spatially averaged temperature.

31. The resulting spatially averaged equations take different forms, depending upon whether the averaging is performed over the depth or the width. Since depth-averaged models are not applicable to the

hydrodynamic modeling of stratified reservoirs, only the laterally averaged equations, with B denoted as the width, are presented below:

$$\underline{\text{Continuity}}: \quad \frac{\partial \tilde{\tilde{u}}_i B}{\partial x_i} = 0 \tag{14}$$

$$\underline{\text{Momentum}}: \quad \frac{\partial \tilde{\tilde{u}}_i B}{\partial t} + \frac{\partial \tilde{\tilde{u}}_i \tilde{\tilde{u}}_j B}{\partial x_j} = -\frac{1}{\rho_o}\frac{\partial \tilde{\tilde{P}} B}{\partial x_i} + \frac{\tilde{\tilde{\rho}} g_i}{\rho_o} + \frac{1}{\rho_o}\frac{\partial}{\partial x_j}\left[B\Gamma_{ij}\left(\frac{\partial \tilde{\tilde{u}}_i}{\partial x_j} + \frac{\partial \tilde{\tilde{u}}_j}{\partial x_i}\right)\right] \tag{15}$$

$$\underline{\text{Energy}}: \quad \frac{\partial \tilde{\tilde{T}} B}{\partial t}\frac{\partial \tilde{\tilde{T}} \tilde{\tilde{u}}_i B}{\partial x_i} = \frac{\partial}{\partial x_i}\left(BC_{ij}\frac{\partial \tilde{\tilde{T}}}{\partial x_j}\right) + \sum \text{sources} - \sum \text{sinks} \tag{16}$$

$$\underline{\text{Equation of State}}: \quad \tilde{\tilde{\rho}} = \tilde{\tilde{\rho}}(\tilde{\tilde{T}}) \tag{17}$$

where the Coriolis terms have been neglected, the water is assumed incompressible, and

where

$\tilde{\tilde{P}}$ = time-averaged and spatially averaged press

$\tilde{\tilde{\rho}}$ = time-averaged and spatially averaged water density

Γ_{ij} = sum of $\varepsilon_{k\ell}$, $\varepsilon'_{k\ell}$, and μ

C_{ij} = sum of eddy diffusivities due to time- and spatial averaging

32. A general discussion of both time averaging and spatial averaging of the equations is presented in Ward and Espey (1971), with additional details of depth averaging given by Leendertse (1967) and lateral averaging by Blumberg (1975) and Edinger and Buchak (1979).

Vorticity-stream function notation

33. The governing equations written with the velocity and the pressure as the dependent variables are often referred to as the primitive form of the equations. An approach that is often used in two-dimensional modeling in the field of aerodynamics, although very rarely

in hydrodynamics, is to write the equations with the stream function and the vorticity as the dependent variables. With the vorticity defined as the curl of the velocity, i.e., $\vec{\omega} = \nabla \times \vec{v}$, it can easily be seen that if the velocity field is two-dimensional, e.g., $\vec{v} = u\hat{i} + v\hat{j}$, where $\hat{i}$, $\hat{j}$ and $\hat{k}$ are unit vectors, the vorticity contains only one component, namely $\zeta\hat{k}$. Therefore, instead of being required to solve two momentum equations for the velocities u and v, a single equation for ζ and a Poisson equation for the stream function are solved. In other words, the number of equations to be solved has in essence been reduced by one. However, one must make additional computations to obtain the velocity field from the computed stream function. Still, when the vorticity-stream function approach is applicable, it is probably faster. Multiple outlets at a dam would, however, prohibit its use.

Subgrid-scale motion

34. The eddy coefficients discussed above enter the equations due to first of all the time averaging (diffusion coefficients) of the equations and then as a result of spatial averaging (dispersion coefficients) to remove one or more of the independent spatial coordinates from the equations. A similar coefficient arises as a result of averaging the governing equations over the numerical grid upon which a numerical solution is sought. The numerical model cannot resolve small-scale local circulation patterns or eddies unless the eddies extend over an area covering several grid points. Thus, as discussed by Deardorff (1970), an averaging operator is applied to the governing equations, with averaging typically being over the grid volume of the numerical calculation to filter out the subgrid scale (SGS) motions. Explicit calculations are then made for the filtered variables after assumptions are made about the SGS Reynolds stresses that arise from the averaging process. All of this, of course, is completely analogous to the manner in which turbulent and dispersive Reynolds stresses arose in the previously discussed time and spatial averaging.

35. The total stress then is the sum of the molecular viscous stress, the diffusive Reynolds stress, the dispersive Reynolds stress,

and the SGS Reynolds stress. In practice, all of these are lumped into one stress term with a single tensor eddy viscosity coefficient. Similarly, the total diffusivity in the transport equation for temperature is the sum of four components that are lumped together with a single tensor eddy diffusivity coefficient.

36. In turbulent flow, these coefficients are not constant as in laminar flow, but depend on the flow itself, i.e., on the processes generating the turbulence. The determination of these eddy coefficients in terms of the mean flow variables is a major problem in hydrodynamic modeling.

37. Up to this point, the eddy viscosity and diffusivity coefficients have been treated as second order tensors. Some researchers actually allow for the tensor behavior as a function of the rate of strain tensor of the mean flow field; however, the more common approach is to neglect all off-diagonal terms and, furthermore, to consider the two components in the horizontal plane to be equal. Some modelers allow for a variation of these coefficients, but others take a rather simplistic approach and treat them as constants over the computational field.

38. As noted by Lick (1976), the vertical eddy coefficients should vary throughout the depth. Causes for their variations are related to the following:

a. Stability of the water column.

b. Action of the wind on the surface.

c. Vertical shear in currents due to horizontal pressure gradients.

d. Presence of internal waves.

e. Effect of bottom irregularities and friction on currents.

One often finds the vertical coefficients related to the stability of the water column as a function of the Richardson number R_i :

$$R_i = - \frac{\frac{g}{\rho} \frac{\partial \rho}{\partial z}}{\left(\frac{\partial u}{\partial z}\right)^2}$$

where z is the vertical coordinate and u is the mean horizontal flow velocity.

39. Horizontal coefficients are generally much greater than vertical coefficients. Based upon various surface dye experiments, primarily in the oceans, it has been found that the horizontal coefficients are proportional to the scale of the turbulence raised to approximately the 4/3 power.

40. Lick indicates that in nonstratified flow, the eddy diffusivity is approximately equal to the eddy viscosity, i.e., the Reynolds analogy holds. Various forms that have been employed for these coefficients will be presented later in discussions on individual models.

Boundary Conditions

41. As noted by Roache (1972), the thing that makes a particular fluid flow problem unique are the boundary conditions that are prescribed. Conditions at the surface of the reservoir, at solid boundaries, and at both inflow and outflow boundaries must be specified in order to obtain a solution of the governing equations previously presented.

Surface conditions

42. In modeling the hydrodynamics of a water body, one of two approaches is taken in the treatment of the water surface. The surface is either treated as a free surface or as a rigid lid. In either case, the heat flux at the surface must be specified as a boundary condition on the temperature.

43. If the surface is treated as free, the assumption is made that a water particle on the surface remains there, i.e., the surface is a streamline. This then leads to the following kinematic condition:

$$\frac{\partial \zeta}{\partial t} + u \frac{\partial \zeta}{\partial x} + v \frac{\partial \zeta}{\partial y} - w = 0 \qquad (18)$$

for the computation of the water surface elevation, ζ. In addition, the internal stresses in the fluid must equal those applied externally to the surface. Considering a vertical-longitudinal two-dimensional (2-D)

reservoir, for laminar flow the normal internal stress at the surface τ_n is

$$T_n = -P + 2\mu \left[n_x^2 \frac{\partial u}{\partial x} + n_x n_z \left(\frac{\partial u}{\partial z} + \frac{\partial w}{\partial x} \right) + n_z^2 \frac{\partial w}{\partial z} \right]$$

and the tangetial internal stress at the surface τ_t can be expressed as

$$T_t = n_x n_z 2\mu \left(\frac{\partial u}{\partial x} - \frac{\partial w}{\partial z} \right) + \mu \left(\frac{\partial u}{\partial z} + \frac{\partial w}{\partial x} \right) \left(n_z^2 - n_x^2 \right)$$

where, as illustrated in Figure 3, n_x and n_z are the x and z

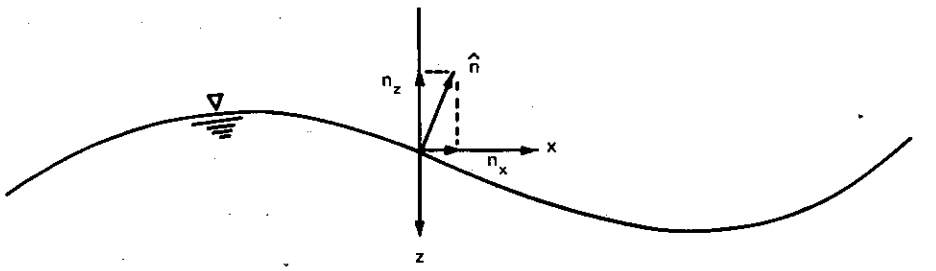

Figure 3. Orientation of unit normal to the surface

components, respectively, of the outward unit normal vector to the surface. The above expressions have been derived from the stress force $\vec{t}$ given by

$$\vec{t} = \hat{n} \cdot \overleftrightarrow{T}$$

where, as noted, $\hat{n}$ is the unit normal to the surface and $\overleftrightarrow{T}$ is the laminar stress tensor for incompressible flow, given by

$$T_{ij} = -P\delta_{ij} + \mu \left(\frac{\partial u_i}{\partial x_j} + \frac{\partial u_j}{\partial x_i} \right)$$

Now the externally applied stress will be a normal stress as a result of

atmospheric pressure and a tangential stress imparted by the wind; therefore, the boundary conditions become

$$2n_x n_z \mu\left(\frac{\partial u}{\partial x} - \frac{\partial w}{\partial z}\right) + \mu\left(\frac{\partial u}{\partial z} + \frac{\partial w}{\partial x}\right)\left(n_z^2 - n_x^2\right) = \tau_{WIND}$$

and

$$-P_a = -P + 2\mu\left[n_x^2 \frac{\partial u}{\partial x} + n_x n_z\left(\frac{\partial u}{\partial z} + \frac{\partial w}{\partial x}\right) + n_z^2 \frac{\partial w}{\partial z}\right]$$

where

τ_{WIND} = wind shear stress

P_a = atmospheric pressure

Thus, in a strict application of the stress boundary condition, the orientation of the surface, i.e., n_x and n_z, would have to be known. Since for a large water body the surface is at least locally flat, the assumption of a flat surface is normally made so that

$$n_x = 0$$

$$n_z = -1$$

The stress boundary conditions then reduce to

$$\mu\left(\frac{\partial u}{\partial z} + \frac{\partial w}{\partial x}\right) = \tau_{WIND}$$

$$P = P_a - 2\mu \frac{\partial w}{\partial z}$$

44. In addition, if the hydrostatic pressure assumption is made, i.e., vertical accelerations are neglected, the above conditions take the form below that is commonly found in the literature, where the molecular viscosity μ has been replaced by its turbulent eddy counterpart, ε_v.

$$\left.\begin{aligned} \varepsilon_v \frac{\partial u}{\partial z} &= \tau_{WIND} \\ P &= P_a \end{aligned}\right\} \text{ at free surface}$$

45. When the surface is treated as a rigid lid, it becomes in essence a solid boundary, and the normal component of the velocity must be zero. In addition, the pressure can no longer be prescribed at the surface, but rather must be computed. The pressure boundary condition now takes the form of a derivative boundary condition, i.e., a Neumman condition as opposed to the Dirichlet condition for the free surface case. The primary reason for assuming that the surface is a rigid lid is connected with stability problems encountered in the numerical solution of the governing equations and will be discussed later. It should be obvious that with the rigid lid approximation, the effect on the internal flow of the piling up of water cannot be accounted for. Modelers such as Liggett (1970) and Lick (1976) have employed the concept in the development of lake circulation models. However, others such as Eraslan* and Edinger** feel that the rigid lid approximation associated with a uniform water surface assumption is not realistic in the development of mathematical models for environmental flow conditions and that the water surface elevation must be considered as an integral part of the general solution of the hydrodynamic problem.

Solid boundaries

46. For viscous fluids, the fluid velocity is actually always zero at a solid boundary; i.e., both the tangential as well as the normal components are zero. This boundary condition is referred to as a "no-slip condition." Although in theory such a condition must always hold at a solid boundary, often in hydrodynamic modeling a slip condition is employed. This condition is implemented by setting the component of the velocity normal to the wall equal to zero but not the tangential; i.e., the flow slides freely along the solid wall. Theoretically, this implies that the flow is inviscid. Therefore, proper boundary conditions for a slip wall are that the normal velocity is zero as well as that the vorticity is zero at the solid wall, since vorticity is created in

---

* Personal communication, May 1979, Arsev Eraslan, Chief Scientist, Hennington, Durham, and Richardson, Knoxville, Tenn.

** Personal communication, May 1979, J. E. Edinger, J. E. Edinger Associates, Inc., Wayne, Penn.

viscous regions. The tangential component of velocity is then determined from the zero-vorticity condition. However, it does not appear that this is the approach usually taken in hydrodynamic modeling. In most cases, as will be discussed later, a staggered grid is used in obtaining a numerical solution such that the tangential component of the velocity is not defined at the wall. Instead, its value must be specified outside the wall. The usual procedure taken by most hydrodynamic modelers for slip walls is to set this value equal to its value inside the field.

47. The major reason for using slip boundary conditions is apparently related to the fact that a relatively large grid spacing is normally required in hydrodynamic modeling for economic reasons. With such a grid spacing near a solid boundary, if no-slip conditions are applied, the boundary layer effect extends farther into the field than it does in reality.

48. In addition to conditions being imposed on the flow field at solid boundaries, information about the heat transfer must also be specified. Either wall temperatures or the heat flux may be prescribed. In all reservoir- or lake-type modeling that has been investigated, the solid boundaries are assumed to be adiabatic, and thus the heat flux through the boundary is set to zero.

Open boundaries

49. Open boundaries are exactly what the name implies, i.e., boundaries that are open such that fluid may either enter or leave the field within which a solution is sought. Such boundaries are known as either "inflow" or "outflow" boundaries.

50. At forced open boundaries (inflows are always forced), either flow, i.e., velocities, or water surface elevations (assuming a free surface), must be prescribed as a function of time along with the temperature. Theoretically, rather than expressing either the flow or surface elevations, one could specify a relationship between the two. Such a boundary condition, known as a rating curve, is often prescribed at the downstream end of one-dimensional unsteady flow models of riverflows.

51. At outflow boundaries that are free rather than forced, e.g.,

free flow from an opening at a dam, one cannot prescribe the flow directly since it obviously is dependent upon conditions within the computational field. In the temperature computations, an outflow boundary is always considered free. A boundary condition that allows phenomena generated in the domain of interest to pass through the boundary without undergoing significant distortion and without influencing the interior solution is needed. Since a physical law to prescribe such a boundary condition does not exist, some kind of extrapolation from the interior must be used. The most common methods used are either a Sommerfeld radiation condition or perhaps one-sided differences when employing finite differences to obtain numerical solutions.

52. The dispersion characteristics in one dimension of the waves needed to prescribe the Sommerfeld radiation condition are known as

$$\frac{\partial \phi}{\partial t} + C \frac{\partial \phi}{\partial x} = 0 \tag{19}$$

where ϕ is any variable and C is the phase velocity of the waves. The dispersion characteristics are not generally known, since C is not generally a constant. A simplification often used to avoid this problem is to assume that the characteristics of the waves will have a slope equal to $\Delta x/\Delta t$ (Δx and Δt being the spatial and temporal grid steps, respectively). Then the extrapolated variable ϕ at the present time t at the boundary point J is given by

$$\phi_J^t = 2\phi_{J-1}^{t-\Delta t} - \phi_{J-2}^{t-2\Delta t}$$

A more accurate use of the Sommerfeld radiation condition, Equation 19, is presented by Orianski (1976). Instead of fixing a constant value for the phase velocity, Orianski numerically calculates a propagation velocity from neighboring points.

PART III: NUMERICAL DISCUSSIONS

53. The governing equations of fluid motion are nonlinear partial differential equations, which in a strict mathematical sense, are classified as being of the parabolic type. However, outside the boundary layer the equations exhibit a strong hyperbolic or wave character due to the convective terms and, thus, are often considered as being of the hyperbolic type. In any case, because of their nonlinearity, analytical solutions do not generally exist and one must resort to numerical methods to obtain an approximation of the continuous solution of the differential equations. Such methods include the use of finite differences and finite elements.

Finite Element Method (FEM)

54. In the finite element approach, the field is divided into finite elements, and the solution is approximated by a chosen function on each element. This function contains free parameters, which are evaluated by requiring the function and perhaps certain of its derivatives to equal the solution and its derivatives at certain points on the element. If the partial differential equations can be expressed in terms of integral variational principles, the variational integrals over each element are evaluated analytically from the chosen approximation functions on each element. The integrals over each individual element are then summed over all the elements to produce the variational integral over the entire field. This result contains the unknown values of the solution and perhaps some of its derivatives at all the points used above in the determination of the parameters in the approximating functions. The variational integral is then minimized in terms of these point values of the solution and derivatives involved. If the partial differential equations cannot be expressed in terms of variational principles, then the method of weighted residuals (Galerkin) must be used. Here the solution is again approximated on each element as above. However, instead of the evaluation of variational integrals, integrals of the products of weight

functions and the partial differential equations are evaluated on each element. This produces a set of simultaneous algebraic equations to be solved for the values of the solution and perhaps some of its derivatives at certain points on the elements.

55. The finite element approach is best suited to partial differential systems that can be expressed in terms of a variational principle. In this case, the boundary conditions can be incorporated naturally by means of Lagrange multipliers. For more general systems, particularly nonlinear systems that are not expressible in terms of variational principles, the finite element approach must use the method of weighted residuals (Galerkin) whereby a functional form of the solution in each element is assumed and integral moments of the partial differential equations are satisfied over the field as noted above. With this procedure, the partial differential equations themselves are not actually satisfied. Boundary conditions are incorporated in the assumed functional form of the solution in the elements adjacent to the boundaries.

56. The finite element method has enjoyed its greatest success in the field of solid mechanics where for the most part variational rather than difference methods are used. As Fix (1975) notes:

> "The reason for this is partly physical. The equations of elasticity can be put into a variational form and engineers have found this to be the most physically natural setting to formulate approximations. In addition, the variational approximations--finite elements--have other properties that are of great value in practice. Complicated boundaries can easily be treated in this setting; singularities in the solution can be modeled in the approximation; and, in dealing with higher order methods with increased resolving power, the practical problems are much less troublesome than with difference schemes."

57. Perhaps the major practical disadvantage of the finite element method as applied to hydrodynamic problems is that a large amount of computing time is required for such time-dependent problems. It might be noted that in most finite element models, differences are still employed in handling the time derivative. The reason the method is slow is that it creates dense matrices to be inverted, as opposed to the sparse

matrices that result from using differences. A common rebuttal by finite element modelers to this criticism is that since implicitness is central to the finite element approximation, implicit time differencing should be employed to yield an unconditionally stable system and thus, the use of larger time steps compensates for the large computing times required to invert the dense coefficient matrices each time step. However, it should be remembered that in addition to stability considerations, one must first of all be concerned with the accuracy of the solution. When using finite differences, it can be shown that as the computational time step becomes increasing larger than that allowed by the Courant condition for gravity waves, e.g., in one dimension

$$\Delta t_c < \frac{\Delta x}{\sqrt{gh}}$$

where

Δt_c = time step restricted by Courant condition

h = water depth

a corresponding increase in the number of spatial points per wavelength must occur to retain the same level of accuracy in the amplitude and phase of the computed wave. Leendertse (1967) indicates that from a practical standpoint, generally the time step should not be greater than 3-5 times Δt_c in the difference scheme he employs to compute vertically averaged flows. Abbott (1979) and his colleagues at the Danish Hydraulic Institute (DHI) have arrived at a similar conclusion for the difference scheme that they employ. Edinger and Buchak (1979) have indicated that for the laterally averaged case, the time step should not exceed 3-5 times the Δt computed from the internal wave condition given by

$$\Delta t \leq \frac{\Delta x}{\sqrt{\frac{\Delta \rho}{\rho} gh}}$$

where

$\Delta \rho$ = change in water density

Such an analysis of the error between the computed and analytic wave in the FEM has not been found in the literature.

58. In the development of a new model, an often stated disadvantage of the finite element method is that the FORTRAN coding is much more cumbersome than with finite differences. Of course, if the model already exists, such a disadvantage is of no concern to the user unless extensive modifications are required, in which case the cumbersomeness of the coding might well become a major consideration in the model selection.

Finite Difference Method (FDM)

59. The vast majority of the numerical hydrodynamic models, whether they be one-, two-, or three-dimensional, employ the use of finite differences to obtain solutions of the governing equations of fluid motion. In the finite difference method, the domain of the independent variables is replaced by a finite set of points referred to as net or mesh points. One then seeks to determine approximate values for the desired solutions at these points. The values at the mesh points are required to satisfy difference equations that are usually obtained by replacing partial derivatives by partial difference quotients. The resulting set of simultaneous algebraic equations is then solved for the values of the solution at the mesh points. If the boundaries do not coincide with mesh points, then the finite difference approach applied to the equations in a Cartesian coordinate system requires interpolation between mesh points to represent boundary conditions.

60. However, through coordinate transformations, irregular boundaries can be accurately handled while still making use of the simplicity of finite differences to obtain solutions. The most general of such transformations, which will be discussed in more detail later in the report, is a method developed by Thompson et al. (1974), which generates curvilinear coordinates as the solution of two elliptic partial differential equations with Dirichlet boundary conditions, one coordinate being specified as constant on the boundaries, and a distribution of the other

specified along the boundaries. No restrictions are placed on the irregularity of the boundaries, and fields containing multiple bodies or branches can be handled as easily as simple geometries. Regardless of the shape and number of bodies and regardless of the spacing of coordinate lines, all numerical computations, both to generate the coordinate system and to subsequently solve the fluid flow equations, are done on a rectangular grid with square mesh.

61. Since the boundary-fitted coordinate system has a coordinate line coincident with all boundaries, all boundary conditions may be expressed at grid points, and normal derivatives may be represented using only finite differences between grid points on coordinate lines. No interpolation is needed, even though the coordinate system is not orthogonal at the boundary.

62. Linear transformations that allow for the physical dimensions to be mapped between the values of 0 and 1 have been employed. For example, as will be discussed later in PART IV, Lick (1976) maps the vertical dimension in such a manner to represent bottom topographies more accurately.

Discrete element concept

63. Eraslan employs a numerical technique that he labels "the discrete element method." However from a conceptual standpoint, the primary difference between the finite difference method as it is normally applied and the discrete element method appears to be that the mathematical development of the discrete element method is based on employing the control volume integral forms of the physical conservation principles; whereas, the usual application of the finite difference method begins with the continuum limit differential equations presented in PART II.

64. Eraslan indicates that the application of the discrete element method to the solution of environmental fluid mechanics problems is based on the following procedure:

a. Divide the flow region into arbitrarily sized discrete elements, preferably with geometrically simple (rectangular) enclosure surfaces except at the boundaries, such that the finite number of discrete elements completely spans the region.

b. Integrate the volume and surface area integrals of the physical conservation equations without assuming uniform values for the flow properties over the surface areas. This produces a governing semidiscretized system of ordinary differential equations in time.

c. Apply proper interpolation techniques for determining transportive values of the flow properties between discrete elements.

65. As an example of the discrete element concept, consider the one-dimensional problem illustrated in Figure 4. Neglecting frictional

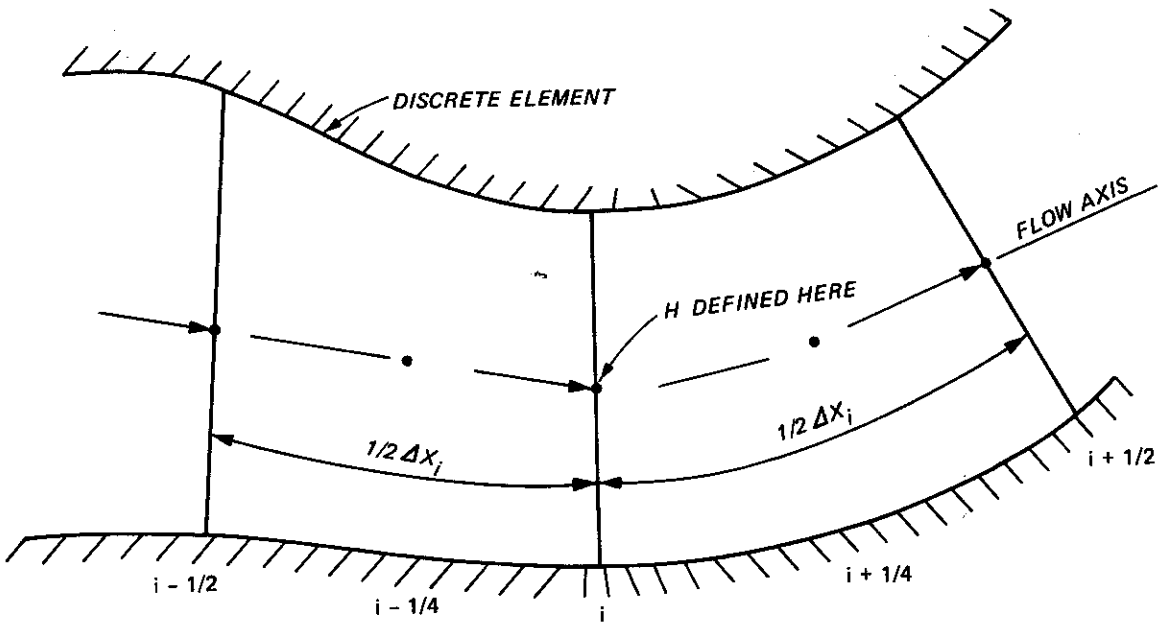

Figure 4. One-dimensional discrete element

effects, the integral forms of the conservation of mass and momentum can be written as

$$\underline{\text{Continuity}}: \quad \frac{\partial}{\partial t} \iiint_{cv} dV_o + \iint_{A_{cv}} \vec{v} \cdot \hat{n} \, dA = 0 \tag{20}$$

$$\underline{\text{Momentum}}: \quad \frac{\partial}{\partial t} \iiint_{cv} \vec{v} \, dV_o + \iint_{A_{cv}} \vec{v}\vec{v} \cdot \hat{n} \, dA = g \iint_{A_{cv}} \vec{f} \, dA \tag{21}$$

where

dV_o = differential volume

cv = volume of discrete element

A_{cv} = Area of discrete element

$\vec{v}$ = velocity vector

dA = differential area

$\vec{f}$ = force vector

Now define

$$G = \iint_{A_{cv}} u \, dA = \text{volumetric flow rate}$$

Therefore, from Figure 4

$$\iint_{A_{cv}} \vec{v} \cdot \hat{n} \, dA = -G_{i-1/2} + G_{i+1/2}$$

also,

$$\frac{\partial}{\partial t} \iiint_{cv} dV_o = \frac{\partial}{\partial t} (\Delta x_i A_i) = \Delta x_i B_i \frac{\partial H_i}{\partial t}$$

where B_i is the surface width and H_i is the surface elevation. Therefore, the discrete element equation for the conservation of fluid mass becomes

$$\frac{\partial H_i}{\partial t} = \frac{1}{\Delta x_i B_i} \left(G_{i-1/2} - G_{i+1/2} \right) \qquad (22)$$

Considering the surface integral for the momentum flux over the cross section A_i at the center of the element yields

$$\iint_{A_{cv}} \vec{v}\vec{v} \cdot \hat{n} \, dA = u_i G_i + \text{Reynolds stress terms}$$

Neglecting the Reynolds stress terms, which arise due to writing the velocity as the sum of a time-averaged and spatially averaged component plus its time and spatial deviations, the integral form of the momentum equation applied to one-half of the discrete element becomes

$$\frac{\partial G_{i-1/4}}{\partial t} = \frac{2}{\Delta x_i}\left(G_{i-1/2}u_{i-1/2} - G_i u_i\right)$$

$$+ \frac{2g}{\Delta x_i}\left[A_{i-1/2}\left(H_{i-1/2} - H_{i-1/4}\right) - A_i\left(H_i - H_{i-1/4}\right)\right] \qquad (23)$$

66. Equations 22 and 23 both take the appearance of finite difference equations in which the time derivative has not been replaced by differences. It appears that from a practical consideration, the primary difference between the discrete element method and the application of finite differences to the differential equation centers around what might be called "the conservation of geometrical properties," as reflected through the definition of the divergence of a variable. In the equations of motion, flux terms such as

$$\iint_{A_{cv}} \vec{\phi} \cdot \hat{n}\, dA$$

appear. Considering the element below,

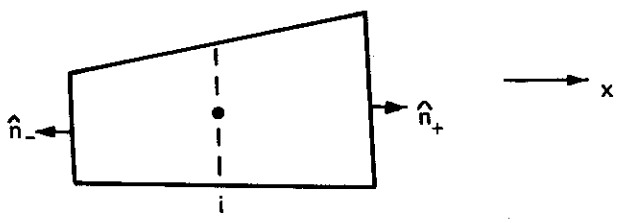

and working with only the x direction, the flux integral above can be evaluated as

$$\iint_{A_{cv}} \vec{\phi} \cdot \hat{n}\, dA = (\phi A)_+ - (\phi A)_-$$

Now, if one employs Gauss's Divergence theorem, the flux integral can be written as

$$\iint_{A_{cv}} \vec{\phi} \cdot \hat{n}\, dA = \iiint_{cv} (\nabla \cdot \vec{\phi})\, dV_o \cong (\nabla \cdot \vec{\phi})_i \Delta x_i A_i$$

where $\nabla \cdot \vec{\phi}$ is the divergence of ϕ. The two previous expressions can be equated, and one can derive an expression for the divergence over the i^{th} element as

$$\left(\nabla \cdot \vec{\phi}\right)_i = \frac{1}{\Delta x_i A_i} [(\phi A)_+ - (\phi A)_-]$$

or

$$\left(\nabla \cdot \vec{\phi}\right)_i = \frac{1}{A_i} \left(\frac{\partial(\phi A)}{\partial x}\right)_i \tag{24}$$

In the usual derivation of the differential form of the equations, the divergence is written as

$$\nabla \cdot \vec{\phi} = \frac{\partial \phi}{\partial x} \tag{25}$$

Equation 24 might be referred to as the "geometrically conservative" form of the divergence; whereas, the normal definition as given by Equation 25 would be referred to as the "geometrically nonconservative" form.

67. Note that physically the difference between the two forms is that in the conservative form (Equation 24), the area through which the flux of ϕ flows is that of the bounding faces through which the flux actually occurs. In Equation 25, however, the influence of the respective areas on the flux through the boundaries is not allowed.

68. It appears that if the conservative form of the divergence is

used in expanding the vector form of the governing differential equations, the finite difference method applied to those equations becomes identical to the discrete element method if the same interpolation scheme is used to provide values of the dependent variables at points where they are not defined in the grid.

Finite difference spatial grids

69. The spatial grid in Cartesian coordinates most commonly used by numerical hydrodynamic modelers appears to be one in which the water surface elevation, temperature, and density are defined at the center of a computational cell; whereas, the velocity components are defined on the faces of the cell. Such a grid is illustrated below for a two-dimensional problem.

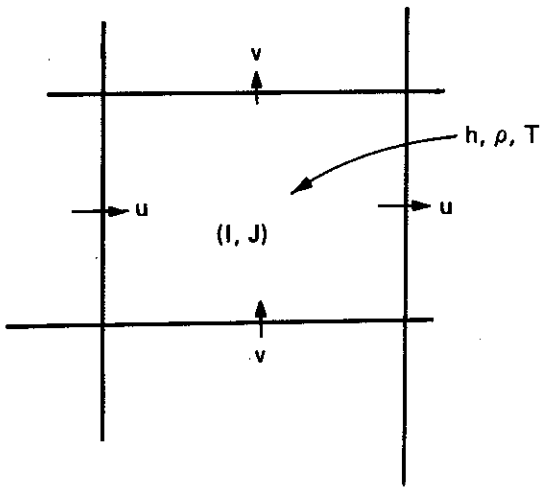

With such a grid, the normal component of the velocity at solid boundaries can easily be set to zero if the boundary is assumed to lie along cell faces, which is the usual assumption.

70. With such a grid one obviously will need values of variables at points where they are not defined in order to numerically solve the governing equations. One solution is to utilize more than one grid, with the variables defined such that a solution on one grid is used to step the solution forward on another grid. As discussed by Simons (1973), such a procedure can result in semi-independent solutions on the different grids. The numerical error associated with the use of more than one grid is known as a "grid dispersion error." The approach

normally taken to provide the variables at net points where they are not computed is to perform an interpolation within the grid. Simons shows that conservation requirements are satisfied if the unknown values are approximated by simple linear interpolation.

71. A grid often used in aerodynamic flow modeling has all variables defined at the same point, i.e., at the cell center. Such a grid (shown below) has been employed by Waldrop and Tatom (1976) in their three-dimensional hydrodynamic modeling work.

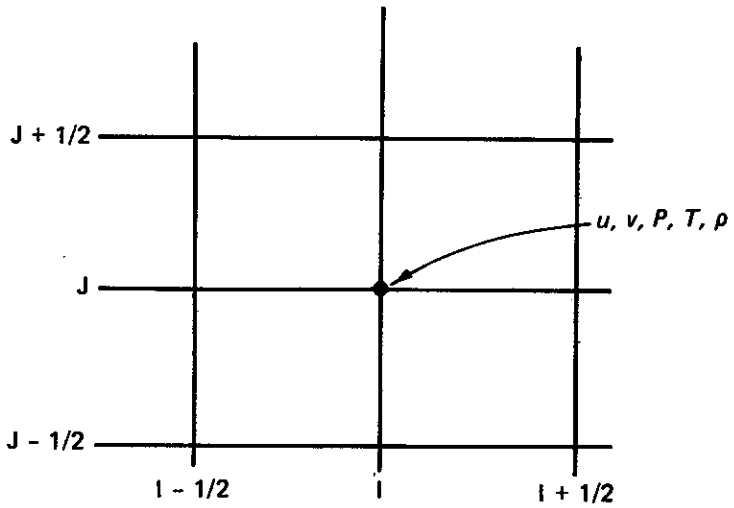

72. Still another grid is currently being employed by Thompson* in the development of a model for use in selective withdrawal studies.

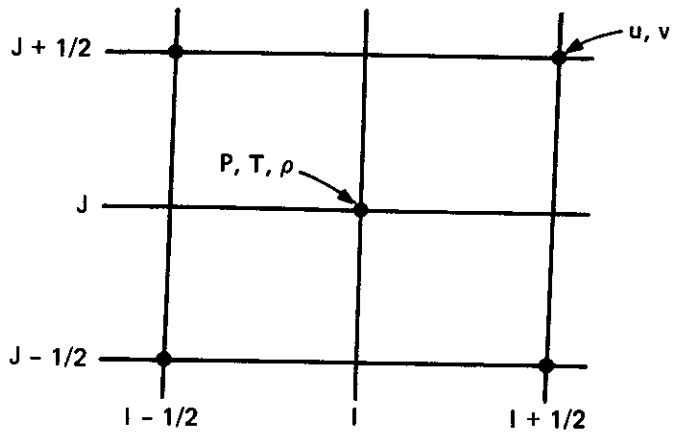

* Personal communication, April 1979, J. F. Thompson, Mississippi State University, Mississippi State, Miss.

In this grid, all velocity components are defined at the same point, i.e., the cell corners; whereas, all thermodynamic variables are defined at the cell center. Thompson indicates such a grid allows for a more natural application of velocity and pressure boundary conditions in a curvilinear coordinate system.

73. Most numerical finite difference hydrodynamic models employ a constant grid size in each direction. However, models have been developed that allow for the size of the computational cell to vary over the region within which flow computations are being made in order to increase the resolution in certain areas. Examples are the 3-D models of Tatom and Waldrop and Thompson's 2-D model that utilizes boundary-fitted coordinates. As discussed by Roache (1972), there are two approaches to the implementation of a variable computational mesh. One can merely solve the given equations on a grid that has physically been constructed such that the computational nodes are not evenly spaced, or one can transform the equations and solve them in a transformed rectangular plane with equal grid spacing, although the grid spacing is not equal over the physical region. Even though the two approaches might appear to be similar, Roache indicates they are fundamentally different. When the untransformed equations are differenced in the variable mesh, the result is a deterioration of formal accuracy, but the transformed equations may be differenced in a regular mesh with no deterioriation in the formal order of truncation error relative to the transformed plane. Roache, therefore, states that the coordinate transformation approach, which can be used for the purpose of aligning coordinates along physical boundaries as well as increasing resolution in certain areas, is to be preferred. As previously noted, Thompson's boundary-fitted coordinate technique provides the most general such transformation that can be attained.

Time differencing

74. As previously noted, time integration is performed by finite differences even in the finite element method. Such time differencing can basically be classified as either explicit or implicit. For either type, one can construct first, second, or even higher order schemes; although Kreiss (1975) indicates that second order schemes are to be

preferred if one combines accuracy with considerations of economy and simplicity. As an additional classification, one often finds time-differencing schemes referred to as one- or two-step schemes.

75. In order that these concepts may be better understood, consider the following basic equation:

$$\frac{\partial \phi}{\partial t} + u \frac{\partial \phi}{\partial x} = \alpha \frac{\partial^2 \phi}{\partial x^2} \tag{26}$$

76. If u is zero, this equation is the parabolic time-dependent diffusion equation in which the dependent variable ϕ can change only through the second order derivative dissipative term. If the diffusion coefficient α is zero, the equation is a hyperbolic wave-type equation in which ϕ can vary only through advection by the velocity u.

77. Assuming that ϕ is continuous and possesses continuous derivatives, a Taylor series expansion in time yields

$$\phi(t + \Delta t) = \phi(t) + \Delta t \frac{\partial \phi}{\partial t} + \frac{\Delta t^2}{2} \frac{\partial^2 \phi}{\partial t^2} + O(\Delta t^3) \tag{27}$$

thus, one can solve for $\partial \phi / \partial t$ as

$$\frac{\partial \phi}{\partial t} = \frac{\phi(t + \Delta t) - \phi(t)}{\Delta t} + \frac{\Delta t}{2} \frac{\partial^2 \phi}{\partial t^2} + O(\Delta t^2)$$

or

$$\frac{\partial \phi}{\partial t} = \frac{\phi(t + \Delta t) - \phi(t)}{\Delta t} + O(\Delta t) \tag{28}$$

This is called a "forward difference" representation of the time derivative and as indicated by the notation $O(\Delta t)$ is only first order. Likewise, one can write the Taylor series as

$$\phi(t - \Delta t) = \phi(t) - \Delta t \frac{\partial \phi}{\partial t} + \frac{\Delta t^2}{2!} \frac{\partial^2 \phi}{\partial t^2} + O(\Delta t^3) \tag{29}$$

so that

$$\frac{\partial \phi}{\partial t} = \frac{\phi(t) - \phi(t - \Delta t)}{\Delta t} + O(\Delta t) \tag{30}$$

which is known as a "backward difference." As with the forward difference, such an expression is only a first order scheme. If one subtracts Equation 29 from Equation 27, the following results

$$\frac{\partial \phi}{\partial t} = \frac{\phi(t + \Delta t) - \phi(t - \Delta t)}{2\Delta t} + O(\Delta t^2) \tag{31}$$

This expression is referred to as a "centered difference" representation and is a more accurate integration scheme as $\Delta t \to 0$, since it is of second order in time.

78. Applying a forward differencing of the time derivative in Equation 26 yields

$$\phi_i^{n+1} = \phi_i^n + \Delta t \left[-u \frac{\partial \phi}{\partial x} + \alpha \frac{\partial^2 \phi}{\partial x^2} \right]_i^n \tag{32}$$

which is known as an "explicit time-integration scheme," since values at the $n + 1$ time level can be computed directly from known values at the previous time level n . In addition, such a scheme is labeled as a one-step scheme, since only one sequence of computations is required.

79. Likewise, applying a backward differencing to the time derivative yields

$$\phi_i^{n+1} = \phi_i^n + \Delta t \left[-u \frac{\partial \phi}{\partial x} + \alpha \frac{\partial^2 \phi}{\partial x^2} \right]_i^{n+1} \tag{33}$$

which is labeled as an "implicit time-integration scheme," since values at the i^{th} spatial point on the $n + 1$ time level are dependent upon

not only values at the n time level but also values of ϕ at surrounding spatial points on the same time line. Implicit schemes require the simultaneous solution of a system of algebraic equations and, thus, are more complicated than the explicit integration schemes. However, as will be discussed later, implicit schemes are more numerically stable. As with Equation 32, Equation 33 would be labeled a one-step method. Various degrees of implictness can be realized by positioning the spatial derivatives between the n and the $n + 1$ time step. (Equation 33, for example, is fully implicit.)

80. If one employs the centered integration scheme, the following results

$$\phi^{n+1} = \phi^{n-1} + \Delta t\left[-u\,\frac{\partial \phi}{\partial x} + \alpha\,\frac{\partial^2 \phi}{\partial x^2}\right]^n \tag{34}$$

which is also an explicit scheme, but as previously noted is of second order in time. It might be noted that the above scheme is unstable if $\alpha \neq 0$. However, it can be made stable by evaluating $(\alpha)\partial^2\phi/\partial x^2$ at the $n - 1$ level. Schemes that utilize centered differences in time are often referred to as leapfrog schemes. A characteristic of centered difference schemes is that in addition to the primary solution, a computational mode can also exist and results in a time-splitting of the solution. Consider the simple equation

$$\frac{\partial f}{\partial t} = 0$$

The analytic solution of this equation is $f = \text{constant}$. However, its numerical solution using centered differences is $f^{n+1} = f^{n-1}$. Thus, the following solutions are possible:

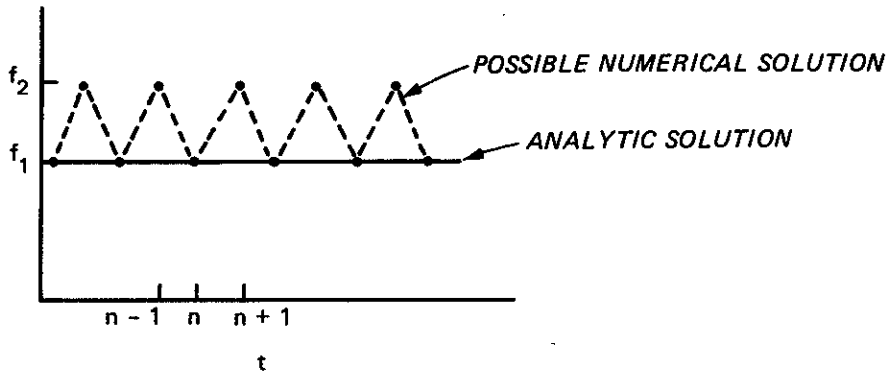

It is easy to see then that a time-splitting of solutions can occur when using centered differences to replace the time derivative. One method of suppressing such a splitting is to employ a smoothing technique at some regular interval of time steps during the computations.

81. All of the time-differencing schemes above are one-step methods. An example of a two-step scheme is that of Heun, as discussed by Roache (1972). In Heun's scheme one first solves for $\tilde{\phi}^{n+1}$ using a forward differencing, i.e.,

$$\tilde{\phi}^{n+1} = \phi^n + \Delta t \left[-u\Delta t \frac{\partial \phi}{\partial x} + \alpha \frac{\partial^2 \phi}{\partial x^2} \right]^n \tag{35}$$

and then ϕ^{n+1} is determined from

$$\phi^{n+1} = \phi^n + \frac{\Delta t}{2} \left\{ \left[-u\Delta t \frac{\partial \phi}{\partial x} + \alpha \frac{\partial^2 \phi}{\partial x^2} \right]^n + \left[-u\Delta t \frac{\partial \tilde{\phi}}{\partial x} + \alpha \frac{\partial^2 \tilde{\phi}}{\partial x^2} \right]^{n+1} \right\} \tag{36}$$

It can be seen then that the solution is obtained from two computational steps and thus Heun's integration scheme is referred to as a two-step scheme.

82. As previously noted, higher order time-differencing schemes can be constructed. These can be devised through the utilization of more time levels or perhaps in the following manner. Consider the hyperbolic equation

$$\frac{\partial \phi}{\partial t} + C \frac{\partial \phi}{\partial x} = 0 \qquad (37)$$

As previously illustrated, a centered time differencing yields

$$\frac{\partial \phi}{\partial t} = \frac{\phi^{n+1} - \phi^{n-1}}{\Delta t} + \frac{\Delta t^2}{3} \frac{\partial^3 \phi}{\partial t^3} + O(\Delta t^3)$$

where five time levels would be required for a centered difference representation of the third order time derivative. However, through a sequence of time and spatial differentiation of Equation 37, one can show that

$$\frac{\partial^3 \phi}{\partial t^3} = C^3 \frac{\partial^3 \phi}{\partial x^3}$$

thus, a third order time-differencing scheme of the basic equation could be written as

$$\frac{\phi^{n+1} - \phi^{n-1}}{\Delta t} = -\left[C \frac{\partial \phi}{\partial x} + \frac{C^3 \Delta t^2}{3} \frac{\partial^3 \phi}{\partial x^3} \right]^n$$

The only numerical hydrodynamic model found in the literature that is of higher order than two in time is a vertically averaged model developed at the Danish Hydraulic Institute, which, according to Abbott (1979), is "close" to third order.

Space differencing

83. As in the discussion on time differencing, either first, second, or higher order differencing of spatial derivatives can be utilized to create different order finite difference schemes. Once again, Taylor series expansions in space yield the following expressions for forward, backward, and centered differences of a spatial derivative:

$$\underline{\text{Forward}}: \quad \frac{\partial \phi}{\partial x} = \frac{\phi_{i+1} - \phi_i}{\Delta x} + O(\Delta x)$$

$$\underline{\text{Backward}}: \quad \frac{\partial \phi}{\partial x} = \frac{\phi_i - \phi_{i-1}}{\Delta x} + O(\Delta x)$$

$$\underline{\text{Centered}}: \quad \frac{\partial \phi}{\partial x} = \frac{\phi_{i+1} - \phi_{i-1}}{2\Delta x} + O(\Delta x^2)$$

Thus, one can see that if a forward difference is used in both space and time, a scheme that is completely first order, i.e., $O(\Delta t, \Delta x)$, results. Likewise, the use of centered differences in both space and time results in an $O(\Delta t^2, \Delta x^2)$ scheme.

84. As with centered differencing of time derivatives, the use of centered differences to replace spatial derivatives can result in a computational mode. This is illustrated by considering the solution of

$$\frac{\partial f}{\partial x} = 0$$

where the analytic solution is f = constant. Thus, similar to its time counterpart, numerically the following solution can develop:

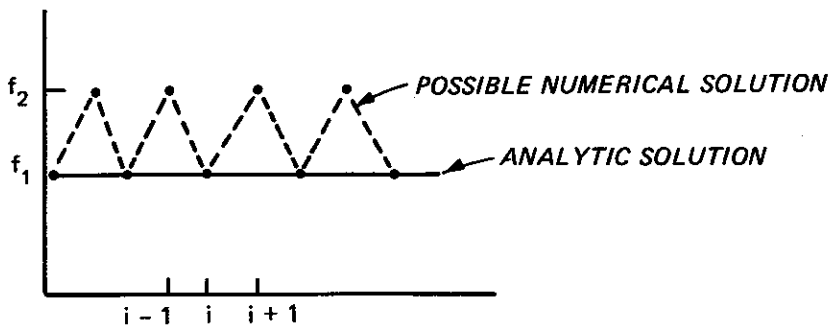

85. A major problem associated with space differencing is the treatment of the nonlinear advective terms. The nonlinear terms tend to generate higher harmonics, which can result in what Phillips (1959) called a "nonlinear computational instability." As noted by Roache (1972), this problem is not unique to nonlinear systems, but can occur whenever

nonconstant coefficients appear in the differential equation. An effective method to suppress higher harmonics is to introduce eddy diffusion or smoothing. One scheme that tends to introduce artificial damping of the higher harmonics without appreciably affecting the long waves, i.e., the solution of interest, is the two-step Lax-Wendroff scheme which combines Lax's forward-in-time and centered-in-space scheme as the first step with a centered-in-time and centered-in-space scheme for the second step.

86. The use of either forward or backward spatial differences to represent the advective terms of the transport equation is closely related to the characteristics of the hyperbolic equation. Consider the case of $\alpha = 0$ in Equation 26. The transport equation then states that $D\phi/Dt = 0$ along the characteristic direction given by $dx/dt = u$. Therefore, from the illustration below

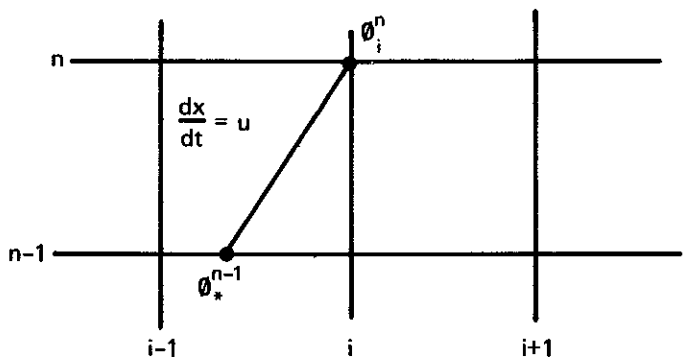

ϕ_i^n must be equal to ϕ_*^{n-1}. If u is positive, the characteristic lies as shown; whereas, if u is negative, it falls between i and $i + 1$ on the $n - 1$ level. The major problem in determining ϕ_i^n is to determine ϕ_*^{n-1}. If linear interpolation is used between i and $i - 1$, the resulting expression for ϕ_i^n corresponds to the use of a forward-in-time and backward-in-space representation of the basic equation. However, if u is negative and a linear interpolation between i and $i + 1$ is employed, the resulting expression is equivalent to the use of forward differences in the spatial derivative. If a linear interpolation from $i - 1$ to $i + 1$ is used, centered differences result. In addition, one could use higher order interpolating schemes such as a quadratic polynomial to interpolate between $i - 1$, i, and $i + 1$ which

yields Leith's scheme (Roache 1972). This scheme is $O(\Delta t^2, \Delta x^2)$, even though only two time levels appear in the difference equation. It can be shown that this approach is equivalent to replacing the second order time derivative in the series expansion by a second order spatial derivative, as previously discussed.

87. One-sided differences, i.e., the forward or backward schemes, introduce an artificial dissipation into the solution similar to the case where $\alpha \neq 0$; whereas, centered differences do not introduce this dissipation. However, the one-sided differences preserve what is labeled by Roache (1972) as the "transportive property," which is not the case with centered differences. The transportive property is related to whether the parameter ϕ is numerically advected solely in the direction of the flow, as theoretically it should be.

88. In the space differencing discussed above, only first or second order schemes have been discussed. However, higher order spatial schemes can be developed and have been utilized, in particular in the work of Abbott (1979). In the DHI models (Hinstrup 1977), Everett's 12-point interpolating polynomial in two dimensions is used to generate a fourth order transport scheme that conserves mass, advects correctly the center of mass, i.e., maintains the transportive property, has no artificial dispersion (proportional to $\partial^2\phi/\partial x^2$), and in addition conserves third and fourth moments of the distribution of ϕ . A disadvantage of such higher order schemes that extend over several grid points is the difficulty encountered near boundaries.

89. Holly and Preissman (1977) present a method of constructing higher order schemes that utilize only two grid points. Their method centers around the use of Hermitian interpolating polynomials rather than interpolating polynomials that extend over several net points. Hermitian polynomials are constructed such that not only the function but also derivatives of the function are required to satisfy known conditions at only two points. Numerical schemes based on this concept are referred to as "two-point higher order" methods to emphasize the fact that by using function derivatives, one can obtain higher order one-dimensional schemes using information at only two points. In fact, the

authors indicate that results from comparative studies show that the use of derivatives to obtain a third degree interpolating polynomial is more accurate than one using a third or fourth degree polynomial based on additional points.

90. Such a method, of course, requires both the dependent variable and its space derivative as initial and boundary conditions. However, through an example application, Holly and Preissman (1977) show that the inconsistencies introduced between the dependent variable and its derivatives as estimated from initial given values of the variable will have a minor influence on the results. Although an extension of the method to two dimensions is not presented, some preliminary computational results are. The authors indicate that such an extension to two dimensions preserves the favorable accuracy characteristics observed in one dimension.

Consistency, convergence, and stability

91. A finite difference scheme is said to be consistent if when one expands the discrete system in Taylor's series form by retaining the higher order terms, all the terms of the differential equation (with possible additional terms) are generated. In addition, in the limit as the time and spatial steps approach zero independently, all of the additional terms must go to zero.

92. In order for a numerical solution to be meaningful, it must be a good approximation of the exact solution of the differential equations. Convergent finite difference schemes are those for which the solution of the difference equations converges to the exact solution as the size of time and spatial steps approach zero. The convergence of finite difference solutions of the nonlinear equations governing fluid motions cannot be proved analytically, and thus, one must resort to the use of intuition or preferably a comparison of numerical results with laboratory and/or field data to demonstrate that the numerical scheme does indeed model the physical processes represented mathematically by the governing differential equations.

93. In a rigorous, mathematical sense, a finite difference scheme is stable if two solutions that are arbitrarily close to each other at a

given time remain arbitrarily close for all time. In a practical sense, one considers a particular scheme stable if the solutions do not grow unbounded. For economic reasons, in the numerical calculation of space- and time-dependent hydrodynamic problems, one desires to use as large a space and time step as possible and still obtain the desired level of accuracy and physical detail. However, in addition to these restrictions, the stability of the finite difference scheme dictates the size of the integration difference steps that can be employed.

94. Explicit finite difference schemes are conditionally stable; i.e., stable computations will result so long as the space and time steps satisfy what are known as "stability criteria." In free surface hydrodynamic modeling, the most severe of these criteria is usually the Courant condition on a gravity wave,

$$\Delta t < \frac{\Delta x}{\sqrt{gh}}$$

which states that the time and spatial steps are restricted such that a gravity wave will not propagate over more than one spatial step within the prescribed time step. Additional stability criteria presented below

$$\Delta t < \Delta x/u$$

$$\Delta t < \Delta z^2/2A$$

$$\Delta t < \Delta x/\sqrt{\frac{\Delta\rho}{\rho} gh}$$

are related to the velocity of a fluid particle, the rate of diffusion, and the speed of internal waves, respectively.

95. All or some of these restrictions may be eliminated by various finite difference schemes. For example, fully implicit schemes can be constructed that are unconditionally stable, at least in a linear sense; whereas, mixed implicit-explicit schemes, such as that of Edinger and

Buchak (1979), may be constructed to remove one or more of the more severe criteria while continuing to be restricted by the less severe ones. Each finite difference scheme has its own advantages and difficulties, and which scheme is best often depends upon the particular problem. For example, one may be able, from a stability standpoint, to use an unlimited time step in an implicit scheme as opposed to perhaps a rather small time step in an explicit scheme. However, if the physical character of the problem, such as rapidly varying input boundary conditions, forces the use of a relatively small time integration step in the implicit code, one may find that an explicit model is actually more economical due to the simplicity of the solution technique.

96. Stability of a finite difference scheme can be related to the concept of artificial viscosity or diffusivity, which has been previously discussed. Using Hirt's method of analysis, as opposed to the more elaborate von Neumann analysis in which the growth of a Fourier component is investigated (see Roache 1972), consider the stability of a forward-in-time and centered-in-space representation of Equation 26:

$$\phi^{n+1} = \phi^{n} - \frac{u\Delta t}{2\Delta x}\left(\phi^{n}_{i+1} - \phi^{n}_{i-1}\right) + \frac{\Delta t\alpha}{2\Delta x}\left(\phi^{n}_{i+1} - 2\phi^{n}_{i} + \phi^{n}_{i-1}\right) \qquad (38)$$

Replacing the discrete values above by a Taylor series expansion and making use of the initial differential equation yields

$$\frac{\partial\phi}{\partial t} + u\,\frac{\partial\phi}{\partial x} = \left(\alpha - \frac{u^2\Delta t}{2}\right)\frac{\partial^2\phi}{\partial x^2} + O(\Delta t) + O(\Delta x^2) \qquad (39)$$

It can be seen that as Δt and $\Delta x \to 0$, the above equation reduces to the original differential equation; therefore, the difference scheme is consistent. However, it will not be stable unless the effective dissipative coefficient $\alpha - u^2\Delta t/2$ is greater than zero, since the physical nature of such a coefficient is to smear a disturbance. Thus, a negative

coefficient is a physical impossibility. The term $-u^2\Delta t/2$ is referred to as the "negative artificial viscosity" or "diffusitivity" of the scheme. One can now see why a forward time integration with centered spatial derivatives will result in a completely unstable scheme when applied to pure hyperbolic equations, i.e., $\alpha = 0$ in Equation 26. If backward differences ($u > 0$) are used to replace the spatial derivative, the effective dissipative coefficient becomes

$$\alpha_e = \alpha + u\Delta x/2 - u^2\Delta t/2$$

Therefore, one-sided differences for spatial derivatives increase the effective dissipative coefficient, which results in a more stable, although theoretically less accurate, scheme.

PART IV: THREE-DIMENSIONAL HYDRODYNAMIC MODELS

97. A relatively wide range of numerical three-dimensional hydrodynamic models currently exist. All that have been investigated utilize finite differences to obtain numerical solutions of the governing equations and furthermore all employ explicit time differencing. The general opinion in the past concerning the use of 3-D implicit schemes has been that due to the extremely large matrices that have to be inverted for a completely implicit model, such schemes would require excessive computing time. In addition, apparently schemes such as Leendertse (1967) employs in his two-dimensional work (alternating direction implicit--ADI) have not been used for various reasons. First, such schemes require all computational arrays to be in the computer's fast memory for efficient computation, which would put a considerable restraint on the array sizes of a three-dimensional model. In addition, such schemes place restrictions on the formulation of the finite difference representation of various terms in the equations.

98. The time-dependent and variable density three-dimensional models of Simons (1973), Lick (1976), Leendertse et al. (1973), Waldrop and Tatom (1976), and Spraggs and Street (1975) are discussed in some detail below. Other less general three-dimensional numerical hydrodynamic models exist, such as those of Gedney and Lick (1970), Liggett (1970), and Bonham-Carter et al. (1973). However, for the computation of flows in stratified reservoirs, only those models that are time-dependent and allow for a variable density are of interest.

Simons' 3-D Lake Model

99. The modeling of stratified fluid flow may be accomplished in two ways: (a) a layered model in which the fluid is made up of discontinuous layers within which all fluid properties such as density and viscosity are uniform and (b) a continuous model in which the density is varied continuously. Historically, in numerical models developed by meteorologists and oceanographers, the three-dimensional model has

been viewed as a superposition of layers of fluid separated by material interfaces. The reason for this is partly physical, since during certain periods a body of water may become so stratified that strong density discontinuities can exist. On the other hand, if the vertical resolution of the model is sufficiently large, any type of stratification can be handled by a straightforward three-dimensional finite difference grid, i.e., a sequence of rigid permeable horizontal levels.

100. Simons' (1973) model is a multilayered model, which employs the principles and terminology of layered models while retaining the capability of treating the layers as being separated by permeable rigid interfaces (either horizontal or sloping) as well as treating the interfaces in the usual layered manner as moving material surfaces. The equations for the layered system are obtained by vertical integration of the governing equations (written in the conservative form) over each layer as opposed to applying the equations at given levels and replacing the vertical derivatives by finite differences. The primary dependent variables are the layer thickness or vertical velocity and the layer-averaged horizontal velocity components as well as the temperature.

101. Simons invokes the Boussinesq approximation and assumes that vertical accelerations are negligible; i.e., the pressure is hydrostatic. With the assumption of the Boussinesq approximation, the equation of mass continuity reduces to the incompressibility condition, which implies that the vertical fluid motion is directly related to the divergence of the horizontal flow. With the hydrostatic pressure assumption replacing the vertical momentum equation, the vertical component of velocity cannot be computed in the same manner as the two horizontal components. Instead, the equation expressing incompressibility is integrated over a layer to yield an equation whose primary purpose is to compute water displacements from a given distribution of horizontal velocities. From this equation, one can determine either the displacement of a material surface or the vertical velocity of the fluid through a rigid interface, if given the appropriate boundary conditions at the free surface, at the interface, and at the bottom. The computation starts with the bottom layer and proceeds upward.

102. The equation of state is such that the density is assumed to be a quadratic function of the temperature. An eddy coefficient model is employed to approximate the exchange of energy between the large-scale flow and the smaller turbulent eddies. It appears that constant, but different, horizontal and vertical coefficients are employed. Simons does indicate that the vertical eddy diffusivity depends on the static stability $\partial\rho/\partial z$ of the water column, and he allows it to attain very large values for unstable situations in order to simulate the net effects of convective overturning.

103. The time integration scheme employed by Simons uses centered differences, where the pressure gradient terms, the divergence terms, the Coriolis terms, and the nonlinear terms are evaluated at a time step centered between the old and new time, while the dissipative and diffusion terms are evaluated at the old time step. Centered differences are also used to replace spatial derivatives, and thus, the finite difference model is almost $O(\Delta t^2, \Delta x^2)$. Linear interpolation is used to provide values of variables at points where they are not defined.

104. An interesting aspect of Simons' model is his use of two different time steps. The surface and internal computations are decoupled such that a small time step governed by the Courant condition is used to compute the water surface elevations; whereas, a much larger time step governed by the speed of a fluid particle is used to compute the internal flow and the temperature. This is accomplished as follows. The layer-averaged equations are added to create a vertically averaged, i.e., one-layer, model for gross fluid flows, which are then used to drive the free surface. The layer-averaged equations then use the results of the vertically averaged model to produce the internal flow field. Simons indicated that in Lake Ontario, with a grid mesh of 5 km, the surface elevation and the vertically integrated flow were computed with a time step of the order of one minute, while the internal flow and temperature were predicted with a time step of the order of 30 min.

Leendertse's 3-D Estuary Model

105. This variable density model (Leendertse 1973) has been

developed for the computation of the hydrodynamics of estuaries and coastal seas. Some of the assumptions and formulations are not directly applicable to freshwater reservoirs where density effects are due to temperature variations rather than salinity; however, it is believed that such an extension would not be difficult.

106. The approach taken in the formulation of the equations is similar to Simons (1973) in that the basic three-dimensional equations are integrated over a vertical layer to yield layer-averaged equations. Unlike Simons, however, Leendertse's model does not allow movable material interfaces. The water body is represented by rigid permeable horizontal surfaces with the thickness of each interior layer constant in space and time, although the thickness of each layer is not necessarily the same. The top layer that contains the surface is, of course, represented by a time-varying and spatially varying thickness.

107. The basic three-dimensional equations are written in the conservative form to insure that mass, momentum, etc., are neither created nor destroyed by the computational scheme. Before the layer integration is performed, the Boussinesq approximation is assumed and the pressure is assumed to be hydrostatic. Therefore, as in Simons' model, the vertical component of the fluid velocity must be computed from the layer-averaged condition of incompressibility.

108. Approximate eddy viscosity models that consider only the diagonal components of the viscosity tensor are employed to represent the subgrid-scale motions. The momentum and mass dispersion coefficients are assumed to be constant in the horizontal dimensions of the flow, although they can differ in the two directions. The vertical exchange coefficients are calculated with a more sophisticated model that takes into account the vertical velocity, the concentration gradient, and the stability of the flow according to the Richardson number.

109. Since the model was developed for an estuarine or coastal environment, the equation of state relates the fluid density to the salinity. If the model were to be applied to a freshwater environment, a new equation of state relating the density to temperature would, of course, need to be substituted. In addition, surface heat exchange

would have to be accounted for through the surface boundary condition.

110. At the boundaries of the water body to be computed, all diffusion coefficients are set to zero, as are the velocities perpendicular to the boundary. In this manner, no mass fluxes or diffusive transports of salt result. At the surface, the boundary stress due to the wind is computed from a quadratic law. A similar quadratic expression employing the Chezy coefficient is used to represent the dissipation of momentum at the bottom through the bottom shear stress. When employing the layer-averaged approach, interfacial shear stress terms show up in the resulting equations for the layer-averaged variables. As for the boundary stress specifications, a quadratic relationship between the interlayer stresses and the velocity differences of adjacent layers is assumed applicable.

111. The spatial grid used in the finite difference formulation is similar to that employed by Leendertse (1967) in his two-dimensional work where velocities are defined on the faces of a cell. However, the water surface elevations, which are determined from an equation obtained by summing the layer-averaged incompressibility equation over the water column, are defined at the corners of the top layer of cells rather than at the cell center as in the 2-D model. Pressure, density, and salinity are defined at cell centers.

112. Centered differences are used for both time and spatial integrations. Therefore, the resulting finite difference scheme is $O(\Delta t^2, \Delta x^2)$ except that the diffusion terms are taken at the lower time level, i.e., $t = (n-1)\Delta t$, since otherwise the computation becomes unstable. Since centered differences are used to replace the time derivatives, initial information at two time levels is required. To reduce the time-splitting tendency of such a scheme, a single forward differencing step is used to obtain initial information on the second time step.

113. Since an explicit time integration scheme has been utilized, the basic stability criterion is once again the Courant condition. Although the computations with the adopted scheme are extensive, Leendertse indicates that the model is well within the range of

practical applications for relatively short-term simulations. For example, Leendertse indicates that a problem with a horizontal grid of about 1000 points and with eight layers required a computation time of 30 min on an IBM 390-61 for a real time simulation of 67 hr in 4000 time steps.

Lick's Thermal Plume Model

114. A variable density, heat-conducting model for studying the near field surrounding the point of discharge of a river or power plant into a body of water has been developed by Lick (1976) at Case Western Reserve University.

115. Basic assumptions made in the model development are that the Boussinesq approximation holds and that the pressure is hydrostatic. As previously discussed, the hydrostatic pressure assumption reduces the order of the system of equations and the computational effort required. A major difference between the Lick model and other three-dimensional models studied is the assumption of a rigid lid at the surface. This approximation, which removes the surface gradient terms from the momentum equations, is made to eliminate surface gravity waves and the small time scales associated with them. This, of course, greatly increases the maximum allowable time step without encountering stability problems. With the rigid-lid approximation, the limiting time step is no longer given by the extremely restrictive gravity wave Courant condition but instead is usually fixed by the speed of a water particle, i.e.,

$$\Delta t < \Delta x/u$$

or perhaps by the speed of an internal wave, i.e.,

$$\Delta t < \frac{\Delta x}{\sqrt{\frac{\Delta \rho}{\rho} gh}}$$

where $\Delta \rho$ is equal to change in water density.

116. With the rigid-lid assumption, the pressure is no longer atmospheric at the surface but instead varies with the internal flow field. Thus, an additional equation must be derived and subsequently solved to yield the surface pressure. Once the surface pressure is determined, internal pressures are determined from the hydrostatic condition.

117. The Poisson equation for the surface pressure is derived by taking the divergence of the vertically integrated momentum equations and making use of the vertically integrated continuity and hydrostatic pressure equations. The form of this equation becomes

$$\frac{\partial}{\partial x}\left(\frac{h\partial P_s}{\partial x}\right) + \frac{\partial}{\partial y}\left(\frac{h\partial P_s}{\partial y}\right) = F(u,v,w,T)$$

where P_s is the surface pressure. Lick indicates that even though a rigid lid has been assumed, one can compute surface displacements (neglecting the transient motion due to gravity waves) by interpreting the surface pressure as a pressure due to a height of water above or below the location of the rigid lid. The numerical solution of the pressure Poisson equation at each time step is accomplished by using the ADI method.

118. The diagonal components of the eddy coefficient tensors are used to account for the turbulent subgrid-scale motions. The horizontal eddy coefficients are assumed constant, but the vertical eddy coefficients are a function of the temperature gradient and other parameters. This dependence on temperature is given by

$$A_v = \alpha - \beta \frac{\partial T}{\partial z}$$

where A_v is the vertical eddy diffusivity and α and β are constants depending on the local conditions. The constant α is equal to the vertical eddy diffusivity under neutral stability conditions. Typical values for α and β are 50 cm^2/sec and 200 $cm^3/°C\text{-}sec$, respectively. Lick handles a static instability in the same manner as Simons; i.e., extensive mixing is assumed.

119. An interesting aspect of Lick's model is his use of a linear transformation in the vertical direction such that the x, y, z Cartesian system is transformed to a x, y, σ system where $0 \leq \sigma \leq 1$, with the bottom corresponding to $\sigma = 0$ and the top to $\sigma = 1$. The σ coordinate is defined by

$$\sigma = 1 + \frac{z}{h}$$

where $h(x, y)$ is the depth of the water body. With such a transformation, irregular bottoms can be handled more accurately and efficiently. For example, the usual finite difference representation of the sloping bottom of the GRH flume (applications to be discussed later) is as shown below.

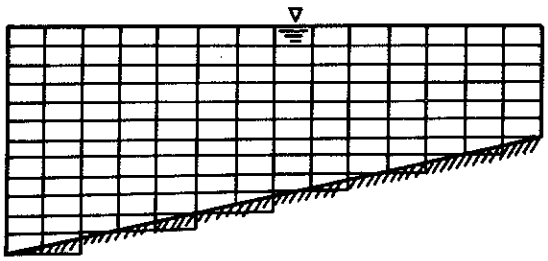

However, the use of the transformation above yields the following physical representation, with the actual numerical computations being performed on a rectangular transformed grid:

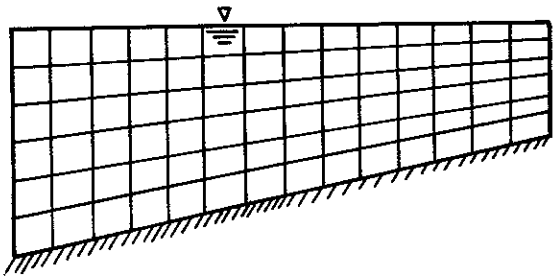

It should be noted, however, that since the transformation is not conformal, when transforming the governing equations, the transformed second derivative diffusive terms contain cross-derivatives of the spatial coordinates. Lick assumes that the diffusive terms containing

derivatives of the depth are negligible with respect to those diffusive terms containing only the depth and thus drops such terms.

120. Solid boundaries are taken as no-slip, impermeable, adiabatic surfaces. A heat transfer condition proportional to the temperature difference (surface temperature minus equilibrium temperature) and a wind-dependent stress are imposed at the surface. Normal derivative pressure boundary conditions are derived from the appropriate vertically integrated momentum equation. At open boundaries far from the point of discharge of the river or plume, the normal derivatives of the velocities and the temperature are zero.

121. As opposed to the layer-averaged approach of Simons and Leendertse, Lick performs a straightforward finite differencing of the governing 3-D equations. A forward time-differencing integration scheme is utilized along with centered differences for the spatial derivatives. Thus, the finite difference scheme is of the first order in time and second order in space, i.e., $O(\Delta t, \Delta x^2)$. The computational grid is such that the horizontal velocity components, u and v , are defined at the cell corners with the vertical component defined at the middle of the top and bottom face of the cell. The pressure and temperature are defined at the cell center, except for the surface pressure, which is computed at the center of the top face.

Waldrop-Tatom 3-D Plume Model

122. There are actually two versions of this extremely versatile three-dimensional variable density model (Waldrop and Tatom 1976). One employs the hydrostatic pressure assumption, and the other retains the complete vertical momentum equation. Both utilize the Boussinesq approximation and both neglect Coriolis effects. It appears from Waldrop and Tatom (1976) that the hydrostatic pressure version solves the nonconservative form of the basic governing equations; whereas, Tatom and Smith (1979a) indicate that the conservative form of the equations are solved in the version that does not make the hydrostatic assumption. Both versions solve the governing equations transformed into orthogonal

curvilinear coordinates. This, of course, allows for more accurate modeling of curved boundaries such as river bends.

123. In the nonhydrostatic version, the pressure is written as the sum of the hydrostatic pressure and the dynamic pressure $1/2\ \rho v^2$, and a Poisson equation for the dynamic pressure is derived for solution over the complete 3-D field. The Richardson iterative technique is employed. It might be noted that in the Poisson pressure equation, terms that involve the horizontal density gradients have been neglected. However, it does appear that horizontal density gradients, as reflected through the hydrostatic component of the pressure, are included in the velocity computations from the momentum equation.

124. With the retention of the complete vertical momentum equation, a fully convective model that can handle buoyancy effects, i.e., unstable density profiles, is realized. The vertical component of the velocity is now determined from the vertical momentum equation as opposed to its solution from the incompressibility condition in the hydrostatic version.

125. The effects of turbulence are included through the use of eddy coefficients. The horizontal eddy viscosity coefficient ε_H is derived from a mixing length equation for open channels in the form

$$\varepsilon_H = 0.16(z - z_B)^2\ (\zeta - z)/(\zeta - z_B)\left|\partial\sqrt{u^2 + v^2}/\partial z\right|$$

where

$z = z_B$ at the bottom

$z = \zeta$ at the free surface

which provides the largest values of ε_H in deep regions with large velocity gradients in the vertical; whereas, in shallow and/or low flow regions ε_H is small. The horizontal eddy diffusivity A_H is related to the eddy viscosity by

$$A_H = 1.33\varepsilon_H$$

126. In turbulent flows, density stratification inhibits the

vertical exchange of both heat and momentum as well as the mass of any constituent. The Waldrop-Tatom models allow the vertical eddy coefficients to be functions of the stratification through their dependence on the Richardson number in the following manner:

$$\varepsilon_v = \varepsilon_H \left(1 + 10R_i\right)^{-1/2}$$

$$A_v = A_H \left(1 + 3.33R_i\right)^{-3/2}$$

where

$$R_i = -(g/\rho)(\partial\rho/\partial z)\left(\partial\sqrt{u^2 + v^2}/\partial z\right)^{-2}$$

It might be noted that although the eddy coefficients are allowed to vary spatially, spatial derivatives of the coefficients have been neglected in the model.

127. At solid boundaries, reflection boundary conditions are imposed to simulate slip boundaries. Therefore, with solid walls assumed to lie between the last two grid points, fictitious values of dependent variables on the opposite side of a wall are set to prevent mass, momentum, or energy transfer through the boundaries. Velocities normal to the wall are set as the negative of the value immediately inside in order to make the normal velocity zero at the wall, but the tangential component is set equal to its value inside since with slip walls, the wall does not influence the tangential flow. Derivatives of the temperature normal to solid walls are set equal to zero to insure no transfer of heat.

128. The velocity profile near the bottom is assumed to be logarithmic. Thus, the equation below is used to help set the horizontal velocity components at all grid points adjacent to the bottom in the solution of the momentum equations:

$$u = \sqrt{T_o/\rho}\left[\frac{1}{0.4}\ln\left(\frac{z - z_B}{k}\right) + 8.5\right]$$

where

τ_o = shear stress

$(z - z_B)$ = height above bottom

k = diameter of the average roughness

The actual values chosen are such that the finite difference representation of the velocity gradients $\partial u/\partial z$ and $\partial v/\partial z$ near the bottom match the gradient specified by the equation above. As noted, this is the procedure for determining bottom velocities for use in the momentum equations. However, in the transport equation for temperature, the velocities at points adjacent to the bottom are determined from an actual fit of the logarithmic profile rather than by forcing the proper gradient. In the computation of the free surface, a control volume is formed between the top grid plane and the free surface. Since the three velocity components from previous computations at a particular time line are known, the mass transported into and out of the control volume can be computed. The free surface is then adjusted to insure conservation of mass. In the current versions of the model, the time integration is essentially a forward difference, but with an additional step that Waldrop and Tatom (1976) indicate helps to stabilize the computations. This is accomplished with the following scheme:

$$u^{n+1} = u^n + \left[\left(\frac{\partial u}{\partial t}\right)^n + \left(\frac{\partial u}{\partial t}\right)^{n-1}\right]\frac{\Delta t}{2}$$

where $(\partial u/\partial t)^{n-1}$ is saved from computations at the previous time step. It would appear that this is equivalent to replacing the time derivative at $t = (n - 1/2)\Delta t$ by a forward difference between $(n + 1)\Delta t$ and $n\Delta t$. Thus, the scheme is still only first order in time. Centered differences are used in the diffusive terms, while one-sided windward (either forward or backward, depending upon the direction of flow) differences are used in the finite difference representation of the advective terms. Thus, it would appear that the solution scheme is $O(\Delta t, \Delta x)$.

129. As noted in a previous section, the computational grid is such that all variables are defined at the same point, with uneven

spacing of those points allowed for more flexible resolution. Waldrop and Tatom indicate that a transformation of the x , y , z coordinates such that even increments in the transformed system produce uneven spacing of the grid points in the physical system is employed. However, details of the transformation are not discussed.

130. The Waldrop-Tatom model is capable of handling branching systems through its modular concept in which the equations are solved simultaneously in different branches or regions. The regions are connected such that when there is free flow between regions, each region uses previously computed information from the adjacent region as a boundary condition. Of course, the fact that an explicit time-integration scheme has been employed greatly decreases the difficulty in incorporating such a concept. The handling of connecting branches, i.e., connecting regions, in an implicit model would be much more difficult to accomplish. The capability of handling connecting regions, allowing for a variable grid, and the use of curvilinear coordinates makes the Waldrop-Tatom model extremely versatile.

Spraggs and Street's 3-D Model

131. The nonhydrostatic version of the Waldrop-Tatom model and the three-dimensional model developed by Spraggs and Street (1975) are the only 3-D numerical models studied that are fully convective models. In other words, the complete vertical momentum equation is retained so that buoyancy effects are modeled directly. As indicated by Spraggs and Street, the primary use of the model is to simulate flows in which the stratification induced by heated effluents sets up in a matter of hours. No claim is made as to the usefulness of the present form of the model for simulating flows over periods extending over the time required for the formation of a natural thermocline. This is because of the excessive computing time required due to the extremely small time step imposed by the explicit nature of the solution.

132. As in the vast majority of hydrodynamic models, the Boussinesq approximation is made, which reduces the conservation of

mass equation to the incompressibility condition. In addition, an eddy viscosity model is used to simulate the transfer of energy from the developing flow to small-scale turbulent eddies, i.e., the subgrid-scale motions. These appear to be the only assumptions made to the basic equations. It should be noted, however, that one important restriction exists in the basic mathematical development of the model due to the manner in which pressure gradients are handled in the horizontal momentum equations.

133. A reduced pressure P_R, which is a measure of the perturbations in the system, e.g., caused by stratification and/or vertical accelerations, is defined as

$$P_R = \frac{(P - P_h)}{\rho_r}$$

where the hydrostatic pressure P_h is

$$P_h = (L_z - \zeta - z)\rho_r g$$

ρ_r is the density of a reference state, L_z is a reference depth, $\zeta(x,y)$ is the water surface elevation, and z is the distance above the reference bottom. With the hydrostatic pressure defined as above in terms of a reference density that is not a function of (x,y), the pressure gradient becomes

$$\frac{1}{\rho_r}\frac{\partial P}{\partial x_i} = \frac{\partial P_R}{\partial x_i} - g\frac{\partial \zeta}{\partial x_i}$$

which does not allow for the effect on the flow of horizontal gradients in the density. It appears that this restriction could be removed by defining the hydrostatic pressure in terms of the spatially varying density rather than of a constant reference density. Both Edinger and Buchak (1979) in the modeling of stratified reservoirs and Hamilton (1975) in the modeling of salinity-stratified estuaries have indicated that the horizontal density gradients are quite important in modeling variable density flows.

134. As is usually the case when the hydrostatic pressure assumption is not made, a Poisson equation for the reduced pressure P_R is derived by taking the divergence of the vector momentum equation and combining with the time derivative of the incompressibility condition. Derivative boundary conditions on the pressure at solid walls are derived from the momentum equations; whereas, the pressure itself is prescribed at the free surface. The solution of the pressure from the three-dimensional Poisson equation is obtained through the iterative method called point Successive-Over-Relaxation (SOR). Spraggs and Street indicate that the pressure solution usually converges within 50 iterations. Such a solution of a 3-D Poisson equation at each time step constitutes a major portion of the total computation time of the model. Thus, one can see why the hydrostatic pressure assumption has been so popular in the past in the development of hydrodynamic models.

135. The mathematical model is rendered dimensionless through the introduction of three length scales, L_x , L_y , and L_z , such that any physical problem is mapped to the interior of a unit cube. Thus, in the numerical model, there are six length parameters--L_x , L_y , L_z , Δx , Δy , Δz . The first three are defined as above, while the second three are determined by the number of computational cells within the unit cube. If $L_x \Delta x = L_y \Delta y = L_z \Delta z$, the numerical model is undistorted, and the computational cells in the physical problem are cubes. Generally, the horizontal length scales will be much larger than the vertical length scale giving rise to a distorted model in which $L_x \Delta x \neq L_y \Delta y \neq L_z \Delta z$.

136. The free surface elevation ζ is computed from the kinematic boundary condition

$$\frac{\partial \zeta}{\partial t} = - w - u \frac{\partial \zeta}{\partial x} - v \frac{\partial \zeta}{\partial y}$$

where the vertical coordinate is positive downward. The solution of the free surface is obtained through the following ADI scheme, which is one iteration of the Peaceman-Rachford scheme with an acceleration parameter of 1.0:

$$\zeta^{*}_{ij} = \zeta^{n}_{ij} - \frac{\Delta t}{2}\left[u^{n+1}\left(\frac{\zeta^{*}_{i+1,j} - \zeta^{*}_{i-1,j}}{2\Delta x}\right) + v^{n+1}_{ij} \times \left(\frac{\zeta^{n}_{i,j+1} - \zeta^{n}_{i,j-1}}{2\Delta y}\right) + w^{n+1}_{ij}\right]$$

$$\zeta^{n+1}_{ij} = \zeta^{*}_{ij} - \frac{\Delta t}{2}\left[u^{n+1}\left(\frac{\zeta^{*}_{i+1,j} - \zeta^{*}_{i-1,j}}{2\Delta y}\right) + v^{n+1}_{ij} \times \left(\frac{\zeta^{n+1}_{i,j+1} - \zeta^{n+1}_{i,j-1}}{2\Delta y}\right) + w^{n+1}_{ij}\right]$$

From the above solution technique, it can be seen that since velocities at the $n + 1$ time level are required, they are computed before the computations for the free surface are made.

137. The Spraggs and Street model is the only 3-D model investigated that allows for tensor eddy coefficients, i.e., the off-diagonal terms are not neglected. The form of the eddy viscosity tensor selected by Spraggs is a function of the rate of strain S_{mn}, i.e.,

$$\varepsilon_{ij} = \Omega \Delta x_i \Delta x_j (S_{mn}\, S_{mn})^{1/2}$$

where the Reynolds stress is

$$\overline{u'_i\, u'_j} = -\varepsilon_{ij}\, S_{ij} \quad \text{(no summation over } i\text{)}$$

and the rate of strain tensor S_{ij} is

$$S_{ij} = \frac{\partial u_i}{\partial x_j} + \frac{\partial u_j}{\partial x_i}$$

As Spraggs and Street note, there is some question as to the value of the scaling parameter Ω, since the range of problems that might be simulated could extend from laboratory flume dimensions to several hundred kilometres in the field. A value of $\Omega = 0.01$ was used by

Spraggs and Street in the initial testing of the model. The eddy diffusivity is similarly defined such that

$$\overline{u_i' T'} = -\alpha_p \varepsilon_{ij} \frac{\partial T}{\partial x_j}$$

where α_p is the turbulent Prandtl number. It should be noted that Spraggs did not allow for the effect of stratification, through the Richardson number, on the eddy coefficients in his initial work, but did indicate that such a modification would be made later.

138. The computational grid employed is one such that the velocity components are defined on the cell faces; whereas, the thermodynamic variables are defined at the cell center. Thus, the grid is in essence a grid similar to that employed by Leendertse (1967).

139. Boundary conditions at solid walls are treated as no-slip. Thus, the normal velocity at a wall is set to zero, and its value at one grid point outside the wall is set as the negative of its value at the first interior point. Tangential velocities are not defined at the wall. However, in order to model the effect of a no-slip wall, its value at one grid point outside the wall is taken to be the negative of its value at one grid point inside. Both inflow and outflow boundaries are assumed to be forced. At the surface, velocities are set using a wind stress condition. The temperature field at all boundaries except the free surface is assumed to have a zero gradient; whereas, surface temperatures, of course, are determined from the surface heat exchange determined by prevailing atmospheric conditions.

140. In the solution of the velocity and temperature fields, forward differences are used to replace time derivatives. Roache's second upwind differencing scheme is used to replace the advective terms. Thus (see Figure 5),

$$\left(\frac{\partial \alpha u}{\partial x}\right)_i^n = \frac{u_R \alpha_R - u_L \alpha_L}{\Delta x}$$

where α_R and α_L depend on the sign of the convecting velocities.

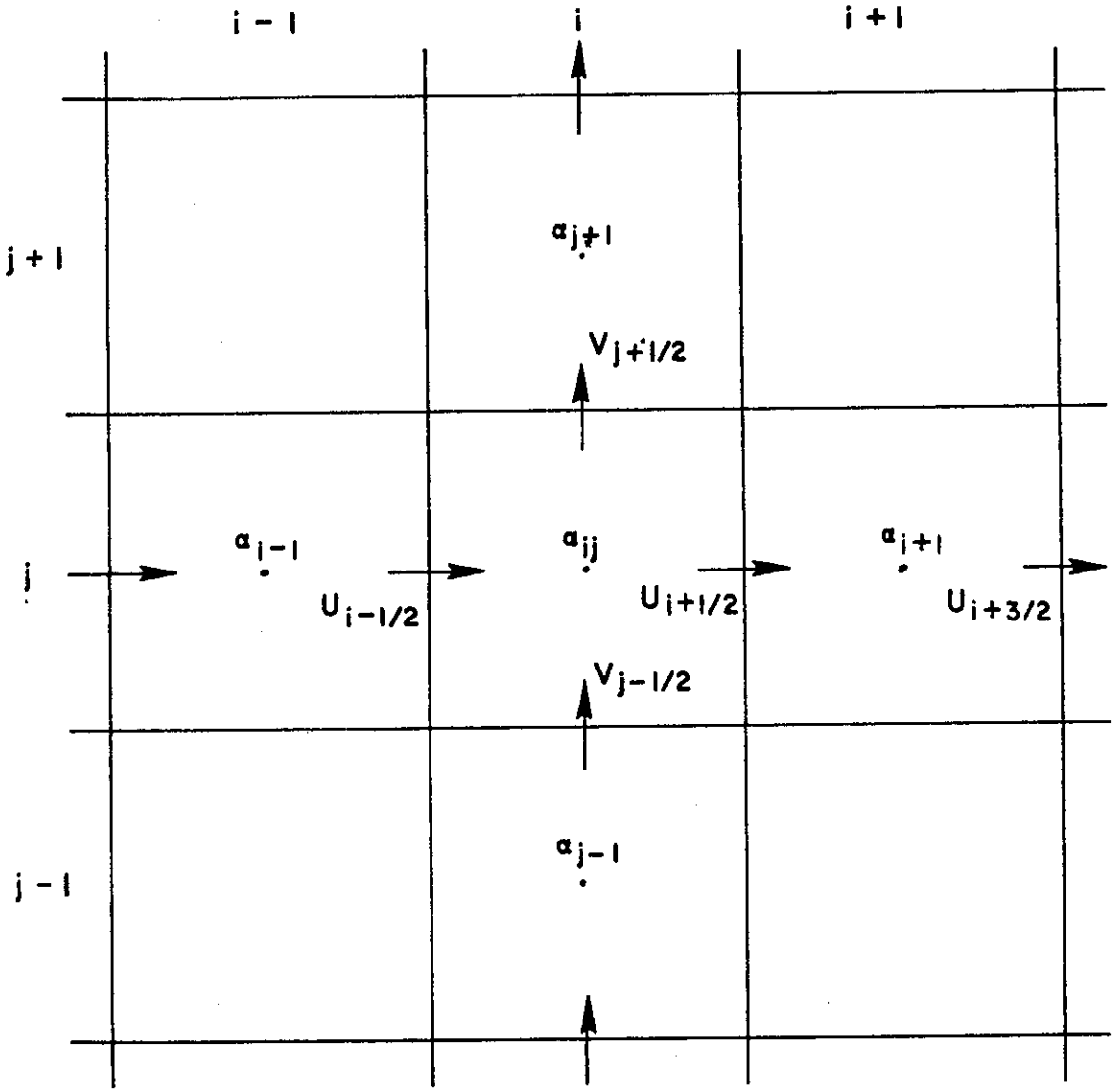

Figure 5. Definitions for upstream differencing

For example, if $u_{i-1/2} < 0$, then

$$u_R = u_{i+1/2}$$

$$u_L = u_{i-1/2}$$

$$\alpha_R = \alpha_{ij}$$

$$\alpha_L = \alpha_{ij}$$

Centered differences are employed in the representation of the diffusive terms. Therefore, the finite difference scheme is in essence $O(\Delta t, \Delta x^2)$. Various schemes of higher order were investigated by Spraggs and Street, e.g., the leapfrog, the Adams-Bashford, and Fromm's (see Roache 1972) second order schemes. The leapfrog scheme was discarded because of the time-splitting nature of the solution, while Fromm's method was not used due to the large percentage of boundary cells encountered in 3-D modeling where the method uses centered spatial differencing. Such a scheme was found to be unacceptable near boundaries with large forced outflows. A similar conclusion was arrived at during computer experimentation with the 2-D Edinger and Buchak (1979) model (page 94). Spraggs and Street indicate that the necessary coding for the Adams-Bashford method remains in the basic numerical model for future development and testing.

Eraslan's 3-D Discrete Element Model

141. Eraslan* is currently working on a fully three-dimensional heat-conducting hydrodynamic model for the Oak Ridge National Laboratory. The code will be a fully convective model with the complete vertical momentum equation retained. The basic solution technique will employ an explicit time-differencing scheme along with the previously discussed concept of discrete elements. Therefore, his formulation will employ integral forms of the governing conservation equations applied to variable-sized discrete elements that span user-specified flow regions. At the present time, there is no published information on the development of the model.

Blumberg and Mellor's 3-D Model

142. After the initial writing of this report, a three-dimensional heat-conducting coastal model developed by Blumberg and

* Personal communication, May 1979, Arsev Eraslan, Chief Scientist, Hennington, Durham, and Richardson, Knoxville, Tenn.

Mellor (1979) at Princeton University was brought to the attention of the author. It appears that the model is in an early stage of application, with only preliminary tests in the Gulf of Mexico having been made.

143. The basic equations solved are statements of the conservation of fluid mass, momentum, and energy along with the conservation of salt equation. The energy equation is written in terms of temperature, and thus the equation of state relates the fluid density to both temperature and salinity. The basic Boussinesq and hydrostatic pressure assumptions are made.

144. The model employs two concepts previously discussed in connection with the Simons and Lick models. Similar to the Simons model, the external flow is computed separately from the internal flow. The external mode, an essentially two-dimensional calculation, requires a short integrating time step; whereas, the three-dimensional, internal mode can be executed with a long step. The result is a fully three-dimensional code that includes a free surface. Similar to the Lick model, the vertical coordinate is transformed into a σ coordinate system with 20 levels in the vertical. The model developers state, "With such a transformation, the environmentally important continental shelf, shelf break, and slope can be well resolved." Furthermore, the model allows for variable grid spacing in the σ coordinate for increased resolution in the surface and bottom layers.

145. Rather than employing the same concept of eddy coefficients as utilized by all the other models investigated, a second moment model of small-scale turbulence as developed by Mellor and Yamada (1977) is employed. Diffusive-type terms proportional to second derivatives in the basic equations are retained only in the vertical direction. The developers indicate that they believe relatively fine vertical resolution results in a reduced need for horizontal diffusion; i.e., horizontal advection followed by vertical mixing effectively acts as a horizontal diffusion in a real physical sense.

146. At the surface, the wind stress, net heat flux, and net evaporation-precipitation freshwater flux are accounted for. Bottom

boundary conditions on the velocity components are supplied by matching the solution to the logarithmic law of the wall.

147. Time differencing is the conventional leapfrog technique. However, the scheme is quasi-implicit, since the vertical diffusive terms are evaluated at the forward time level. Thus, small vertical spacing is permissible near the surface without the need to reduce the time increment or restrict the magnitude of the mixing coefficients. The spatial differencing is not discussed, but Blumberg and Mellor (1979) state that the overall solution is accurate to the second order in space and time.

148. As previously discussed, leapfrog time differencing introduces a tendency for the solutions at even and odd time lines to split. The time-splitting here is removed by the use of a weak filter where the solution is smoothed at each time step by

$$F_s^n = F^n + \frac{\alpha}{2}\left(F^{n+1} - 2F^n + F_s^{n-1}\right)$$

where $\alpha = 1/10$ and F_s is a smoothed solution. This technique introduces less damping than either the Euler backward or forward stepping techniques (see Roache 1972).

PART V: TWO-DIMENSIONAL VERTICAL FLOW HYDRODYNAMIC MODELS

149. Various two-dimensional numerical hydrodynamic models have been studied and range from vertically averaged models to laterally averaged models to pure two-dimensional vertical-longitudinal models in which the width is constant. There are many two-dimensional vertically averaged estuarine models in existence. However, since such models are not applicable to stratified reservoir flows in which the allowance for a variable density and variations in the vertical direction are crucial, they are not discussed here. The only interest in such models in connection with this study was in the numerical techniques employed. All of the models studied, except for one that employs the finite element method, utilize the finite difference method for solving the governing 2-D equations. Unlike all of the 3-D models, which were explicit models, some of the 2-D models employ an implicit or perhaps semi-implicit time integration scheme so that time steps much larger than that given by the Courant condition are allowed. A few of the 2-D vertical models investigated were developed originally for application to reservoirs, and thus surface heat exchange and the variability of density with temperature are treated. The Edinger and Buchak (1979), Waldrop and Farmer (1976), and Roberts and Street (1975) models are examples. Other 2-D vertical models, such as those of Hamilton (1975) and Blumberg (1975) were initially developed for salinity-stratified estuaries and additional modifications would be needed for application to reservoirs. Additional density-varying models that consider flow in a vertical plane have been investigated and include those of Thompson*, Poseidon, Inc.,** Norton, King, and Orlob (1973), and Slotta et al. (1969).

Hamilton's 2-D Estuary Model

150. Hamilton's (1975) 2-D model was developed to represent the

---

* Personal communication, April 1979, J. F. Thompson, Mississippi State University, Mississippi State, Miss.

** Personal communication, May 1978, Personnel of Poseidon, Inc., Calif.

vertical structure of current and salinity along an estuary of varying width and depth but with a rectangular cross section, i.e., $B \neq B(z)$. A feature of the model is the numerical approach to the basic equations, which considers the depth-dependent variables as continuous. This is in contrast with layered models where the equations are integrated over the separate layers and exchange of momentum and salt between layers parameterized in terms of the mean velocities and salinities of the layers. Hamilton indicates that a continuum approach allows better treatment of the surface and bottom boundary conditions.

151. The basic 3-D equations are reduced to a set of laterally averaged 2-D equations as previously outlined. The only difference here is that the width is not a function of the vertical coordinate and, thus, derivatives of the width with respect to the vertical coordinate z are zero. The resulting laterally averaged equations, with the Bouissinesq approximation and the hydrostatic pressure assumption, are written in nonconservative form. Salinity is related to the density through a linear equation of state.

152. Boundary conditions at the head of freshwater flow consist of a vertical velocity profile and zero salinity. At the ocean boundary, the tidal elevation is prescribed as a function of time, and the salinity is specified to be that of the ocean. It does not appear that Hamilton delineates an inflow and an outflow boundary at the ocean end. To conserve salt, the vertical salinity gradient at the estuary surface and the bed is set to zero. Surface wind stress is neglected, and the bottom stress is assumed to obey the quadratic friction law such that the bottom stress is related to the velocity at a distance above the bottom representative of the frictional layer, e.g., 1 m.

153. As in all hydrostatic models, the vertical component of velocity is obtained by solving the laterally averaged incompressibility condition from the bottom upward. The equation for the free surface is obtained by vertically integrating the incompressibility equation. One restriction imposed on the free surface by the code logic is that the surface elevation does not differ by more than the vertical grid spacing (assumed to be constant) between successive horizontal grid points.

154. The finite difference grid is such that salinity, the vertical velocity, and the vertical eddy viscosity and diffusivity are defined at the center of a cell; whereas, the horizontal velocity is defined at the cell corners. This is illustrated below.

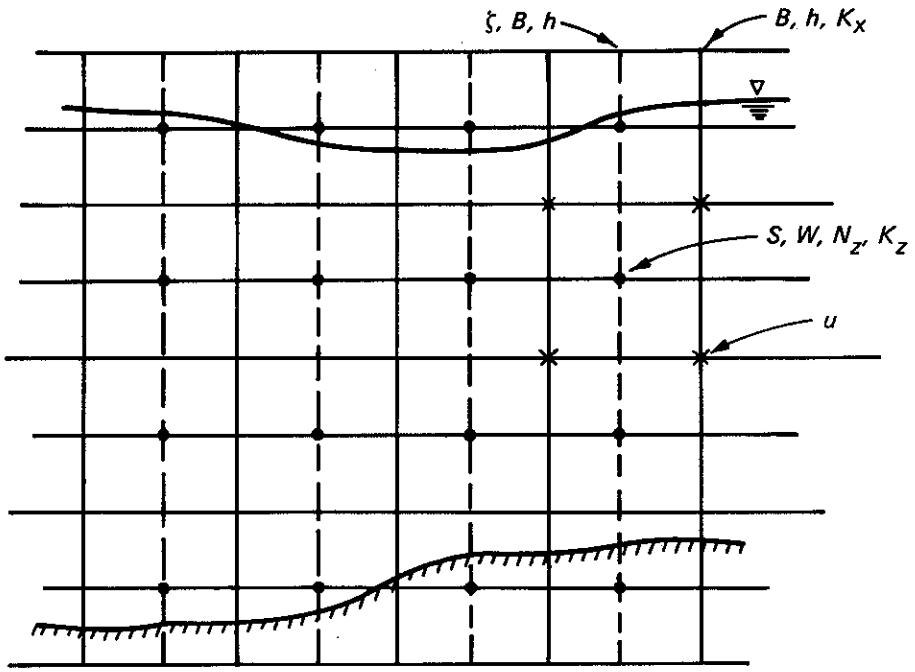

155. The time integration is a combination forward and backward time-differencing scheme such that the diffusive and frictional terms in the conservation of salt and momentum equations, respectively, are taken at the $n + 1$ time level, while all other terms such as the advective terms are taken at the n time level. Spatial differences are replaced by centered differences, except in the horizontal advective term of the conservation of salt equation, i.e., $u\partial s/\partial x$, in which Hamilton appears to make use of Roache's (1972) first upwind differencing. Thus, the finite difference scheme is in essence $O(\Delta t, \Delta x)$. The basic stability criterion is the Courant condition. Therefore, even though the scheme might be called a semi-implicit one because the second derivative terms are taken at the $n + 1$ time level, which does remove diffusive-type stability criteria, the scheme probably offers no real stability advantages over a purely explicit scheme.

Blumberg's 2-D Laterally Averaged Estuary Model

156. Like the Hamilton model, Blumberg's (1975) laterally averaged model was developed for application to an estuary. Thus, the density is related to the salinity through an equation of state and, of course, no surface heat exchange is included, since temperature is not modeled. Unlike the Hamilton model, however, this model does not assume a rectangular cross section and thus $B = B(x,z)$.

157. Additional assumptions made to the basic equations, which are written in conservative form, are that the pressure is hydrostatic, the Boussinesq approximation is applicable, and that eddy coefficients can be employed to represent the effect of subgrid-scale motions. Vertical velocities are thus computed from the incompressibility condition, and the free surface equation results from a vertical integration of the equation for incompressibility.

158. Boundary conditions imposed consist of the inflow of fresh water with zero salinity at the head of the estuary; whereas, salinity and tidal elevations are specified at the ocean end. Unlike Hamilton, Blumberg allows for the ocean boundary to be alternately an inflow and then an outflow boundary. When inflow occurs, the salinity is set to be that of the ocean; during outflow, it is determined from an extrapolation of values inside. To prohibit the flux of salt through the surface and the bottom, the vertical salinity gradients are set to zero at those locations. The boundary condition on the velocity at the surface is determined from the wind stress. Similarly, the bottom stress determines the boundary condition at the bottom. Extrapolation from the hydraulic theory of flow in open channels allows the friction acting on a tidal current, because of the estuary's bottom, to be expressed using the quadratic law

$$T = ku|u|$$

where u is evaluated 1 m away and k depends primarily on the boundary roughness.

159. The basic finite difference grid is of the MAC-type used by Leendertse (1967). Pressure and salinity are defined at cell centers, but velocities are defined on the faces of the cells. Water surface elevations are defined on columns corresponding to cell centers. Similar to the layered approach of Leendertse, the governing equations are integrated vertically over each layer where the thickness of each layer is constant except for the top one. The top layer, of course, contains the influence of the surface gravity wave, and its thickness varies in time and space.

160. Both a horizontal and a vertical eddy viscosity coefficient as well as a horizontal and vertical diffusivity coefficient are computed. The horizontal coefficients are computed from

$$A_H = \varepsilon_H = \left(\frac{C\Delta x}{\sqrt{z}}\right)^2 \left|\frac{\partial u}{\partial x}\right|$$

where

C = adjustable constant

while the vertical coefficients are related to the Richardson number in the following manner:

$$A_v = k_1^2 z^2 \left(1 - \frac{z}{h}\right)^2 \left|\frac{\partial u}{\partial z}\right| \left(1 - \frac{R_i}{R_{i_c}}\right)^{1/2}$$

and

$$\varepsilon_v = \frac{A_v}{1 + R_i}$$

where A_v is the eddy diffusivity and ε_v is the eddy viscosity, k_1 is a constant whose value is ~0.10 and R_{i_c} is a critical Richardson number taken to be 10. It should be remembered that Blumberg's model was developed for an estuary. Therefore, the functional form of the coefficients above are probably not applicable to deep reservoirs. As was done in the 3-D quasi-static models, the eddy diffusivity is assumed large when unstable stratification develops. The salinity in the unstable layers is replaced by the averaged value of the adjacent layers.

161. The time-integration scheme is a centered difference or

leapfrog scheme, except for the diffusive and frictional terms, which are taken at the old time step. All spatial derivatives are replaced by centered differences. Thus, as with the Simons 3-D model, the finite difference scheme is almost $0(\Delta t^2, \Delta x^2)$. As previously noted, the use of centered differences in time and space results in a second order difference equation as the approximation to a first order differential equation, and the solutions at odd and even time lines tend to split. Blumberg attempts to remove this time-splitting through averaging results from three successive time steps with weights of 0.25, 0.50, and 0.25, respectively, every 25 time steps.

162. The centered difference time-integration scheme has the property of not introducing artificial horizontal diffusion and viscosity. Thus, to control nonlinear instabilities, damping must be input into the scheme. This is the major reason for incorporating the expressions previously given for the horizontal diffusivity and viscosity, A_H and ε_v , respectively.

Poseidon's 2-D Vorticity-Stream Function Model

163. There are no published reports on Poseidon's* 2-D, longitudinally and vertically dimensional, variable density model. The major reasons for noting the model's existence are first because it is the only hydrodynamic model discovered that is based on the vorticity-stream function representation of the governing equations and secondly, because of the manner in which the advection terms,

$$\frac{\partial(u\zeta)}{\partial x} + \frac{\partial(v\zeta)}{\partial y}$$

where ζ is vorticity, are numerically modeled. As noted before, the basic problem with these terms is that of achieving numerical stability without numerical diffusion. The Poseidon code uses a flux-corrected transport algorithm called SHASTA (Sharp and Smooth Transport Algorithm).

---

* Personal communication, May 1978, Personnel of Poseidon, Inc., Calif.

Fluxes are first advected according to a scheme that is stable but diffusive, e.g., the two-step Lax-Wendroff algorithm. Then the amount of numerical diffusion is computed at each grid point, and the appropriate amount of antidiffusion flux is applied to each cell, provided no new extrema are created. A discussion of SHASTA is given by Boris and Book (1973). Again it should be noted that such a model would not be applicable to a reservoir containing multiple outlets.

Slotta et al.'s 2-D NUMAC Model

164. A group directed by Slotta (Slotta et al. 1969) at Oregon State University has developed the computer model NUMAC (Nonhomogeneous Unconfined Marker and Cell) for analyzing transient, incompressible, variable density, viscous flows with a free surface. As the name implies, the model is based upon the MAC method developed by Welch et al. (1966), which uses a mixed Eulerian-Lagrangian scheme. In this scheme, the velocity and pressure are considered as Eulerian variables defined at the mesh points of a fixed grid, but the density is considered a Lagrangian variable localized to fluid particles. It appears that the major differences between NUMAC and MAC lie in NUMAC's ability to better handle inlets and outlets and in the use of the SOR technique for solving the Poisson equation for the pressure.

165. The basic Navier-Stokes equations for laminar flow written in the vertical and longitudinal directions, in the conservative form, are solved along with the conservation of mass equation. The Boussinesq approximation is not made, and thus, the density is actually solved for from a transport equation with ρ as the dependent variable. However, the incompressibility condition is still invoked in the derivation of the Poisson equation for the pressure.

166. Many different types of boundary conditions are allowed. At material boundaries, the normal component of the velocity vanishes. At a free surface, the boundary conditions are that the normal and tangential components of the stress must vanish. Two inlet velocity boundary conditions are allowed. One holds the inlet velocity constant,

while the other requires the normal derivative to vanish. The normal derivative of the density at an outlet is set to zero. Both slip and no-slip solid boundaries are allowed with the derivative boundary condition on the pressure determined from the momentum equation.

167. The finite difference scheme is basically one in which the time derivatives are replaced by forward differences and the spatial derivatives by centered differences. However, it does appear that Roache's (1972) second windward-type differencing is used in the evaluation of momentum flux terms such as $\partial(\rho uv)/\partial y$, etc. Thus, theoretically, the scheme is close to $O(\Delta t, \Delta x^2)$.

168. As noted previously, the MAC calculations are a combination of Eulerian and Lagrangian steps. The NUMAC computation cycle is summarized in the following steps:

a. Compute new densities from the mass transport equation.

b. Using new densities, solve Poisson equation for the pressure.

c. Using new densities and pressures, calculate new velocities from momentum equations.

d. Move the Lagrangian particles by use of the new velocities.

e. Calculate new densities and viscosities at the mesh points by averaging the densities and viscosities of the particles that now surround each mesh point.

f. Compare this density with the value computed in step a. If different, go to step b with these densities. If they are essentially the same, continue.

g. Recompute the pressure from the Poisson equation.

h. Recompute the velocities from the momentum equations.

i. Move the particles using velocities from step h.

j. Increment the time and go to step a.

169. Several stability criteria for this explicit scheme are presented; however, once again the basic criterion is related to the speed of a gravity wave.

170. Obviously, NUMAC, or any of the related MAC codes, is an extremely powerful numerical model for analyzing variable density fluid flows, since the model is fully convective. However, computing times

required for long-term transient problems are excessive due to the explicit time differencing plus solving a Poisson equation for the pressure. Slotta indicates that one time cycle on a (Control Data Corporation) CDC 6600 computer requires 7 sec for a problem with 800 cells and 3000 particles.

Norton, King, and Orlob's 2-D Vertical Flow FEM Model--RMA-7

171. Under a contract with the Walla Walla District of the U. S. Army Corps of Engineers, Water Resources Engineers, with Norton and King as principal investigators, developed two 2-D hydrodynamic models using the finite element method for obtaining numerical solutions of the governing flow equations (Norton, King, and Orlob 1973). One of the models is a variable density, laterally averaged model that describes the behavior of velocity, temperature, and pressure in the vertical plane.

172. The basic equations solved are the 2-D laterally averaged horizontal and vertical momentum equations along with the continuity equation reduced to the incompressibility condition as a result of the Boussinesq approximation and an energy equation written in terms of temperatures. These four equations along with an equation of state relating the fluid density to the temperature are solved for the five unknowns--u , v , T , P , and ρ .

173. The exchange of energy to the unresolvable turbulent eddies is accomplished through the use of eddy coefficients, which are treated as constants within each element but can vary from element to element. It should be noted that unlike most models, the off-diagonal terms of the eddy viscosity tensor are retained.

174. The equations are written in the nonconservative form without the usual hydrostatic approximation. Thus, the complete vertical momentum equation is retained and the model is a fully convective model.

175. The governing equations are solved by the finite element method using Galerkin's method of weighted residuals. A mixed set of basic functions is employed in the overall permutation. Quadratic functions are used for all state variables except pressure where a

linear function is used. The linear pressure function implies a constant element density, which is calculated as a function of average nodal temperatures. An implicit, Newton-Raphson computation scheme is employed to achieve a solution to the set of nonlinear equations that define the model. The resulting computer program accommodates triangular and/or quadrilateral isoparametric elements.

176. Both a bottom stress term and a wind shear term are incorporated in the bottom and top row of elements, respectively. The use of the isoparametric formulation with interelement geometric slope continuity allows the user to specify slip or parallel boundary flows. In addition, no-slip walls can be easily handled since zero values of u and v would be inserted at the proper nodes of boundary elements. The surface heat flux at the air-water interface is computed through the use of the coefficient of surface heat exchange and local equilibrium temperature as calculated from meteorological data.

177. A recent version of the model accounts for the movement of the free surface, although in a very limited fashion, since the movement must be stipulated by the user. The free surface pressure boundary condition is based upon the assumption of a locally flat surface so that the pressure boundary condition is for atmospheric pressure. The model developers are currently incorporating into the model a procedure for internally computing the location of the free surface utilizing the atmospheric pressure boundary condition.

178. As noted in previous discussions, finite element models for transient problems require large computing times. Therefore, such models may not be applicable to the simulation of the natural stratification cycle of a reservoir for economic reasons.

179. It might be noted that although laterally averaged models provide a better representation of real reservoirs than pure 2-D models, the momentum flux through an outlet at the dam is not accurately modeled. In the horizontal momentum equation, the horizontal advection of momentum is represented by $\rho_o \partial(\tilde{\tilde{u}}^2 B)/\partial x$, where $\tilde{\tilde{u}}$ is the laterally averaged velocity in the x direction. In actuality, the momentum flux passing a cross section is not $\rho_o \tilde{\tilde{u}}^2 B$, but instead is given by the integral

$$\rho_o \int_o^B \bar{u}^2 dy$$

Using a procedure borrowed from open channel hydraulics, one can set

$$\rho_o \int_o^B \bar{u}^2 \, dy = \beta \rho_o \tilde{u}^2 B$$

where β is referred to as a "momentum correction factor." For the plan and side view of a reservoir near the dam, the u-velocity profile would be

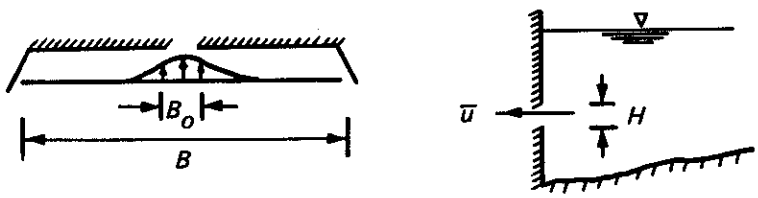

The discharge Q is assumed known and is equal to $\bar{u}B_oH = \tilde{u}BH$, where H is the height of opening at the dam. Thus, $\tilde{u} = Q/BH$ and $\bar{u} = Q/B_oH$. Therefore,

$$\int_o^B \left(\frac{Q}{B_oH}\right)^2 dy = \beta\left(\frac{Q}{BH}\right)^2 B$$

and, if one writes the integral as a sum of integrals over B_o and $(B-B_o)$, then

$$\left(\frac{Q}{B_oH}\right)^2 B_o = \beta\left(\frac{Q}{BH}\right)^2 B$$

since the integral over B is zero except on B_o. The above can then be solved for β to yield

$$\beta = \frac{B}{B_o}$$

Thus, since $B > B_o$, β is much larger than 1.0 near the dam and decreases in some manner with the x coordinate upstream of the dam until

a value of 1.0 is reached. However, the usual procedure is to assume a value of 1.0 everywhere, in which case the flux of momentum at the downstream boundary is not properly modeled.

Thompson's 2-D Model--WESSEL

180. This is a laterally averaged 2-D model that is currently being developed to assist the Corps in selective withdrawal studies. Because of the concern for the quality of water downstream of reservoirs, there is a growing effort to control the quality of water released from reservoirs. The concept of controlling the quality released from a density-stratified impoundment is called "selective withdrawal." Because the quality of water and its density can vary from the surface to the bottom of a lake, it is often possible to selectively withdraw the most desirable qualities. A basic problem is to determine before construction whether the design of an outlet will provide the desired selective withdrawal characteristics.

181. An empirical method developed by Bohan and Grace (1969) can be utilized for selective withdrawal predictions for simplified outlet and approach geometries. However, for complex geometries, physical and/or mathematical models are required.

182. Thompson's model utilizes the concept of boundary-fitted coordinates to obtain a solution of the governing flow equations on a nonorthogonal curvilinear coordinate system. The coordinate system is generated from the elliptic generating system

$$\xi_{xx} + \xi_{yy} = P$$

$$\eta_{xx} + \eta_{yy} = Q$$

where P and Q are functions chosen to cause the ξ, η coordinate lines to concentrate as desired. With one coordinate being specified as constant on the boundaries and a distribution of the other specified, a coordinate system that follows all boundaries, no matter how

irregular, results. A rather detailed discussion of the method and its possible application to hydrodynamic problems is presented by Johnson and Thompson (1978). In addition, an extensive list of references describing Thompson's work with the technique is presented in the work cited.

183. The next step is the development of a numerical model to solve the governing fluid flow equations on the coordinate system computed above. Such a model will be able to accurately model the influence of boundary geometry on the developing flow.

184. The basic laterally averaged 2-D equations solved in Thompson's model are the Navier-Stokes equations, mass conservation, energy conservation, and an equation of state relating temperature and density. These equations are transformed to the ξ , η system in a fully geometrically conservative form such that the finite difference representation is equivalent to the discrete element method. Essentially no assumptions other than assuming an incompressible fluid are applied to the basic equations; e.g., the Boussinesq approximation is not made and the model is fully convective with the vertical velocity obtained from the full vertical momentum equation. In the vicinity of outlets, vertical accelerations may become large and a solution of the full vertical momentum equation is probably required.

185. The pressure is computed using Chorin's method. This method is based upon the concept that if a fluid is incompressible, the function of the pressure is to insure that the velocity field satisfies the incompressibility condition, i.e., $\nabla \cdot \vec{v} = 0$. An iterative algorithm for the pressure field is thus set up such that

$$\left(p^n\right)_{ij}^{s+1} = \left(p^n\right)_{ij}^{s} - \alpha\left(\nabla \cdot \vec{v}^{n+1}\right)_{ij}^{s}$$

where the pressure field at time step n is determined such that the velocity field at time step $n + 1$ will satisfy incompressibility. The advantage of Chorin's method over the use of a Poisson equation is that only velocities are required on the boundaries, rather than pressure and/or velocity derivatives.

186. The finite difference grid is such that both velocity components are defined at cell corners, while the pressure, temperature, and density are defined at the center of a cell. It should be noted that the transformation of the equations into the boundary-fitted coordinate system is such that all computations are performed on a rectangular (ξ , η) grid with square grid mesh.

187. The model being developed will be extremely general so that any number of inlets and/or outlets can lie on any boundary. In addition, any number of bodies can lie in the interior of the field, with a constant coordinate line following each body. Boundary conditions can be either slip or no-slip on solid boundaries, with the option of either specifying wall temperatures or the heat transfer rate at such boundaries.

188. The basic finite difference scheme utilizes second order backward differences to replace time derivatives and centered differences to replace spatial derivatives. The model will allow the option, however, of selecting windward differencing of advective terms. The finite difference scheme is thus fully implicit and of $0(\Delta t^2, \Delta \xi^2)$ or almost $0(\Delta t^2, \Delta \xi^2)$, depending upon whether Roache's (1972) first or second differencing is employed. The SOR iterative method with a variable optimum acceleration parameter field is utilized to obtain a solution.

189. With such an unsteady, fully convective, variable density, free surface model that models the flow phenomena in a natural coordinate system that fits the boundaries of the field, a wide range of hydraulic phenomena can be accurately simulated. However, due to the fully implicit nature of the solution and the resulting iterative solution technique, the computing time required for long-term simulations will probably be large. For selective withdrawal studies in which only the steady-state solution is sought, the computing cost should not be a major factor.

Roberts and Street's 2-D Reservoir Model

190. Roberts and Street's (1975) variable density model is quite

similar to Spraggs and Street's (1975) 3-D model with the major exceptions being the dropping of the lateral dimension and the assumption of a hydrostatic pressure distribution, eliminating the need for a separate pressure equation and the attendant costly solution procedure. The basic finite difference grid, solution technique, and eddy viscosity model are all essentially the same as employed in the 3-D model, but are now reduced to two dimensions. The model is thus a pure 2-D vertical-longitudinal model in which a varying width is not allowed.

191. With the hydrostatic pressure assumption, the vertical velocity is solved from the condition of incompressibility, and a large vertical diffusivity is invoked to simulate convective overturning, which cannot be dealt with explicitly. Unlike some of the hydrostatic models that integrate the incompressibility equation over the vertical to yield an equation for the free surface, Roberts and Street determine the free surface directly from the kinematic boundary condition at the surface. As in the 3-D Spraggs and Street model, an implicit solution of the surface equation is obtained. Once again, however, because of the lack of coupling between the velocity field and the free surface at time level $n + 1$, the Courant condition is still the controlling stability criterion.

192. Limited-slip solid boundaries are assumed. The velocity orthogonal to the boundary is set to zero, but the tangential velocity is defined by the Chezy-Manning formula for boundary shear stress such that the proper velocity profile near the boundary can be achieved. Forced flow boundaries, of course, require the specification of the velocity. At solid boundaries, temperature gradients are set to zero to model an adiabatic wall.

193. At the free surface, the velocity boundary condition is determined by the wind stress, and temperatures are determined by a surface heat-exchange equation.

194. The basic finite difference scheme for the internal flow utilizes forward differencing in time and centered differencing in space, except for the advective terms where Roache's (1972) second

upwind differencing is utilized. The overall solution is, thus, almost of $O(\Delta t, \Delta x^2)$.

Waldrop and Farmer's TVA 2-D Reservoir Model

195. Waldrop and Farmer's (1976) model is an explicit laterally averaged hydrodynamic model for analyzing flows in stratified reservoirs or long river reaches. The model is designed to accommodate hourly changes in boundary conditions consisting of dam discharges, tributary inflow conditions, steam plant intake and discharge conditions, river inflow rates and temperatures, meteorology and wind shear.

196. Very little detailed published material on the model exists, although Waldrop and Walter Harper of TVA are currently in the process of writing such a report. It should be noted that Harper has been responsible for most of the coding and testing of the model; thus, the model should probably be called the Waldrop-Harper model. From the limited material available, it appears that the nonconservative form of the laterally averaged fluid flow equations and the temperature transport equation, in which the Boussinesq approximation and the hydrostatic pressure assumption have been made, are solved. The effect of turbulence is included through eddy coefficients, which are modeled by using a mixing length theory as in Waldrop and Tatom's 3-D model. The retarding effect of stratification upon vertical mixing is included by damping the vertical eddy coefficients as a function of the local Richardson number.

197. Free surface boundary conditions on the temperature and velocity are provided by the specification of the surface heat flux and the wind shear, respectively. The surface heat flux q_s is prescribed as a quadratic function of the temperature, given as

$$q_s = a(t)*T_s^2 + b(t)*T_s + C(t)$$

where a , b , and c are coefficients dependent upon meteorological conditions, and T_s is the surface temperature; wind shear is given by

$$T_{WIND} = C*(U_{WIND} - U_s)^{4/3}$$

where C is a coefficient, U_{WIND} is the wind velocity, and U_s is the surface water velocity.

198. The basic finite difference grid appears to be a 2-D version of the 3-D model, and thus, solid boundaries are treated as in that model. In other words, slip boundary conditions are assumed at vertical walls; whereas, a limited-slip condition is applied at the bottom by using a logarithmic profile to set the velocity near the bottom. With such a technique, the bottom never actually lies on a grid point.

199. With the same basic finite difference scheme as employed in the 3-D model; i.e., a form of forward differencing in time and centered differencing in space, except for Roache's (1972) first windward differencing of advective terms, the basic scheme is probably of $O(\Delta t, \Delta x)$.

Edinger and Buchak's Laterally Averaged Reservoir Model--LARM

200. Edinger and Buchak's (1979) LARM (Laterally Averaged Reservoir Model) is a numerically efficient 2-D laterally averaged free surface, variable density, heat-conducting model developed for the Ohio River Division, U. S. Army Corps of Engineers, for use in simulating flows in stratified reservoirs. As noted by Edinger and Buchak, "Such a model is needed in long, narrow reservoirs that exhibit density flow, epilimnetic wedges and titled isotherms and in deep power plant discharge canals with bottom intrusion of cold water and backwater density wedges from such discharges to rivers."

201. In the initial development of the model, it was anticipated that its primary use would be for long-term simulations extending over a natural stratification cycle of a reservoir. Thus, it was deemed necessary to develop a solution technique that would allow for time steps significantly larger than those imposed by the free surface gravity wave. To allow this, finite difference techniques have been employed to solve the governing equations such that the water surface

elevations are computed implicitly. The velocity components in the longitudinal and vertical directions are then computed explicitly, and finally the temperature field is computed implicitly. The density is then, of course, computed from an equation of state. Unlike the Roberts and Street (1975) model, which also implicitly computes the water surface, Edinger and Buchak's model couples the internal flow and the free surface, and thus, the scheme has been found to be stable so long as the volume of water entering a finite difference cell within a time step is less than the volume of the cell.

202. Edinger and Buchak utilize the layer-averaged concept of Leendertse and Simons. The governing equations that are solved are thus laterally and layer-averaged 2-D equations with layer-averaged variables as the dependent variables. The equations are written in the conservative form with the Boussinesq and hydrostatic approximations. In addition, eddy coefficients are utilized to model the influence of turbulence.

203. The horizontal coefficients of eddy viscosity and eddy diffusivity are assumed to be constant; whereas, in a recent development, the vertical eddy diffusivity and eddy viscosity--related to the internal friction coefficient that results from the layer averaging and replaces vertical viscous terms as related to second derivatives--are allowed to be dependent upon the Richardson number. The form of this functional dependence is

$$A_v = A_{v_o}(1 + 3.33R_i)^{-3/2}$$

$$\varepsilon_v = \varepsilon_{v_o}(1 + 10R_i)^{-1/2}$$

Unstable stratification is modeled by allowing ε_v to increase to the diffusive stability limit of $\Delta z^2/2\Delta t$ when $R_i < 0$.

204. As in other hydrostatic models, the vertical component of the velocity is obtained from the incompressibility equation, with the solution beginning at the bottom and progressing up the column of

layers. An equation for the water surface elevation is then obtained by summing the layer-averaged incompressibility equation over the water column. This equation takes the form

$$\frac{\partial(\zeta B)}{\partial t} = \sum_{\text{layers}} \frac{\partial(uBH)}{\partial x}$$

where ζ is the deviation from the top of the top layer of fluid, positive downward. Edinger and Buchak then replace the time derivative by a backward difference to yield an implicit solution for ζ. However, the velocities are unknown at the $n + 1$ level. This problem is overcome in the following manner. The horizontal momentum equation takes the form

$$\frac{\partial(uBH)}{\partial t} - gBH \frac{\partial \zeta}{\partial x} = F$$

in which a forward time differencing is used in relation to all the terms comprising F, while the $\partial\zeta/\partial x$ term is taken implicitly, i.e., at the $n + 1$ time step. The expression for $(uBH)^{n+1}$ from the momentum equation is then substituted into the finite difference form of the free surface equation. The resulting difference equation then contains the unknowns ζ_{i+1}^{n+1}, ζ_i^{n+1}, ζ_{i-1}^{n+1}, i.e., a tridiagonal system results, which can be efficiently solved by the Thomas algorithm.

205. With such a coupling of the internal flow and the free surface computations, the Courant stability criterion is removed. The time step is now limited by the internal flow speed, plus perhaps diffusive criteria, rather than the speed of the surface gravity wave. It is the removal of the Courant condition that makes the Edinger and Buchak (1979) model so attractive with regard to long-term simulations of stratified reservoirs.

206. With the free surface elevations computed at the $n + 1$ time step, the horizontal velocity component is then computed explicitly, followed by an explicit computation of the vertical component. The temperature is then computed from its transport equation, using the new velocities. This, however, now requires an implicit solution

for the temperature since if the velocity in the advective term is taken at the (n+1) level, the temperature must be taken at that level also; i.e., terms such as $\partial(uBHT)/\partial x$ are taken completely at the new time level. To avoid having a 2-D implicit computation, which would require either an iterative solution or perhaps the use of an ADI scheme, the horizontal diffusive term is taken at the $n + 1$ time level, but the vertical diffusive term is taken at the old or n time level. The resulting difference equation takes a tridiagonal form also and thus is solved in the same manner as is the free surface equation.

207. Spatial derivatives are replaced by centered differences in all terms, except the advective terms in the temperature equation where Roache's (1972) first windward differencing is used. In addition, in computer experimentation with the model, it was concluded that windward differencing is also required in the momentum advective terms in cells adjacent to forced outlets. This will be discussed later in connection with application of the model to the GRH flume. Since the windward differencing is Roache's first kind in which simple forward or backward differencing is utilized, it appears the solution scheme is $0(\Delta t, \Delta x)$. As previously noted, such a scheme preserves the transportive property but not the conservative property and in addition is only of the first order. If Roache's second upwind differencing had been employed, the resulting scheme would be almost $0(\Delta t, \Delta x^2)$, and both the transportive and conservative properties would be preserved. It might be noted that by solving the temperature equation implicitly, the time step limit of $W/\Delta z$ that can be more severe than $u/\Delta x$ has been removed.

208. Boundary stresses at the surface and the bottom are incorporated directly into the layer-averaged equations through the following expressions:

$$\tau_{WIND} = \frac{C^*}{\rho} \rho_a W_a^2 \cos \phi$$

and

$$\tau_b = \frac{g}{C^2} u|u|$$

where

C_* = resistance coefficient (2.6×10^{-3})

ρ_a = air density ($1.2\ kg/m^3$)

W_a = wind speed at 10-m height ($msec^{-1}$)

ϕ = angle between wind and reservoir axis

C = Chezy coefficient ($m^{1/2}/sec$)

209. With the use of the layer-averaged approach, the boundary stresses are incorporated directly as terms in the equations, and boundary conditions on the tangential velocity at the bottom cannot be prescribed. In addition, with the MAC-type grid employed and with the vertical velocity determined from the incompressibility condition, no specification of the tangential velocity at a vertical wall is allowed. Of course, at all solid boundaries, the normal component of velocity is set to zero. In addition, all eddy coefficients are set to zero at solid boundaries to prevent heat transfer at such boundaries.

210. The net rate of surface heat exchange is expressed by:

$$h_n = -CSHE\ (T_s - ET)$$

where CSHE and ET are dependent upon shortwave solar radiation, air temperature, dew point temperature and wind speed.

PART VI: APPLICATION OF SELECTED MODELS TO THE GRH FLUME

211. Two of the 3-D models and three of the 2-D models have been applied to a bottom density current problem in the Generalized Reservoir Hydrodynamics (GRH) flume at WES. In addition, before this report was published Arsev Eraslan provided results from application of the automatic 2-D version of his general 3-D model.* The 3-D models were that of Spraggs and Street (1975) and the Waldrop-Tatom (1976) model; while the 2-D models were LARM, the TVA model, and the RMA-7 finite element model. The two attempts at a 3-D simulation, as well as the TVA's 2-D simulation, were made by the respective model developers at the request of WES, with the Waldrop-Tatom simulation being made by Tatom at WES on WES's Texas Instrument-Advanced Scientific Computer (TI-ASC) computer. The simulations with LARM were conducted by Edinger and Buchak on the CDC 7600 computer located at Boeing in Seattle, Wash. In addition, WES personnel have made similar computations on the CYBER 176 located at Kirtland Air Force Base, N. Mex. The application of the finite element model RMA-7 was made by Bob MacArthur at the Hydrologic Engineering Center (HEC) on CDC equipment located at Berkeley University and on a Prince 550 minicomputer located in Lafayette, Calif.

212. The primary reason for application of the models to the bottom density flow problem was to provide an assessment of relative economy of the more promising models and their ability to simulate a real problem that commonly occurs in reservoirs, whether it be as the result of a coldwater inflow or the plunging of a sediment-laden stream. With an application to a laboratory flume, test conditions could be accurately controlled and temperature and velocity profiles readily obtained. Although temperature data are available, as far as is known, a detailed set of reservoir field data including velocities and results from dye tracer tests does not exist. It seems reasonable to believe that if a mathematical model can accurately simulate laboratory

---

* Personal communication, March 1980, Arsev Eraslan, Chief Scientist, Hennington, Durham, and Richardson, Knoxville, Tenn.

conditions, the expectation of reasonable field applications is justified. This is true because the only scaling effects in the mathematical models is in the specification of the eddy coefficients. Thus, although an accurate simulation of a laboratory test may not justify a quantitative confidence in the ability of the model to yield similar accuracy in the field, it does demonstrate qualitatively the model's ability to simulate basic flow phenomena.

Description of GRH Flume and Test Conditions

213. A photograph of the GRH flume is provided in Figure 6. The flume is 24.38 m long with a 0.91-m × 0.91-m cross section at the downstream end. The cross section at the upstream end is 0.30 m × 0.30 m

Figure 6. The Generalized Reservoir Hydrodynamics (GRH) flume

and linearly grows in width over the first 6.10 m to a cross section 0.30 m deep and 0.91 m wide. The bottom of the flume is horizontal for the first 6.10 m and then drops a total of 0.61 m linearly over the final 18.29 m of the flume. Both plan and side views are given in Figure 7. The water in the flume was at rest and homogeneous at the initiation of the test, with the temperature being 70.6°F. Cold water was input at 0.46 m from the upstream end at a temperature of 62.0°F. A baffle restricted the cold water to enter over about the bottom 0.15 m of the cross section. The inflow rate was 0.00063 m^3/sec with the outflow rate at the downstream end being the same. The outflow was removed from a port with a 2.54-cm diameter located 0.15 m above the bottom of the flume and 0.46 m from either side. Thus, as previously discussed, the 2-D laterally averaged models will not accurately model the momentum flux from the system. In fact, neither will a 3-D model unless the lateral and vertical dimensions of a cell are of the same size as the port.

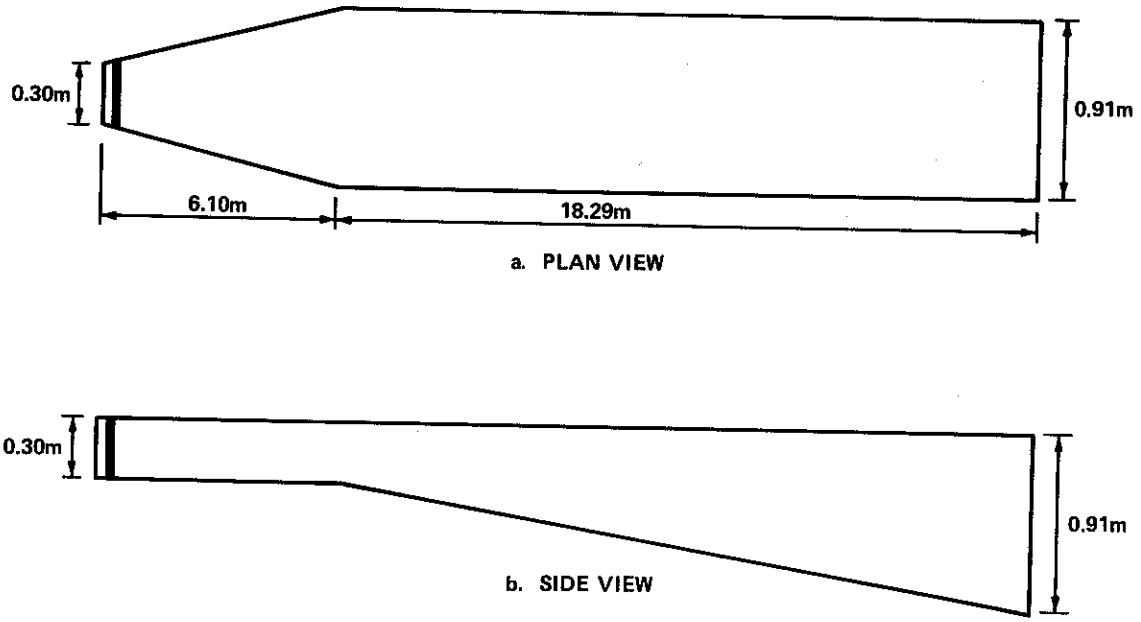

Figure 7. Schematic of GRH flume

Observed Flow Phenomena

214. The coldwater input was dyed for easy visual observation. The basic flow phenomena that developed was the classical density

underflow discussed by Harleman (1966). From a visual observation, the depth of the darkest or most dense fluid appeared to be about 7.5 cm with an overlying intermediate shade of about 5.0 cm and above this a much lighter shade of perhaps another 7.0 to 10.0 cm. The use of dye streaks to determine velocity profiles quickly revealed a reverse flow pattern above the density underflow. An example is presented in Figure 8.

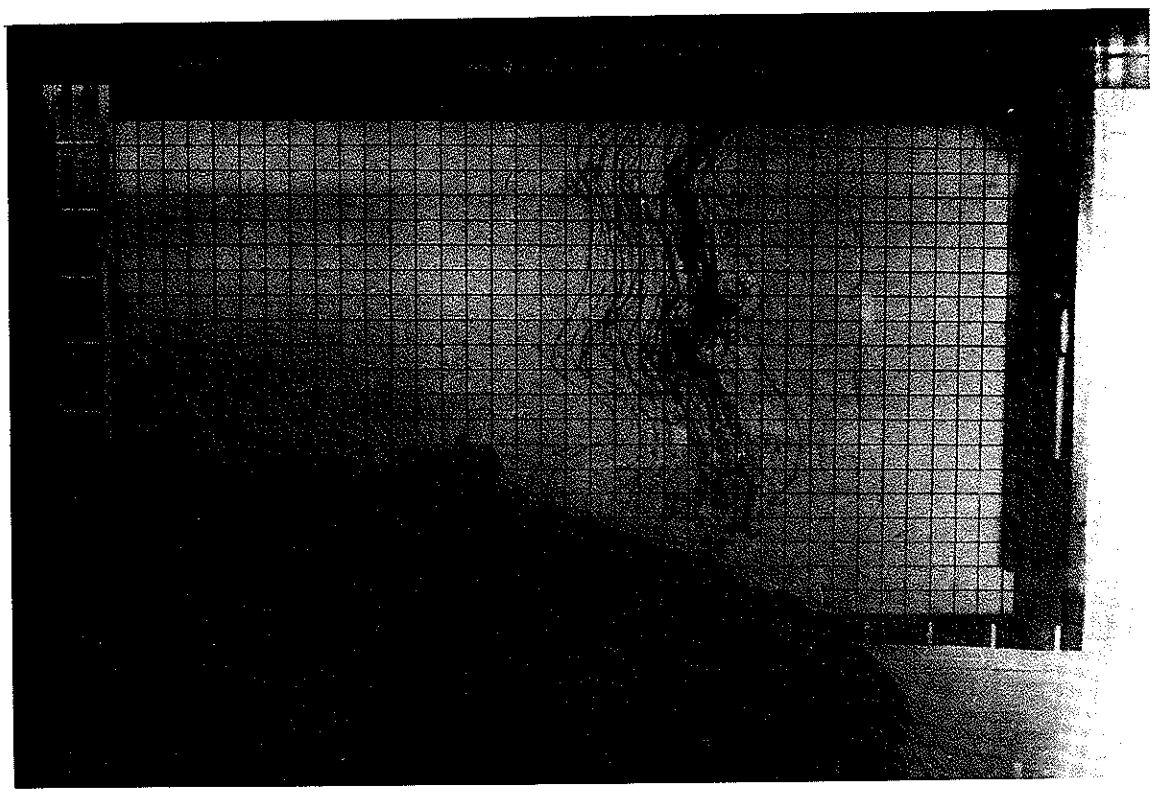

Figure 8. GRH flume simulation of an underflow density current

215. From a visual observation of the phenomena, it was concluded that the relatively smooth flow was probably in the laminar flow range. However, the Reynolds number based upon a density underflow height of 7.5 cm, an average velocity of 0.022 m/sec based upon the time required for the underflow to reach the downstream end, and a molecular viscosity of water of 1.5×10^{-6} m^2/sec, has a value of 1140. Harleman (1966) indicates a value of 1000 is the critical Reynolds number for turbulent flow. Thus the flow is probably in the transition zone between laminar

and turbulent flow, rather than being completely laminar.

216. Using Harleman's equation for the average velocity of a laminar density underflow,

$$\overline{U} = 0.375\ R_e^{1/2} \left(\frac{\Delta\rho}{\rho}\ h_{DF} S\right)^{1/2}$$

where

h_{DF} = height of density underflow, ft
S = slope
R_e = Reynolds number
$\Delta\rho/\rho$ = 0.001121

a value of $\overline{U} = 0.012$ m/sec is obtained. If the equation for the average velocity of a turbulent density underflow is used, i.e.,

$$\overline{U} = \sqrt{8\ \frac{\Delta\rho}{\rho}\ \frac{h_{DF}\ S}{f(1+\alpha)}}$$

where f, the nondimensional friction factor, is taken as 0.003, corresponding to a Chezy value of 55 $m^{1/2}$/sec, and as suggested by Harleman $\alpha = 0.43$; a value of $\overline{U} = 0.04$ m/sec is computed.

Application of Three-Dimensional Models

217. The flow in the flume is essentially a two-dimensional flow, except, of course, in the vicinity of the outlet. However, as an aid in the assessment of 3-D models, an attempt at applying both the Spraggs and Street (1975) and the nonhydrostatic version of the Waldrop-Tatom (1976) models to the coldwater inflow problem has been made. As discussed below, neither of these attempts was very successful.

Application of Spraggs and Street's THERMAC

218. Dr. Lynn Spraggs at McGill University made an application of THERMAC with the computing facilities available to him in Montreal,

Canada.* After much investigation without success into the use of time steps larger than that allowed by the Courant condition, Spraggs concluded that using the existing 3-D THERMAC model to simulate the flow in the flume was not economically feasible. His work with the larger time steps included different schemes for temperature acceleration, rigid-lid approximations and differential time-stepping. His estimate for simulating 30 min of real time in the flume is 25 to 40 hr of CPU (central processing unit) time on a CDC 7600. Therefore, it is obvious that numerical schemes that allow for much larger time steps must be devised before an explicit 3-D model such as THERMAC can be economically applied to relatively long-term reservoir simulations.

219. Spraggs was able to simulate only 600 sec of the flume problem. The computed temperature field at 549 sec is presented in Figure 9.

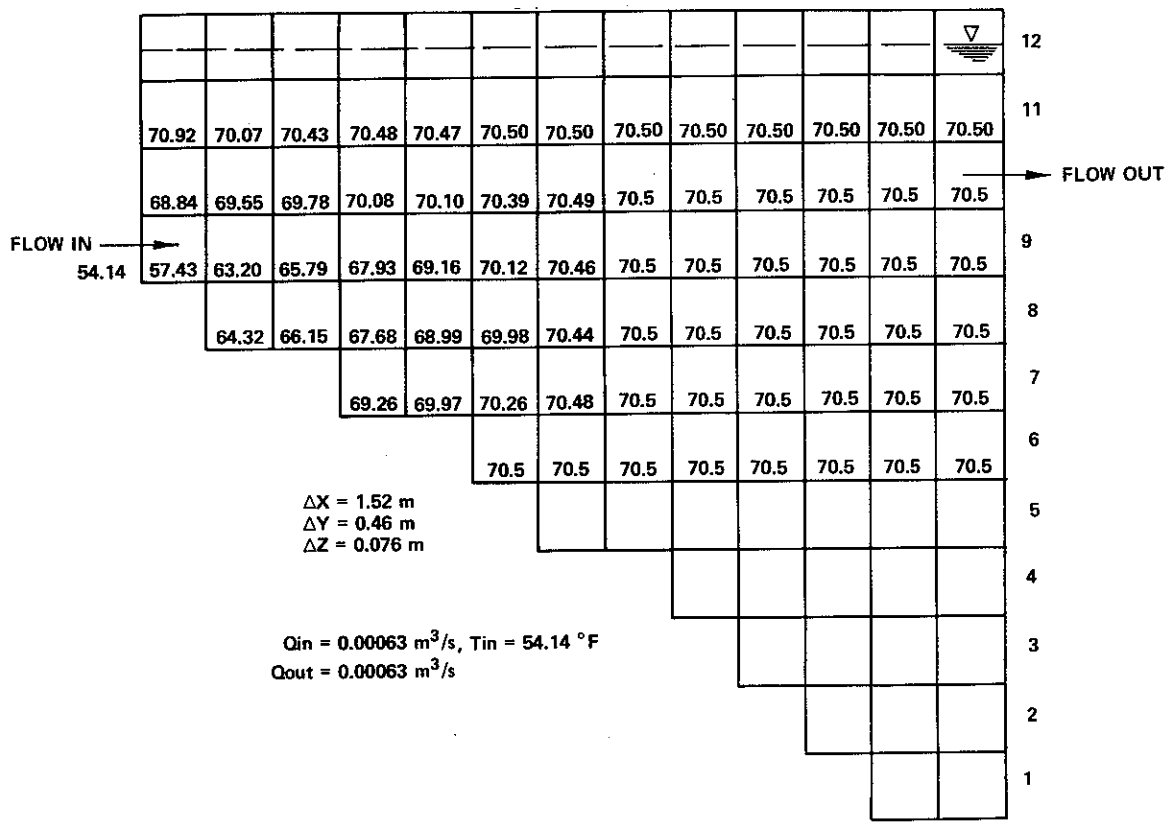

Figure 9. THERMAC Model results after 549 sec, cooled jet

* Personal communication, November 1979, Lynn Spraggs, McGill University, Montreal, Canada.

As can be seen, the simulation was conducted with outflow from the top rather than the bottom. Spraggs indicates that the reason for the temperatures of the cells at level 11 being greater than 70.6°F is that the simulation is unstable at the surface and continuity is not being conserved. It should be noted that in THERMAC the unstable stratification resulting from the stair-stepping effect at the bottom is handled in a fully convective manner, since the complete vertical momentum equation is retained and buoyancy effects are thus convectively modeled.

220. Spraggs also made an additional simulation with a heated bottom inflow. Resulting temperatures are presented in Figure 10. The simulation shows that the model seems to be performing correctly. However, a much longer simulation time is required before definitive conclusions can be drawn.

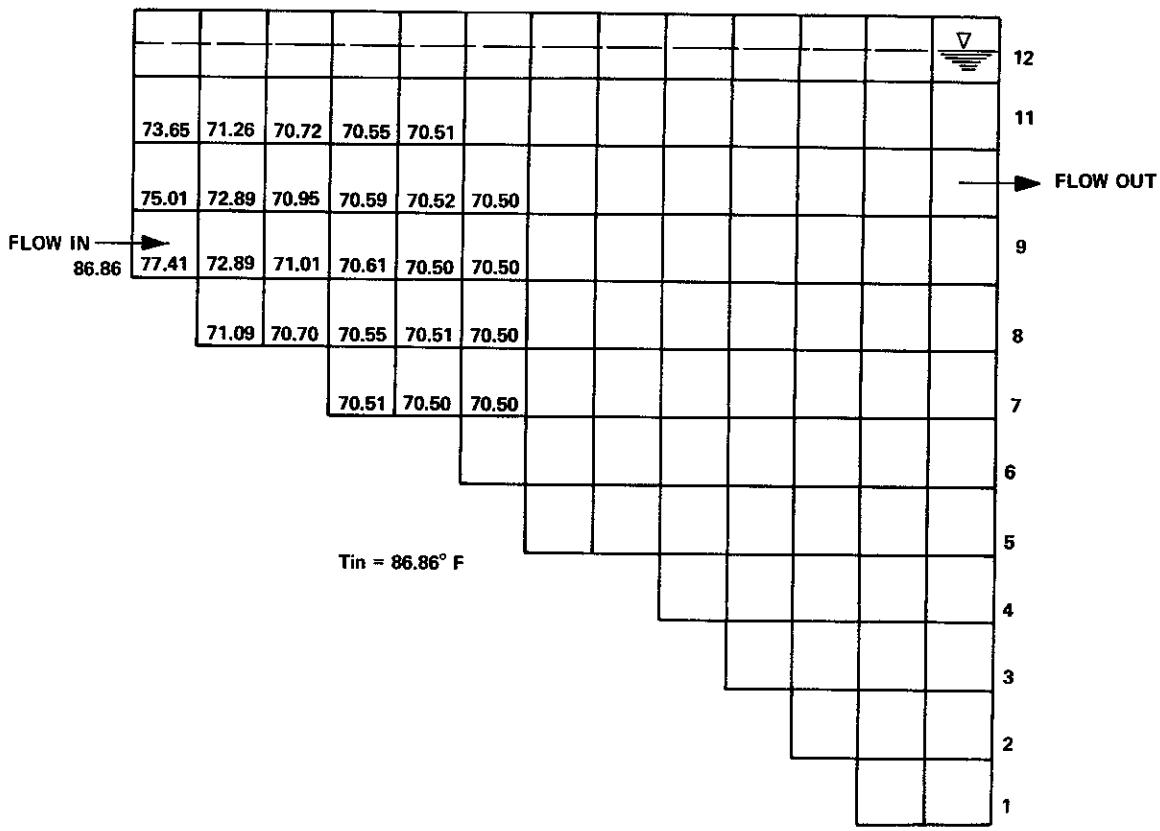

Figure 10. THERMAC Model results, heated jet

Application of
Waldrop-Tatom 3-D PLUME

221. As previously noted, the application of the nonhydrostatic version of the Waldrop-Tatom model to the density underflow problem in the GRH flume was made by Tatom and Smith (1979a) on the TI ASC computer located at WES.

222. The numerical schematization of the flume is illustrated in Figure 11. As shown, the varying width at the upstream end is modeled with three regions, each with a constant width. The axis of the flume is considered to be a plane of symmetry so that only half of the flume in the lateral direction is modeled. As can be seen from Figure 11, the bottom never falls on a grid point, and solid walls are assumed to lie halfway between the last two rows of points. Variable grid spacing in all three dimensions is allowed in the model for extra flexibility. Very little documentation of the code has been published.

223. Initially, it was realized that excessive computing time would be required if the time step was restricted by the Courant condition. With a lateral spatial dimension of 7.62 cm and a maximum depth of 0.91 m, the Courant criterion restricts the time step to be less than approximately 0.025 sec. Therefore, the initial decision was made to model the problem using a rigid-lid assumption to allow for larger time steps. Tatom incorporated this by forcing the water surface to remain at its initial level and specifying a derivative boundary condition at the surface on the dynamic pressure. The results did not resemble the density underflow observed in the flume. Basically, the coldwater inflow tended to spread over the complete depth of the flume and no flow reversal was computed.

224. It was then decided that the rigid-lid assumption was not appropriate, and the derivative pressure boundary condition was replaced with a pressure boundary condition that corresponded to a free surface. Actually the surface was allowed to be free only in the longitudinal direction; i.e., no transverse variations were allowed. Applying the Courant condition only to the longitudinal direction gives a stability restriction such that the time step must be less than about 0.50 sec. A

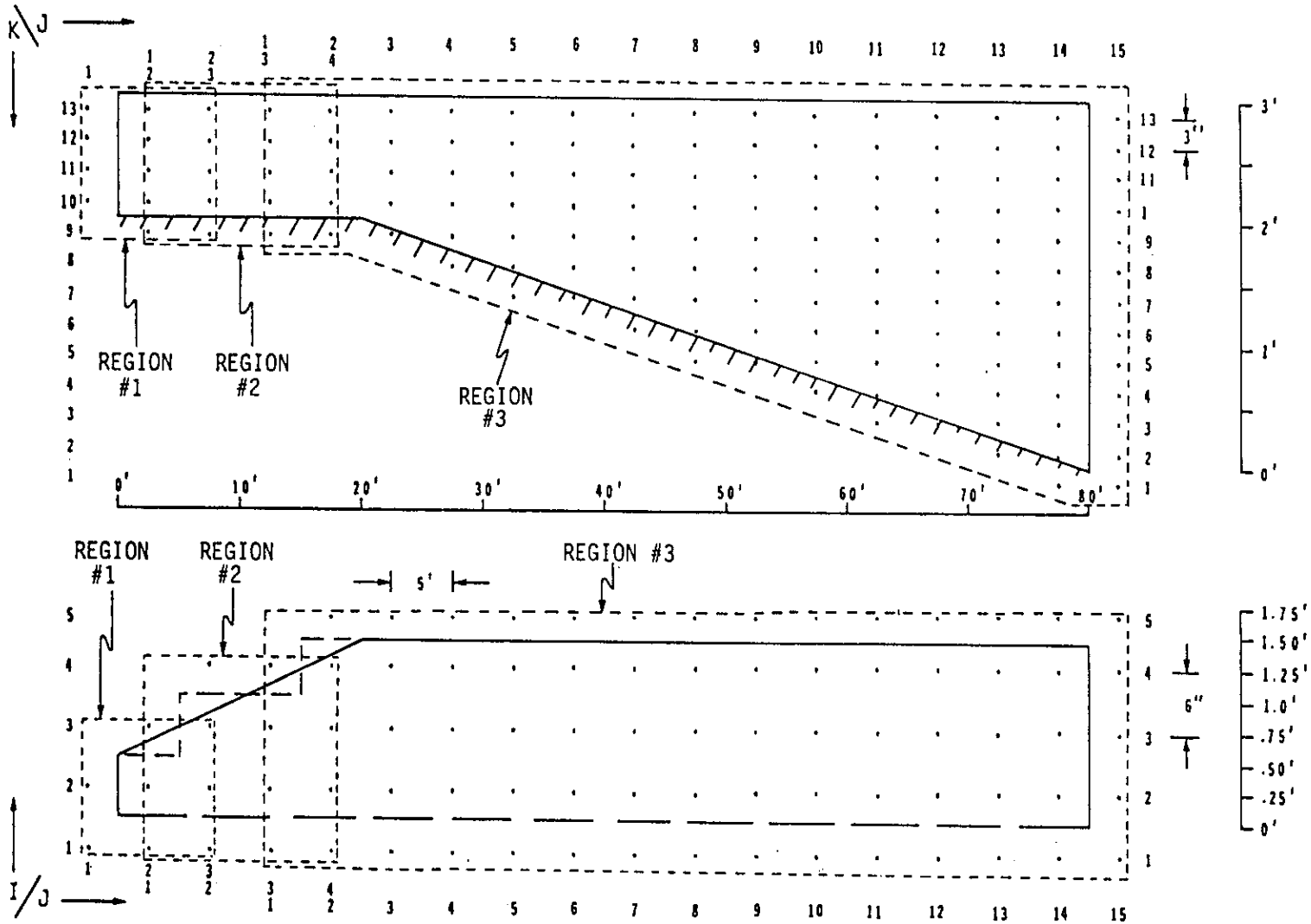

Figure 11. Three-dimensional grid system

time step one-tenth of this, i.e., 0.05 sec, was then employed. With the problem set up in this fashion, there still was no real improvement in the computed flow field. In addition, the computing time was excessive. Approximately 12 to 15 hr of CPU time on the TI ASC computer would have been required to simulate 30 min of real time in the flume.

225. Various portions of the code were investigated in an attempt to resolve the inability of the model to properly simulate the density underflow; e.g., molecular values of the eddy coefficients corresponding to laminar flow were used instead of the turbulent open channel coefficient model, differencing of the convective terms near the bottom was changed, and the pressure boundary condition at the surface was modified. The first two changes above made little or no difference. When the pressure boundary condition was changed such that the dynamic pressure at the first row of grid points inside the fluid was set to zero, some improvement was noted. A slight flow reversal was computed above the density underflow. However, the temperature of the water near the bottom was too high and the underflow moved much too slowly.

226. At this point, Tatom decided again to invoke the complete rigid-lid assumption to allow for a much larger time step but to retain the zero dynamic pressure condition at the surface. Results from this run and a list of input parameters are presented in Appendix A. The general conclusion is that the density underflow is still not properly simulated. As can be seen from the computed results, very little flow reversal is computed, and the computed flow moves much more slowly than observed in the flume. Only about 18-19 min is required for the density underflow to traverse the complete length of the flume, i.e., 23.93 m, but the model indicates a travel distance of only approximately 9.14 m in 33 min. Since funding provided for this application was limited, the reason for the inability of the model to properly compute the density underflow has not been determined. It should be noted that in a mathematical sense a Dirichlet-type boundary condition, i.e., setting the dynamic pressure equal to zero at the surface, is not allowed when imposing the rigid-lid approximation.

227. As described in Tatom and Smith (1979b) in an attempt to

reduce the CPU time required by 3-D PLUME, Tatom and Smith recoded portions of the model to better utilize the vector features of the ASC computer. From the results presented in Appendix B, it can be seen that this effort resulted in a 56-percent reduction in CPU time over the original version of the model that utilized the automated vector features of the machine.

Application of Two-Dimensional Models

Application of Edinger and Buchak's LARM

228. Because the Corps funded the initial development of LARM, an early version of the basic computer code was available for computer experimentation by WES personnel. During this experimentation, several general changes were made to LARM. These centered around making the model more general in the specification of inflows and outflows.

229. During the application of LARM to the GRH flume, as well as in the computer experimentation, it was observed that a common occurrence at the downstream boundary in front of an outlet was that of a flow reversal. Various steps were taken to try to alleviate this problem, including an attempt to incorporate a momentum correction factor and a momentum sink term under the assumption that perhaps the improper modeling of the momentum flux through an outlet was causing the problem. In addition, in an effort to create a larger pressure gradient near the outlet to force the flow in the proper direction, the hydrostatic pressure was decreased by $1/2\ \rho\ u^2$, i.e., the dynamic pressure. None of these attempts proved successful.

230. Finally it was discovered that the use of centered differences in the convective terms of the x-momentum equation is unacceptable near a forced outlet. This is related to the fact that centered differences do not possess the transportive property. This is illustrated by the problem below in which the initial flow field is stationary and a forced outflow with velocity U_o is prescribed.

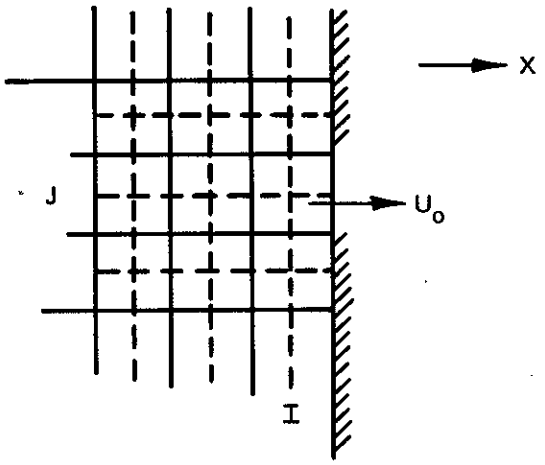

Using centered spatial derivatives and a forward time derivative, the x-velocity at time $t = \Delta t$ at $(i-1/2,j)$ is

$$U_{i-1/2,j}^{t=\Delta t} = U_{i-1/2,j}^{t=0} - \frac{\Delta t}{\Delta X}\left[U_{i,j}^2 - U_{i-1,j}^2\right]^{t=0} + F^{t=0}$$

With the flow field at $t = 0$ stationary,

$$U_{i-1/2,j}^{t=\Delta t} = 0 - \frac{\Delta t}{\Delta X}\left[\left(\frac{0 + U_o}{2}\right)^2 - 0\right] + 0$$

or, the initial computation for the velocity in front of the outlet yields a flow reversal, i.e.,

$$U_{i-1/2,j}^{t=\Delta t} = -\frac{\Delta t}{4\Delta X} U_o^2$$

As noted by Spraggs and Street (1975), the use of windward differencing near an outlet corrects the problem. Therefore, the original centered difference representation of the horizontal advective term $\partial(u^2BH)/\partial x$ has been replaced with a one-sided difference near an outlet.

231. In the initial application of LARM to the GRH flume by WES personnel, it was observed that the coldwater inflow in essence moved to the dam in the horizontal plane in which it entered. The reason for

this was that in the original version of LARM, the eddy coefficients were not treated as functions of the Richardson number and thus vertical variations in density were not considered. Edinger and Buchak have since modified LARM to allow for the Richardson number dependence previously presented. Thus, when an unstable stratification arises, i.e., $R_i < 0$, the vertical eddy viscosity and diffusivity are increased to their maximum values based upon the diffusive stability criterion. This procedure forces either a maximum diffusion upwards or downwards depending upon whether the density of the cell is less than or greater than the surrounding density. The results provided by Edinger and Buchak* (and presented in Figures 16-30) were obtained from simulations in a 22.87-m flume rather than the actual length of the GRH flume traversed by the underflow, i.e., 23.93 m. Values of the various coefficients and other input parameters are presented in Table 2. A longitudinal

Table 2

LARM Input for GRH Flume Application

Parameter	Value
Spatial step	$\Delta x = 1.524$ m
Layer thickness	$H = 0.0762$ m
Time step	$\Delta t = 5.0$ sec
Horizontal viscosity	1.5×10^{-6} m^2/sec
Horizontal diffusivity	1.4×10^{-5} m^2/sec
Vertical viscosity at neutral stability	1.5×10^{-6} m^2/sec
Vertical diffusivity at neutral stability	1.4×10^{-5} m^2/sec
Chezy coefficient	70 $m^{1/2}/sec$
Inflow	0.00063 m^3/sec
Outflow	0.00063 m^3/sec
Inflow temperature	62.0°F

* Personal communication, November 1979, J. E. Edinger and E. M. Buchak, J. E. Edinger Associates, Inc., Wayne, Penn.

spatial step of 1.524 m and a constant layer thickness of 0.0762 m was utilized. The schematization is presented in Figure 12. Approximately 5 sec of CPU time on a CYBER 176 was required to simulate 30 min.

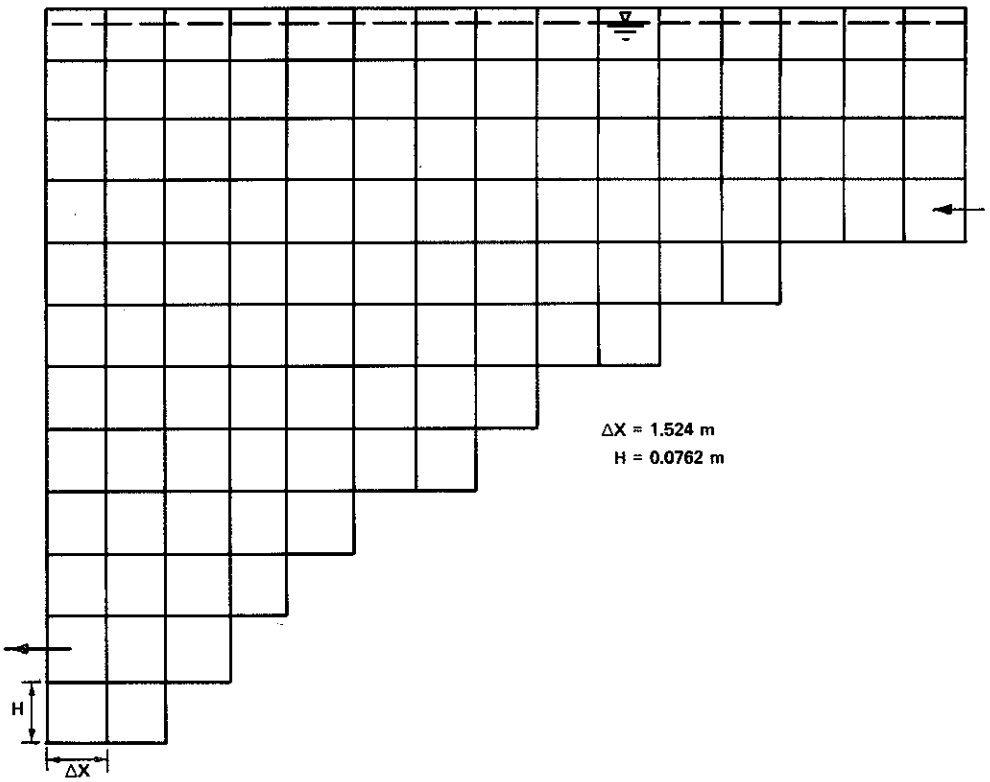

Figure 12. LARM schematization of GRH flume

232. Figure 13 indicates that the density underflow computed by LARM moves too slowly. Approximately 18 min is required for the underflow to travel 23.93 m; whereas, LARM computations result in a travel time of about 21 min to traverse 22.87 m. Neither varying the horizontal eddy diffusivity and viscosity nor the Chezy coefficient resulted in a significant change in the computed travel time. A comparison of the velocity profiles presented at approximately 12 m from the upstream end (see Figure 14) reveals that LARM tends to compute a thicker density underflow than observed in the flume. It is believed this is primarily due to the stair-stepping representation of the bottom, along with perhaps the effect of indirectly modeling buoyancy effects as discussed above. Figure 15, showing a comparison of computed outflow temperatures from LARM

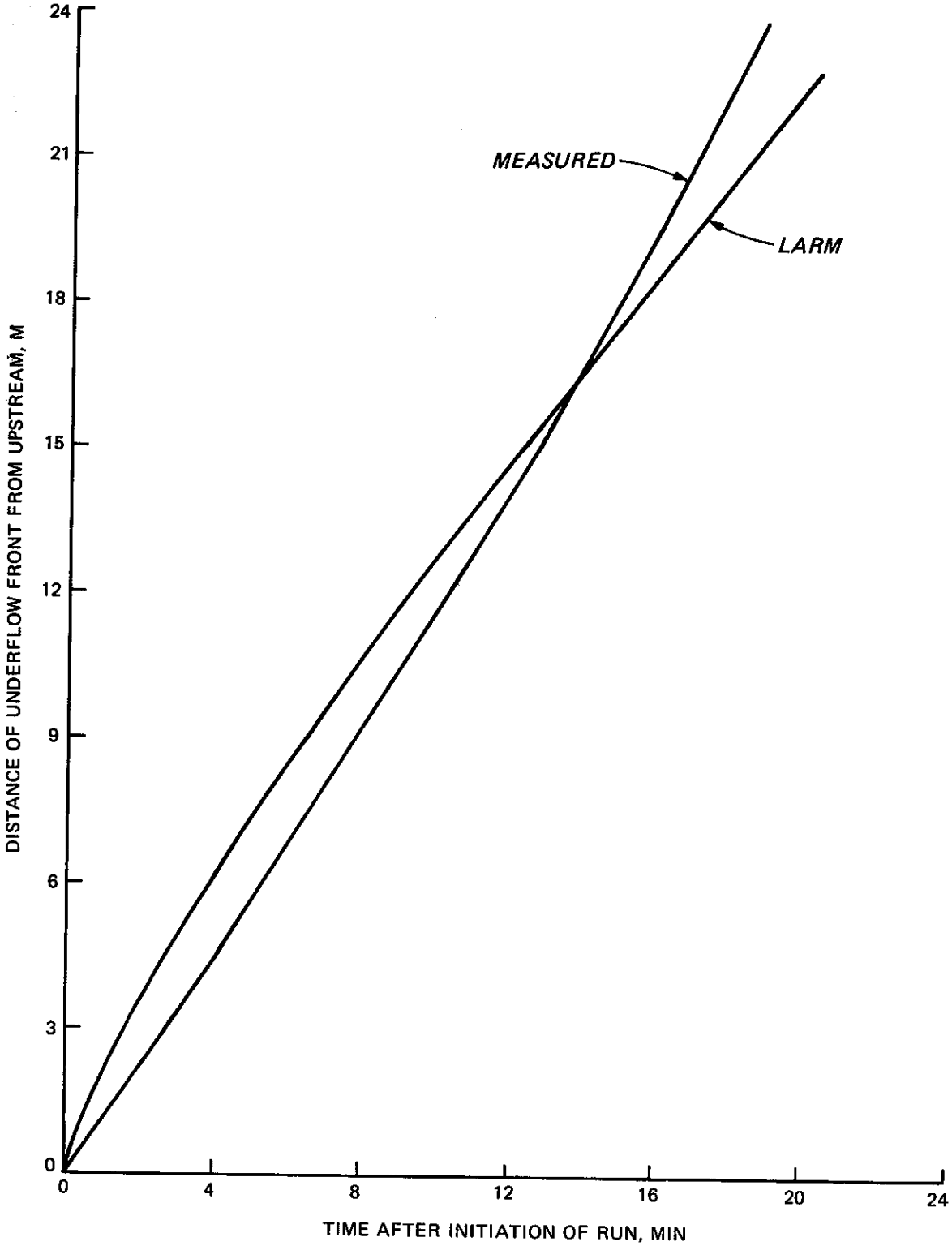

Figure 13. Comparison of LARM computed and recorded underflow speed

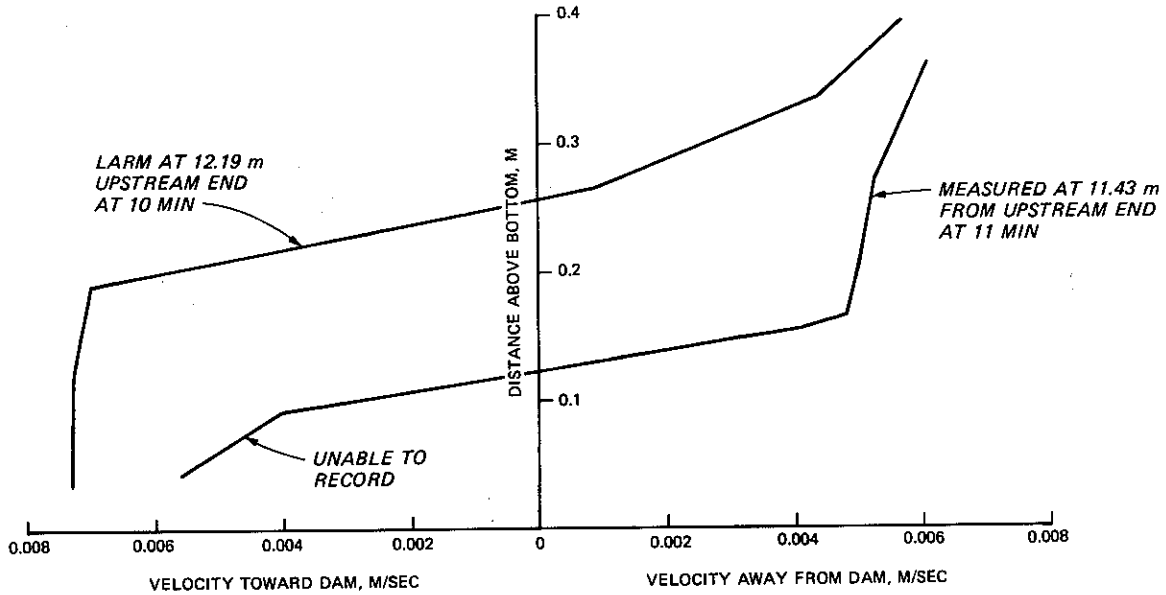

Figure 14. Comparison of LARM computed and recorded horizontal velocities

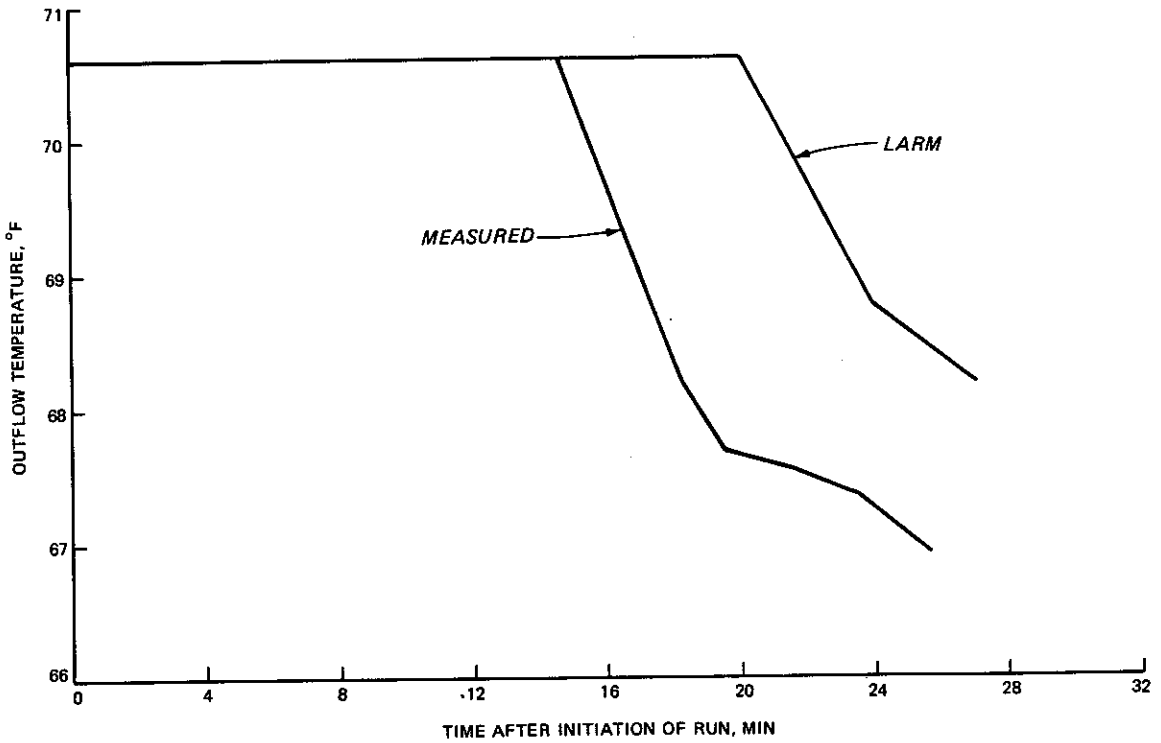

Figure 15. Comparison of LARM computed and recorded outflow temperature

and those recorded, tends to substantiate the conclusion that the density underflow is not being forced to "hug" the bottom enough. The stair-stepped bottom appears to result in too much mixing of the coldwater underflow with the warmer water lying below the next stair-step, which results in higher computed outflow temperatures than those recorded. The computed 2-D mass flux field for 60 min after initiation of the inflow at 4-min increments is presented in Figures 16-30.

233. It should be realized that the above problem in the modeling of the density underflow is not unique to LARM. Any model that represents the bottom boundary in such a stair-stepping fashion will encounter the same problem of too much mixing and a resulting slower, thicker, and warmer density underflow.

234. As a final note, the results presented here were computed with windward differencing of the convective terms throughout the flow field. Much smoother computations were realized than when centered differences were used everywhere except near the outlet. A comparison of the relative magnitude of various terms in the horizontal momentum equation revealed that the convective terms are approximately the same magnitude as the density gradient terms. In real reservoirs, convective terms usually dominate only in the backwater. In addition to the windward differencing being employed, the upstream boundary condition was modified to force the temperature in the most upstream column to remain at the upstream temperature of 62°F, which resulted in a slightly faster underflow current.

Application of Waldrop's TVA Model

235. Dr. Bill Waldrop and Walter Harper at the Tennessee Valley Authority in Norris, Tenn., have made an application of the 2-D reservoir model to the density underflow problem in the GRH flume on the computing facilities available to TVA and have provided results to WES.* Two different runs were made. The first allowed the heavier inflow to seek its own level at the upstream boundary, but in the second run, the

* Personal communication, November 1979, B. Waldrop and W. Harper, Tennessee Valley Authority, Norris, Tenn.

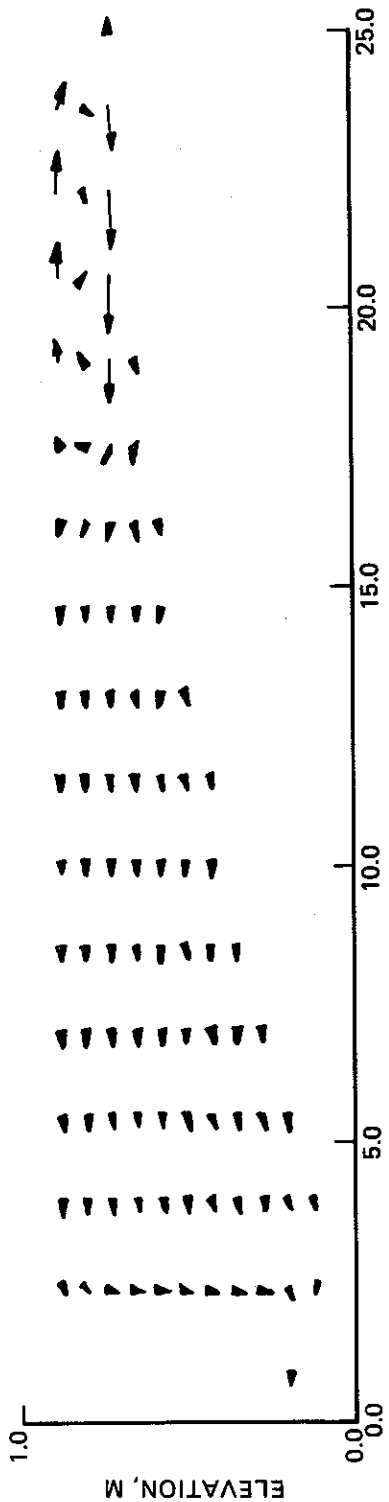

Figure 16. Computed mass flux profile from LARM at T = 4 min

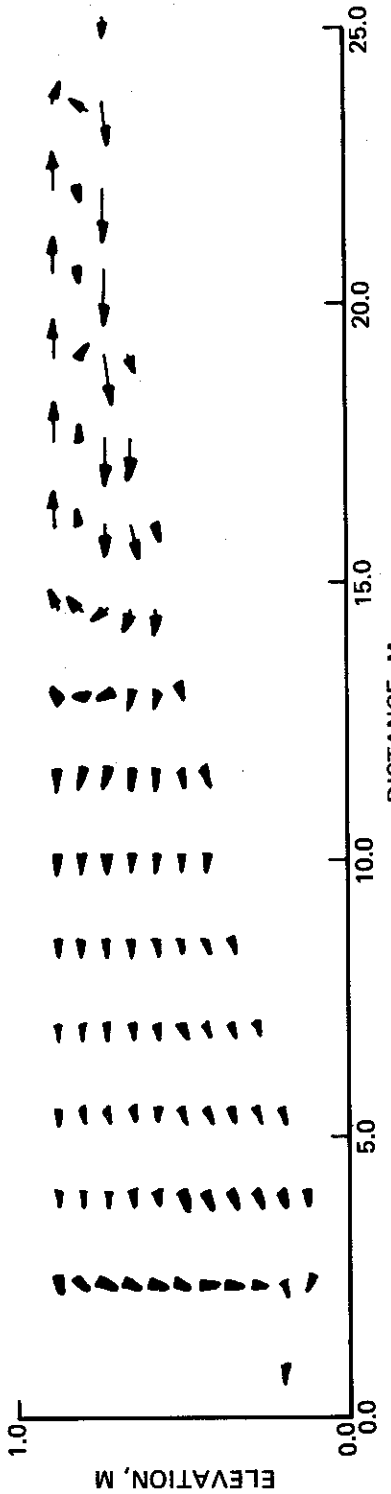

Figure 17. Computed mass flux profile from LARM at T = 8 min

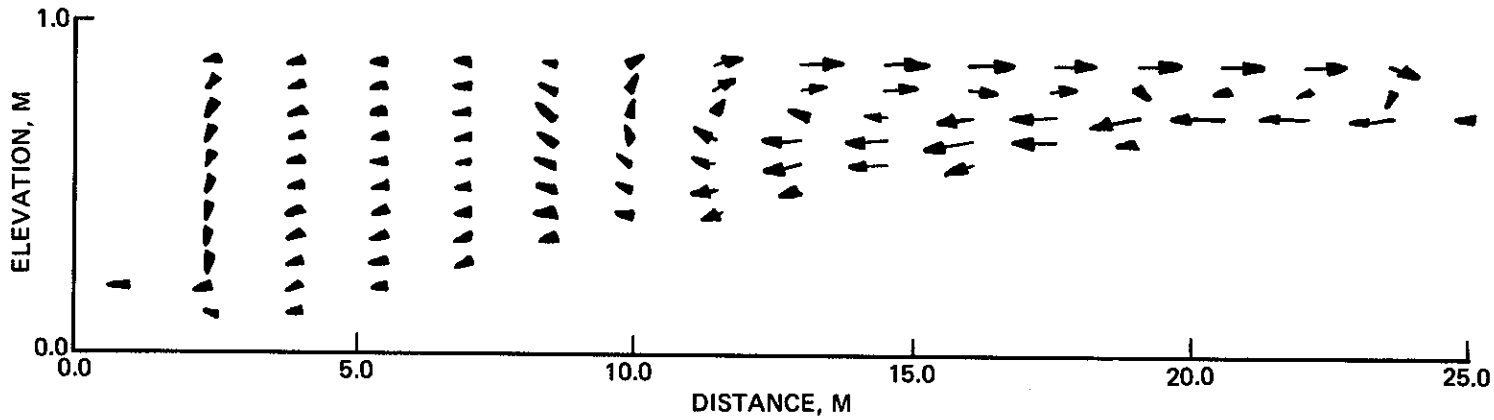

Figure 18. Computed mass flux profile from LARM at T = 12 min

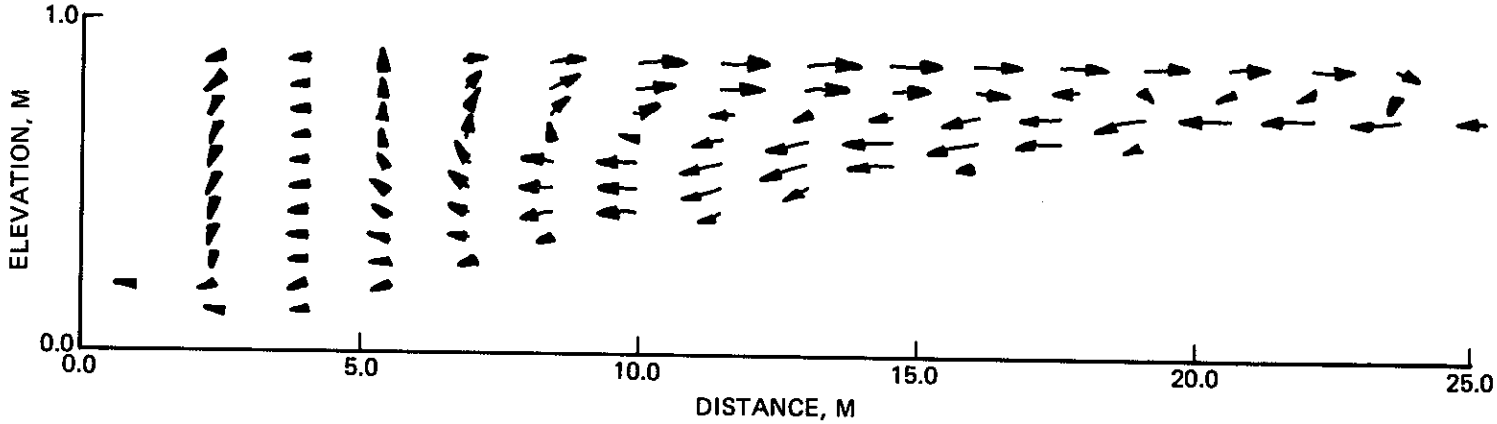

Figure 19. Computed mass flux profile from LARM at T = 16 min

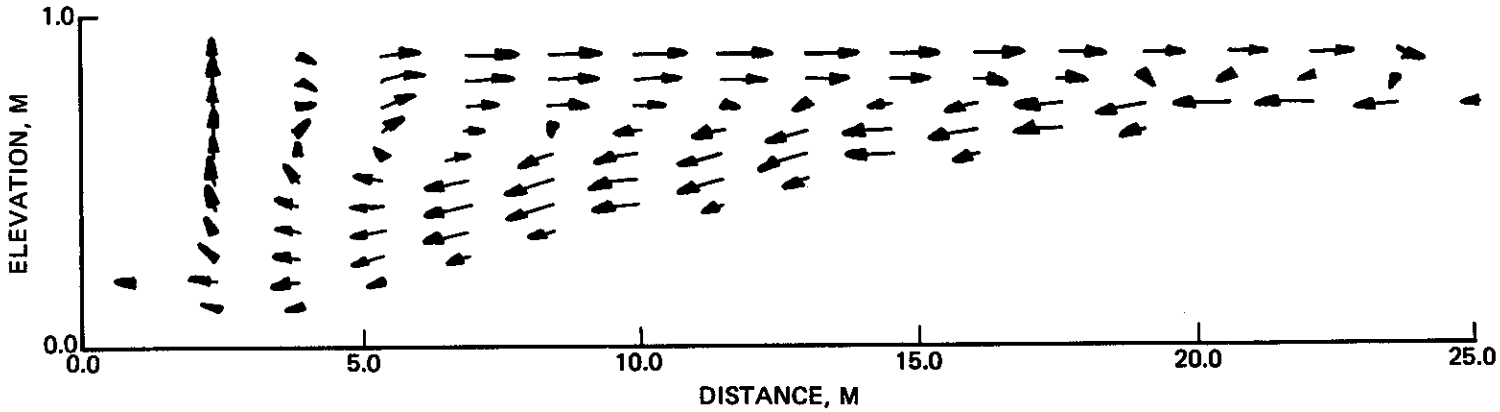

Figure 20. Computed mass flux profile from LARM at T = 20 min

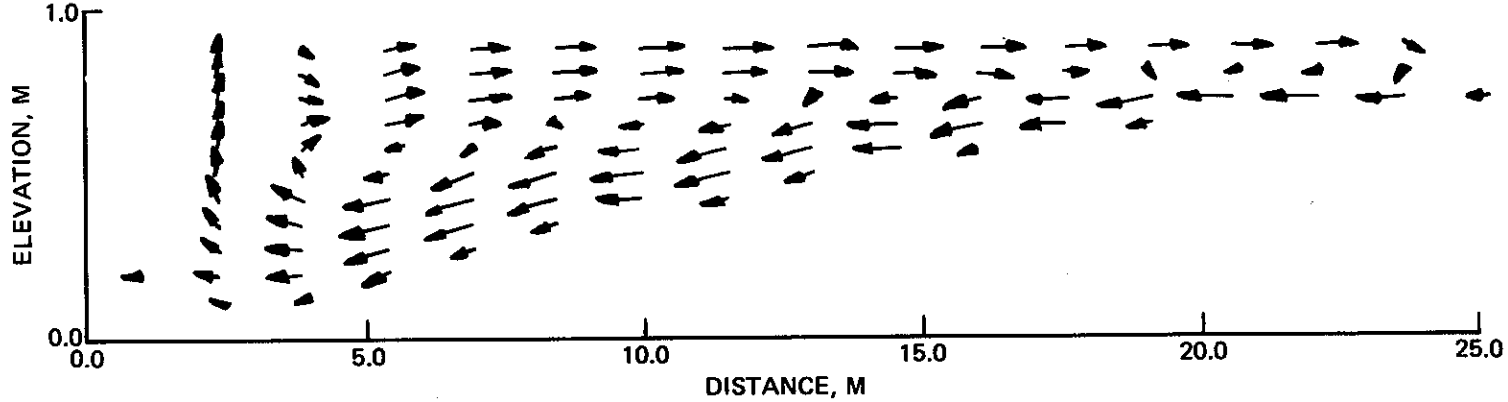

Figure 21. Computed mass flux profile from LARM at T = 24 min

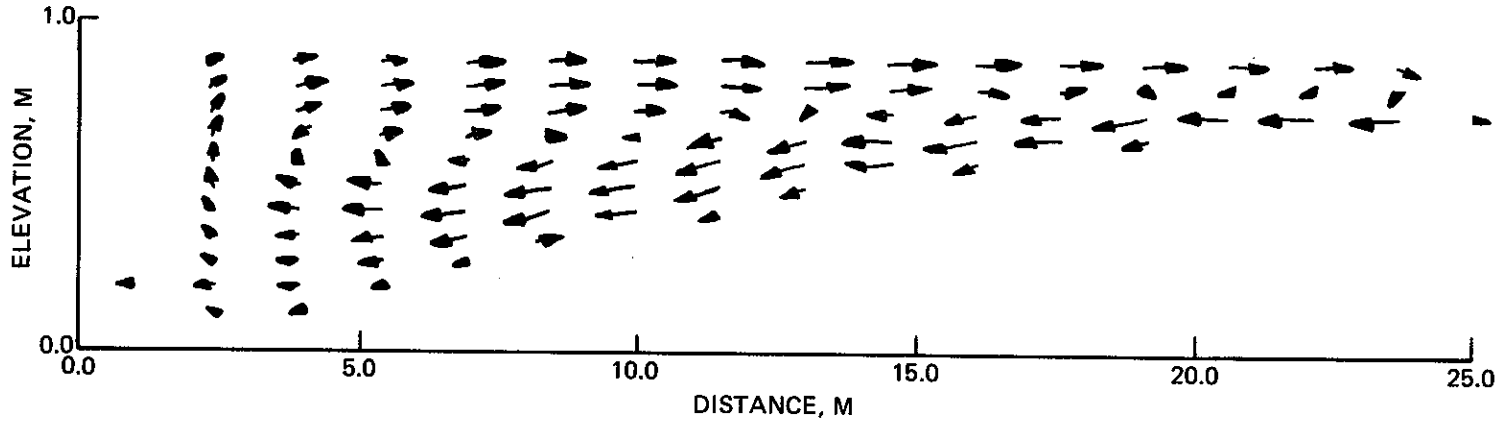

Figure 22. Computed mass flux profile from LARM at T = 28 min

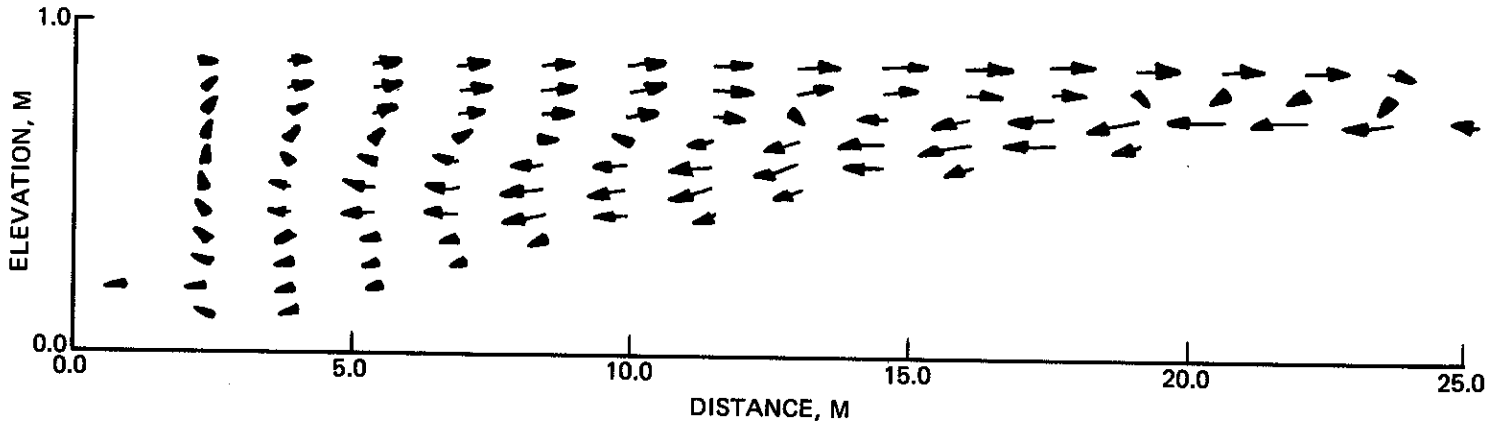

Figure 23. Computed mass flux profile from LARM at T = 32 min

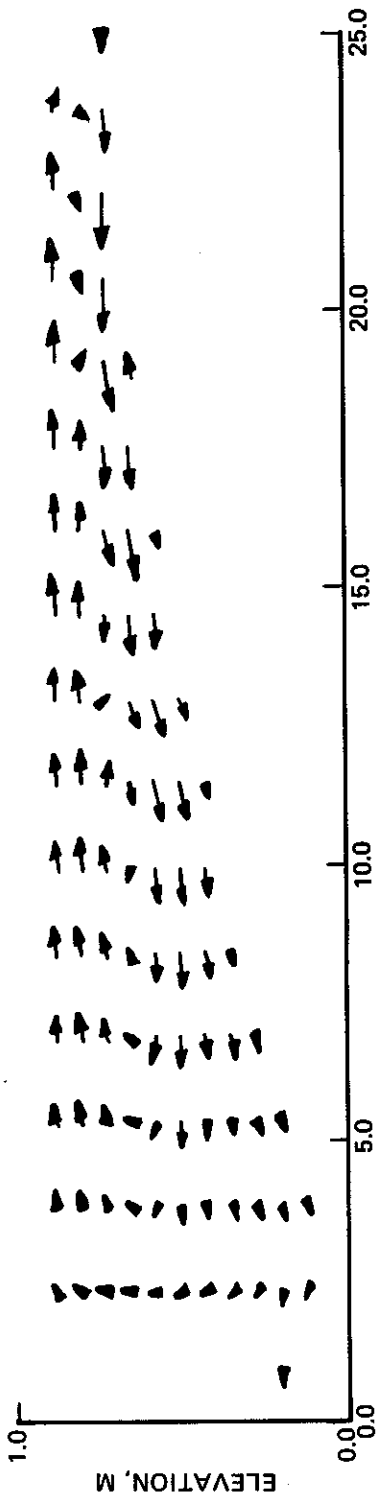

Figure 24. Computed mass flux profile from LARM at T = 36 min

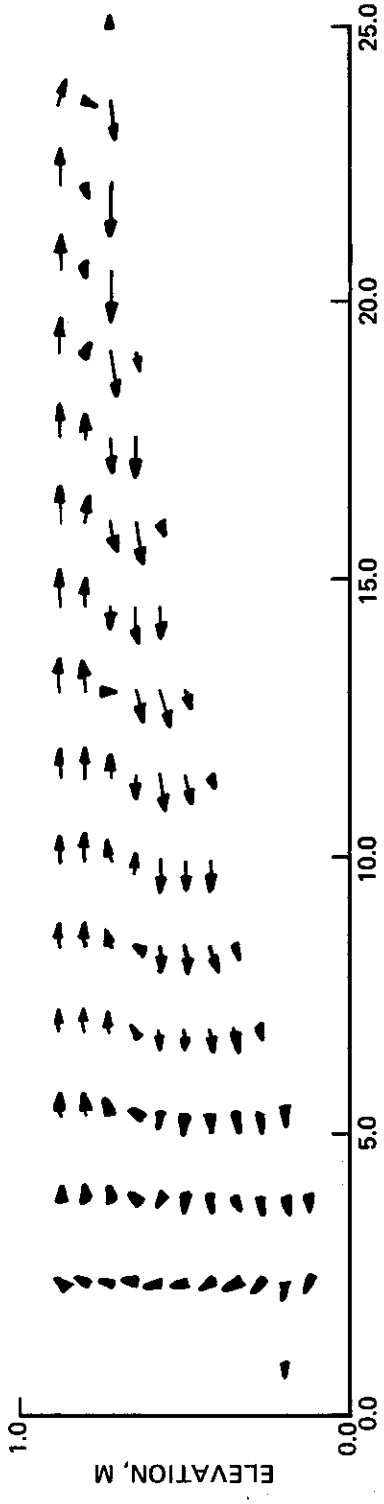

Figure 25. Computed mass flux profile from LARM at T = 40 min

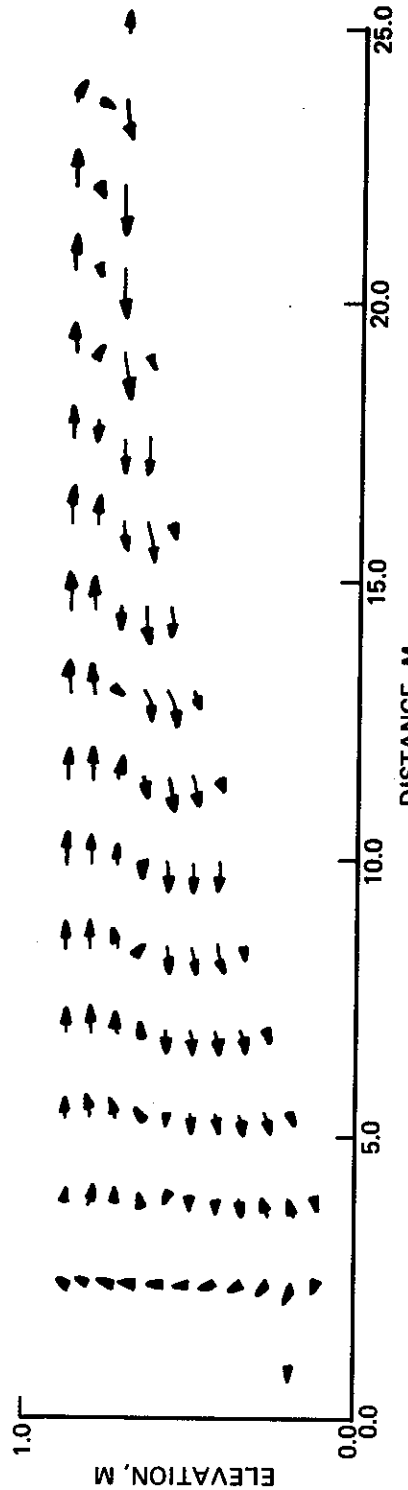

Figure 26. Computed mass flux profile from LARM at T = 44 min

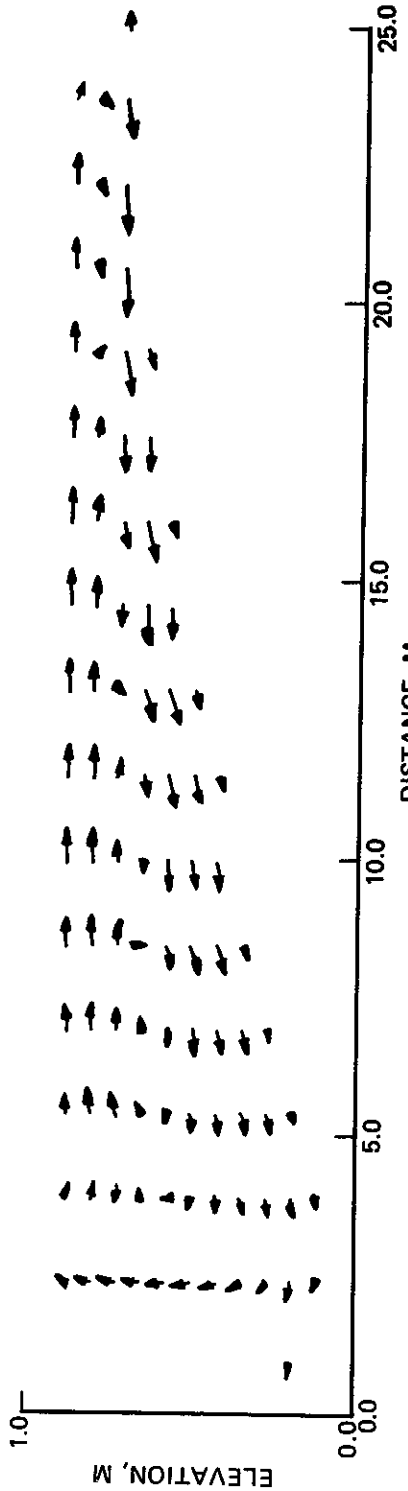

Figure 27. Computed mass flux profile from LARM at T = 48 min

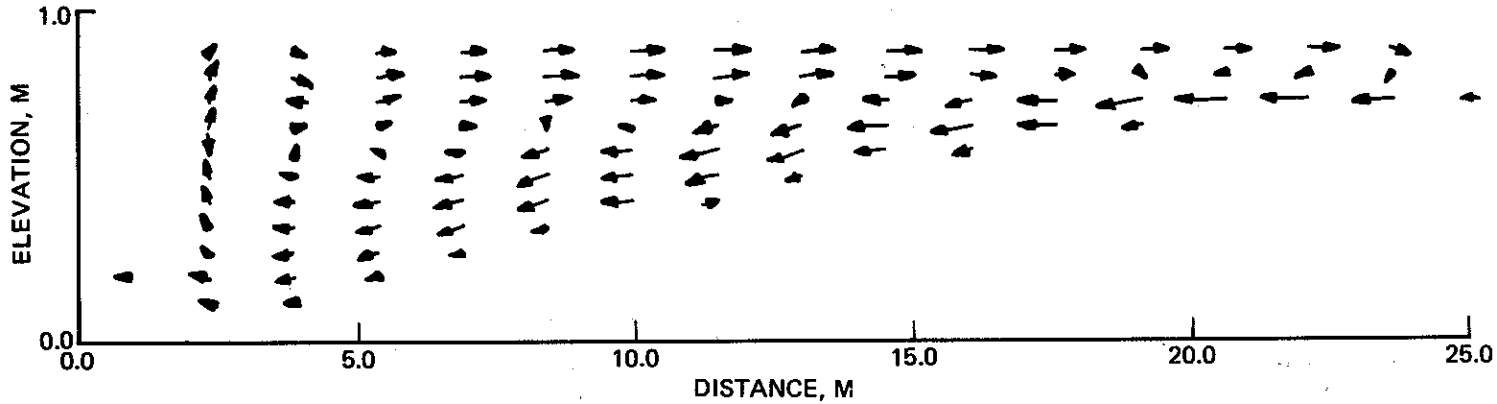

Figure 28. Computed mass flux profile from LARM at T = 52 min

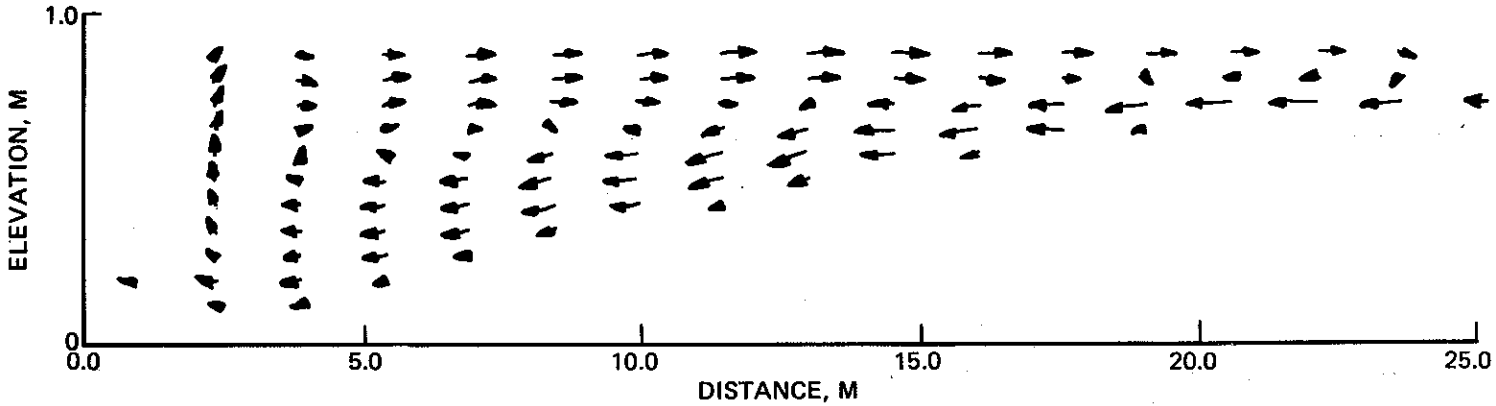

Figure 29. Computed mass flux profile from LARM at T = 56 min

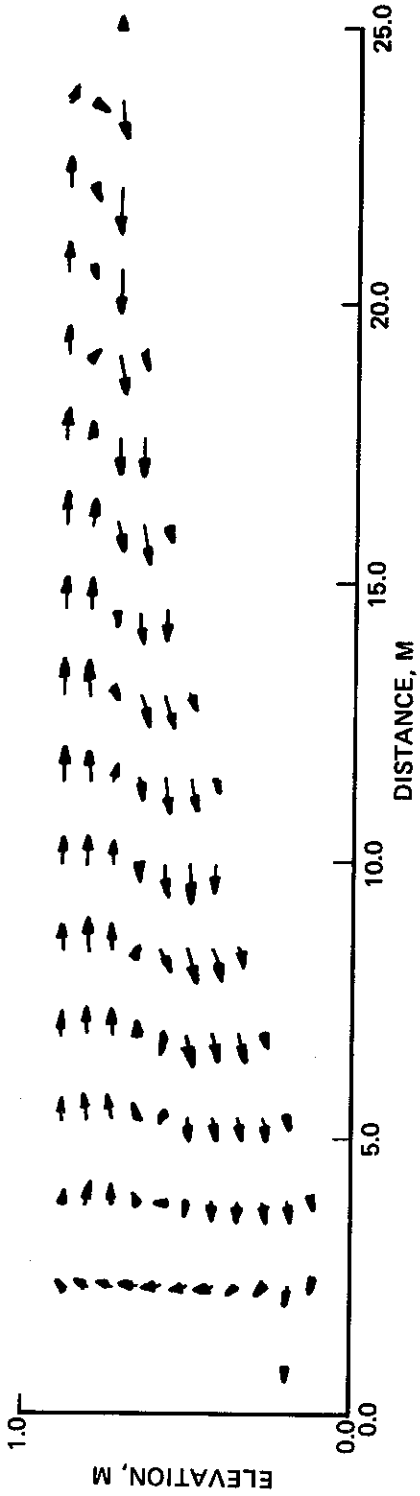

Figure 30. Computed mass flux profile from LARM at T = 60 min

coldwater inflow was forced to enter the bottom layer, as was the case in the Edinger and Buchak application. Figure 31 demonstrates that the

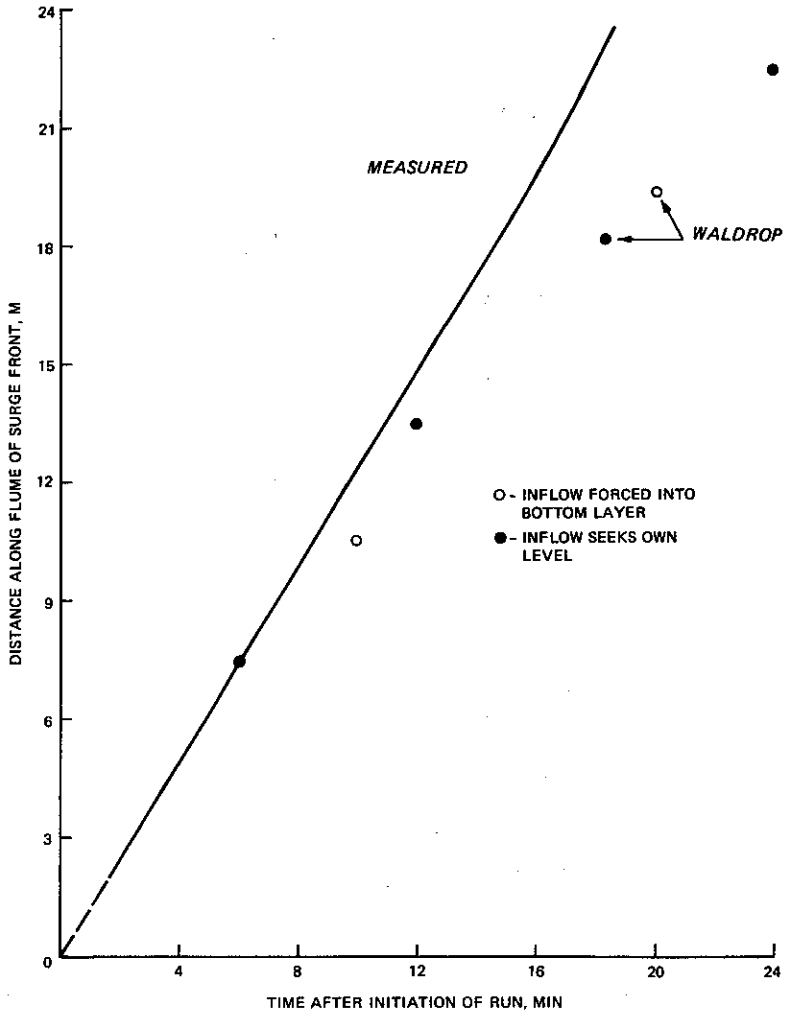

Figure 31. Comparison of TVA computed and recorded underflow speed

computed underflow moves too slowly. Results from both runs indicate a computed travel time in excess of 24 min, although it should be noted that the travel time for the underflow to traverse the horizontal portion of the flume agrees quite well with recorded results. Once again it would seem these results tend to substantiate the previous statements made concerning the stair-stepping effect of the bottom. This effect is further indicated from the plot of computed versus recorded outflow temperatures presented in Figure 32. Computed velocity fields and isotherms

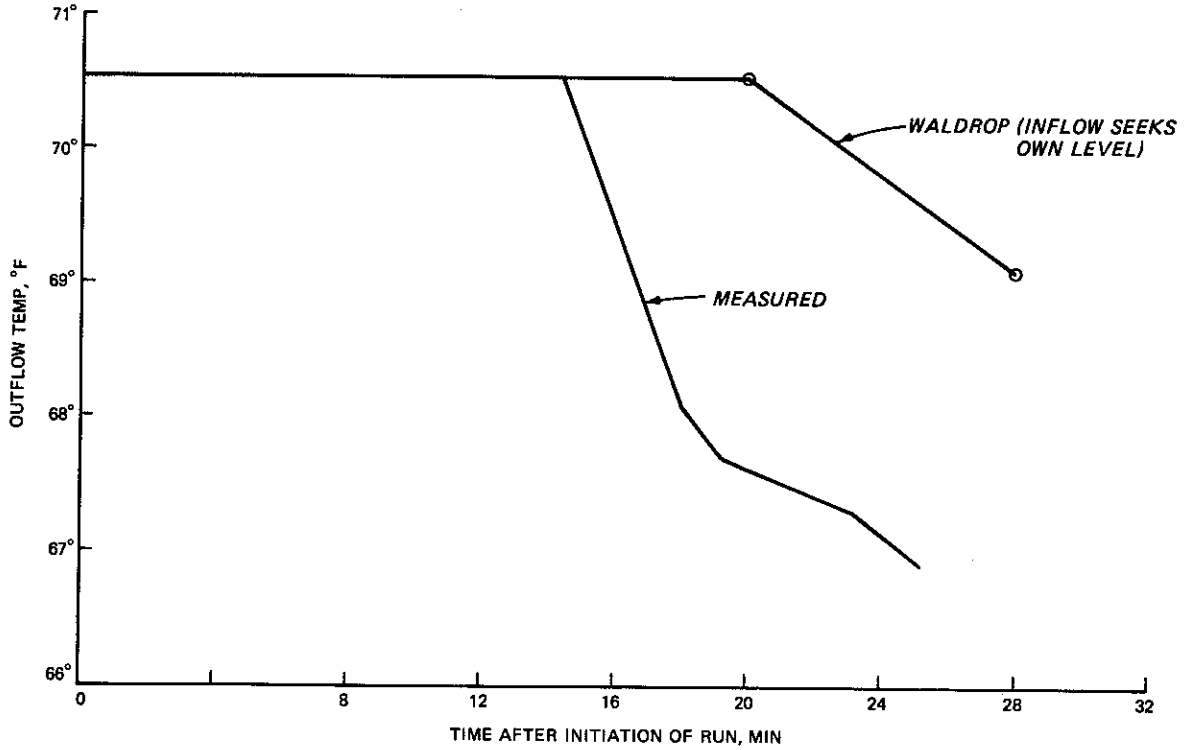

Figure 32. Comparison of TVA computed and recorded outflow temperature

from the first application are presented in Figures 33-37 at times of 6, 12, 18, 24, and 30 min after initiation of the inflow. Similar plots from the second application are presented at 10, 20, and 30 min in Figures 38-40. The only results provided for a direct comparison of computed and recorded velocities at a particular location are presented in Figure 41. There a comparison of the computed velocities at 10.67 m from the upstream end at 10 min after initiation is made with recorded velocities at 11.43 m from the upstream end at 11 min after initiation.

236. As previously noted, the Waldrop model is an explicit FDM and thus the time step at which computations are made is restricted by the speed of the surface gravity wave. For this application, the maximum allowable time step is computed to be about 0.50 sec. Waldrop indicates that a time step of 0.30 sec was actually used, which resulted in 46 sec of CPU time on a CDC 7600 computer for 6000 time steps.

237. As a final note, Waldrop has indicated that he also has encountered flow reversals in front of forced outlets. However, rather

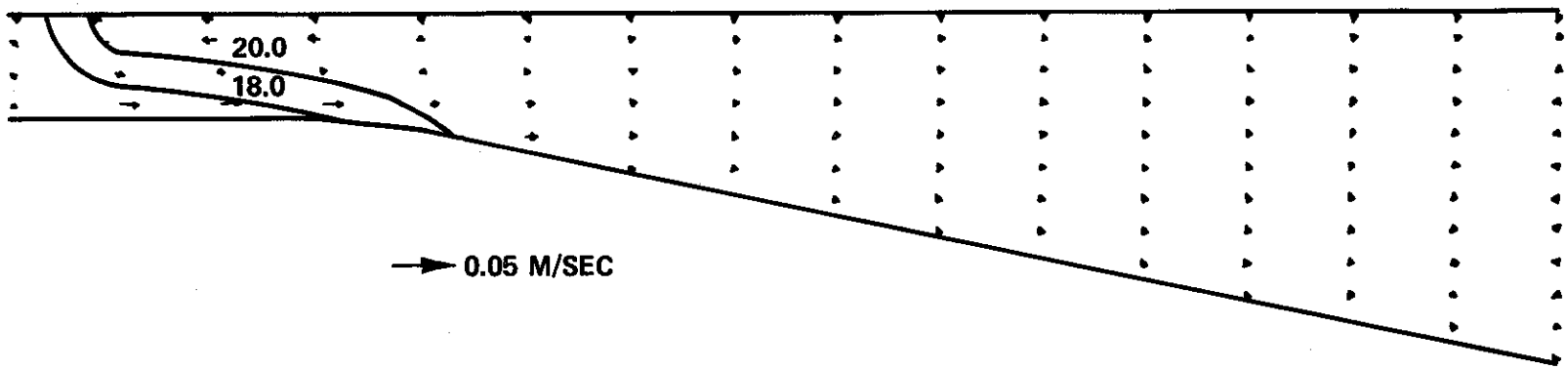

Figure 33. Velocities and isotherms from TVA Model at T = 6 min with inflow seeking its own level

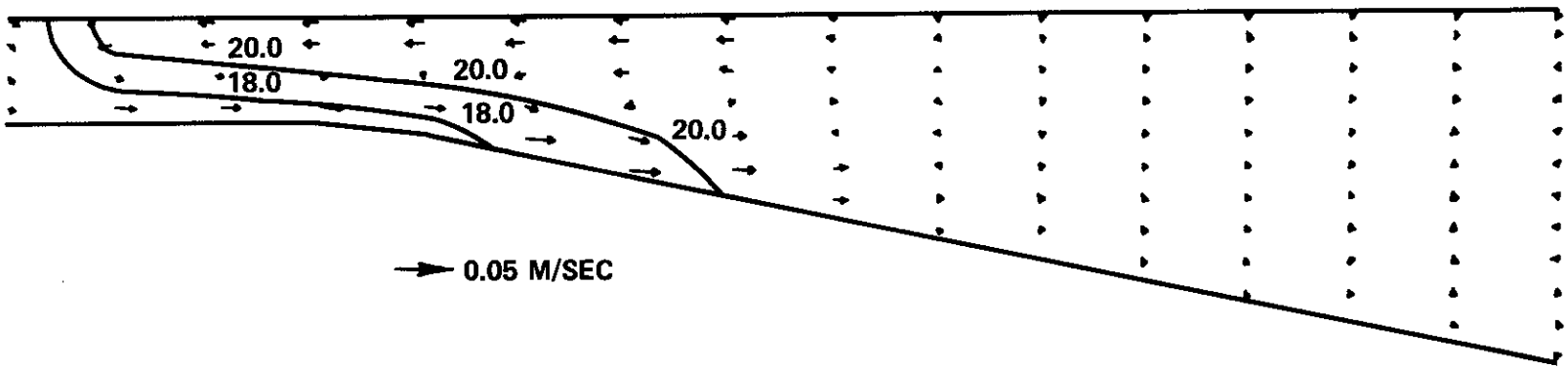

Figure 34. Velocities and isotherms from TVA Model at T = 12 min with inflow seeking its own level

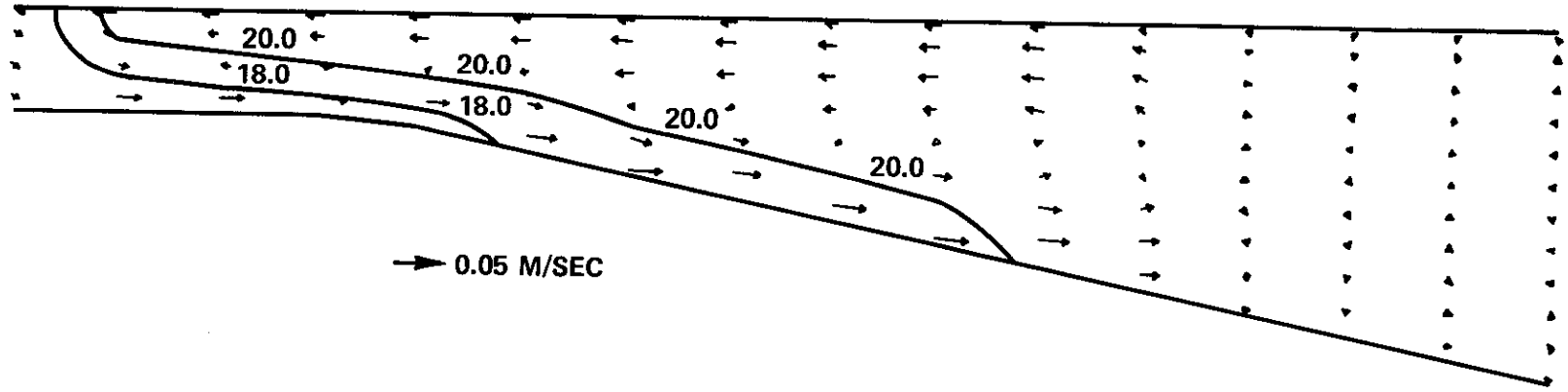

Figure 35. Velocities and isotherms from TVA Model at T = 18 min with inflow seeking its own level

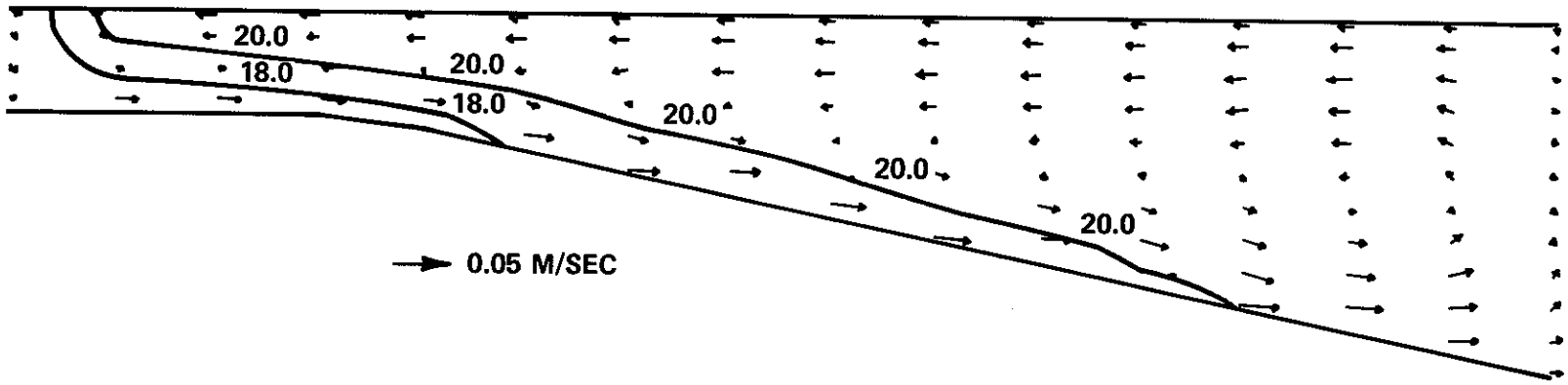

Figure 36. Velocities and isotherms from TVA Model at T = 24 min with inflow seeking its own level

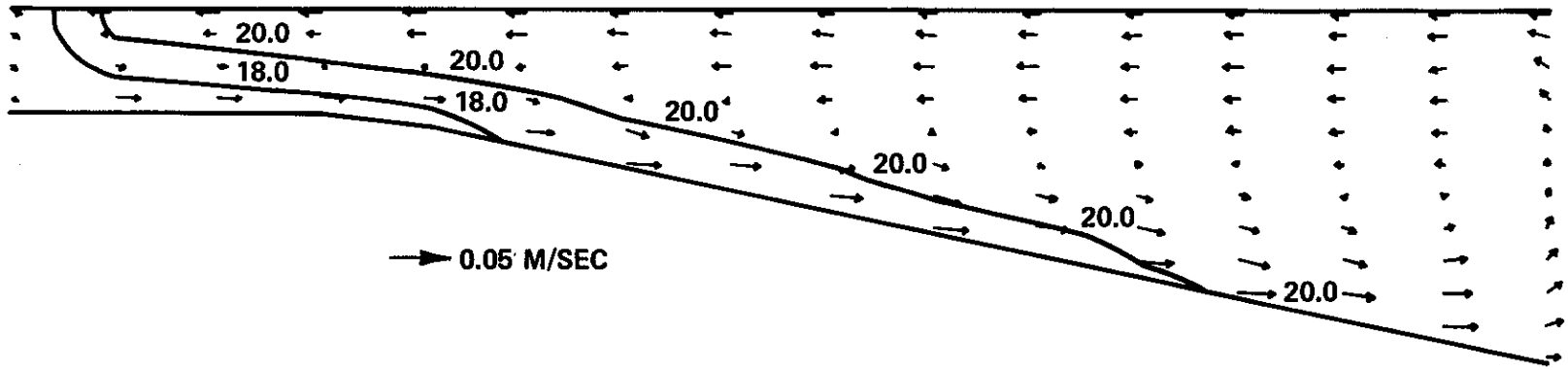

Figure 37. Velocities and isotherms from TVA Model at T = 30 min with inflow seeking its own level

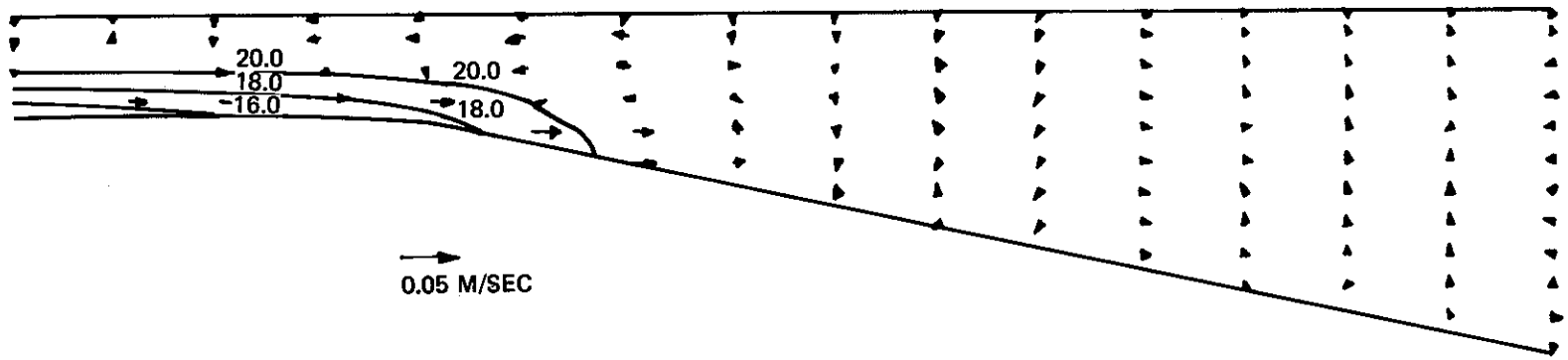

Figure 38. Velocities and isotherms from TVA Model at T = 10 min with inflow forced over lower half

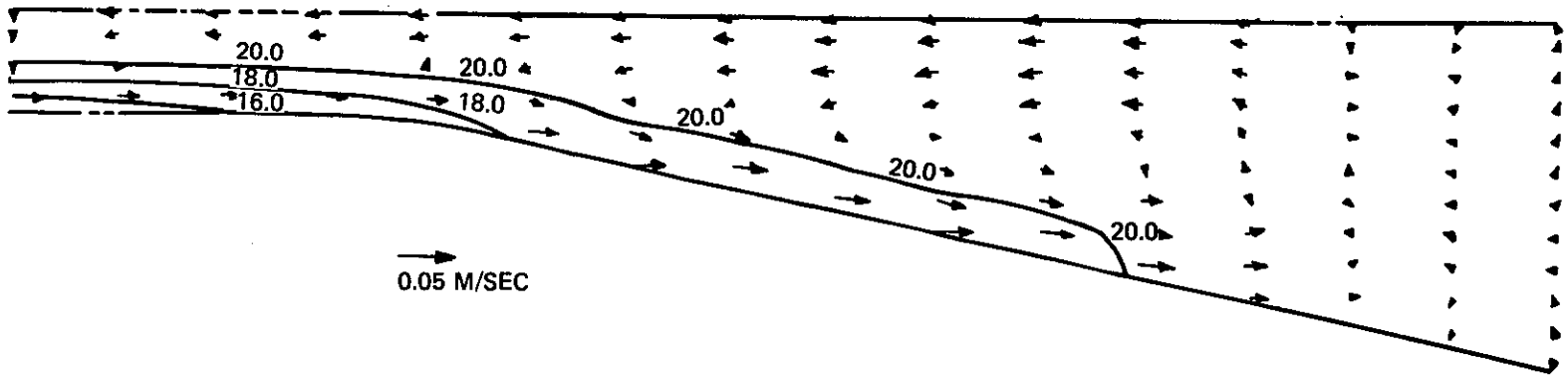

Figure 39. Velocities and isotherms from TVA Model at T = 20 min with inflow forced over lower half

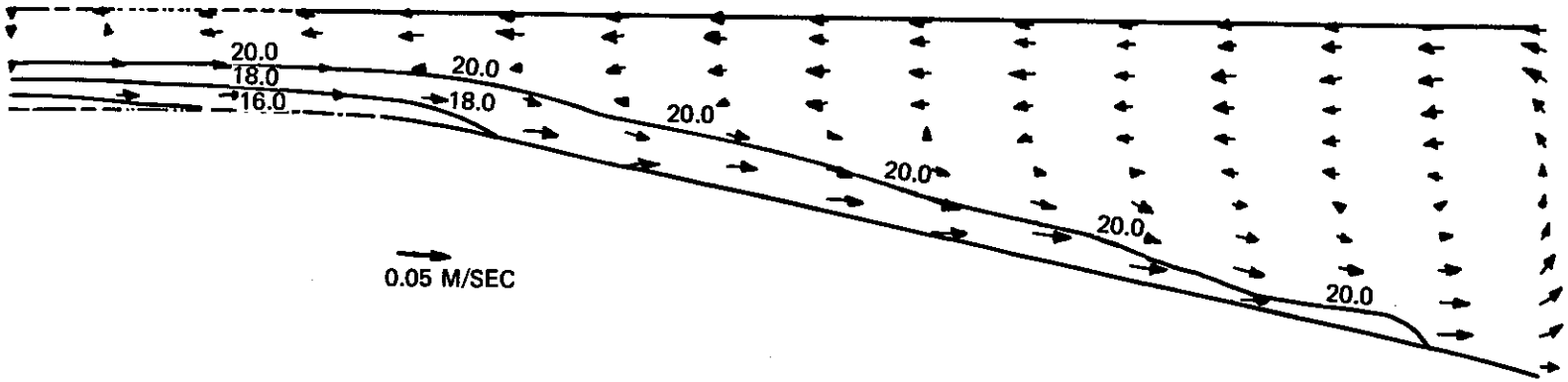

Figure 40. Velocities and isotherms from TVA Model at T = 30 min with inflow forced over lower half

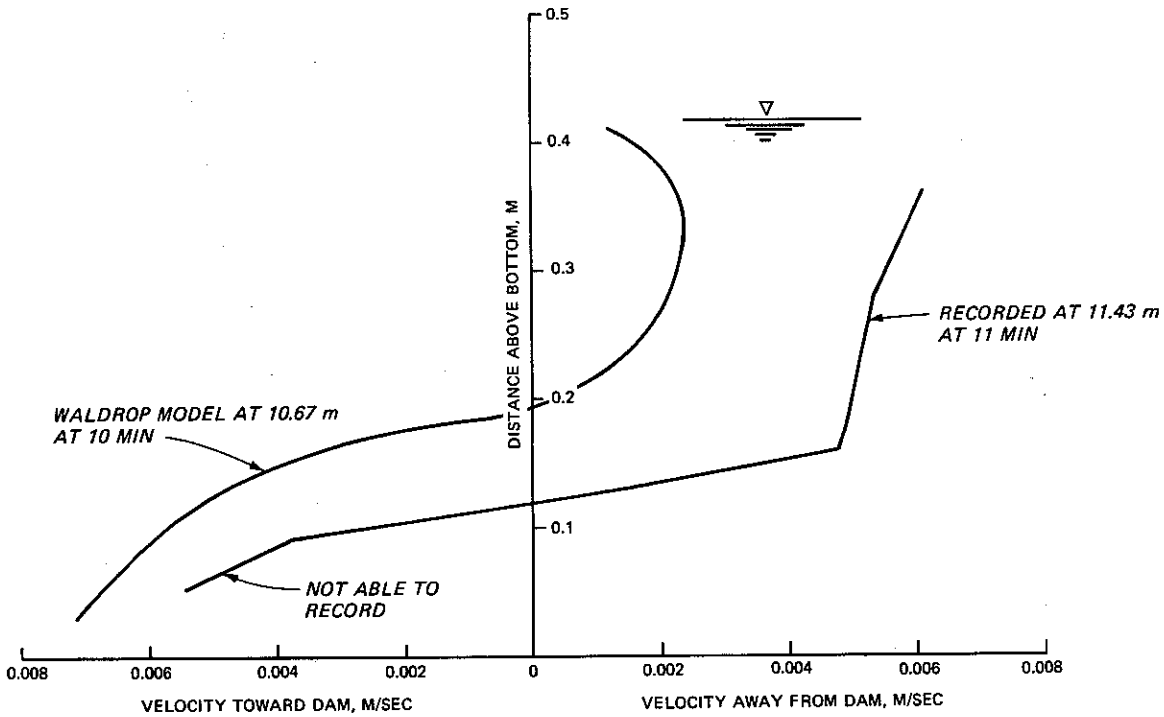

Figure 41. Comparison of TVA computed and recorded horizontal velocities

than using windward differencing near the outlet, he reduces the pressure by subtracting the dynamic pressure $1/2\rho U_o^2$ where U_o is the outlet velocity, to force the flow in the proper direction. This is easy to implement, since his basic computational cell, as is illustrated below, has the velocity components defined at the center of the cell with pressures defined on the vertical faces.

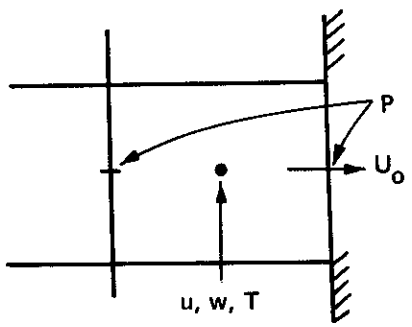

Application of
Norton-King-Orlob FEM--RMA-7

238. The application of the Norton-King-Orlob FEM to the density

underflow in the GRH flume was made by Bob MacArthur of the Hydrologic Engineering Center (HEC) in Davis, Calif.* As in the previous model applications, the initial conditions consisted of zero flows (zero velocity throughout) and isothermal water temperatures throughout at 70.6°F. After time zero, a constant coldwater inflow of 0.00063 m^3/sec at 62.0°F was imposed entering near the bottom of the flume as an upstream boundary condition. MacArthur indicated that a zero pressure, free discharge boundary condition was prescribed at the outlet so the inflow rate would equal the outflow and the free water surface would remain horizontal. Values of the eddy coefficients used are presented in Table 3.

Table 3

Values of the Turbulent Exchange Coefficients Used for the GRH Flume Applications

Turbulent Exchange Coefficients (Eddy Viscosity)	Value
ε_{xx}	10 lb-sec/ft^2 (0.48 m^2/sec)
ε_{xy}	0.004 lb-sec/ft^2 (1.9×10^{-4} m^2/sec)
ε_{yx}	10 lb-sec/ft^2 (0.48 m^2/sec)
ε_{yy}	0.01 lb-sec/ft^2 (4.8×10^{-4} m^2/sec)
Turbulent Diffusion Coefficients (Eddy Diffusivity)	**Value**
D_x	2.0 ft^2/sec (0.19 m^2/sec)
D_y	0.01 ft^2/sec (9.3×10^{-4} m^2/sec)

239. Using a time step of 3 min, a total time of 18 min was simulated. Results furnished by MacArthur for the first three time steps are presented in Figures 42, 43, and 44. The finite element network used to simulate these results is shown in Figure 45. Although comparative plots are not presented, MacArthur stated that travel times for the

* Personal communication, November 1979, R. C. MacArthur, Hydrologic Engineering Center, Davis, Calif.

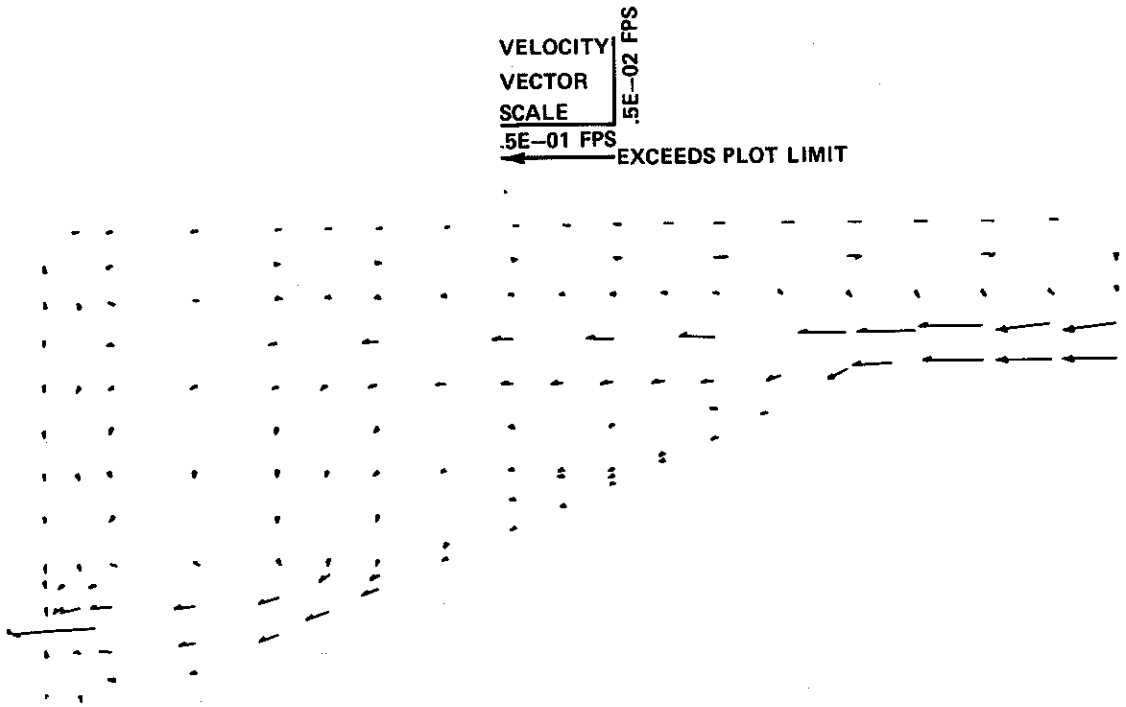

Figure 42. Velocities computed by RMA-7 at T = 3 min

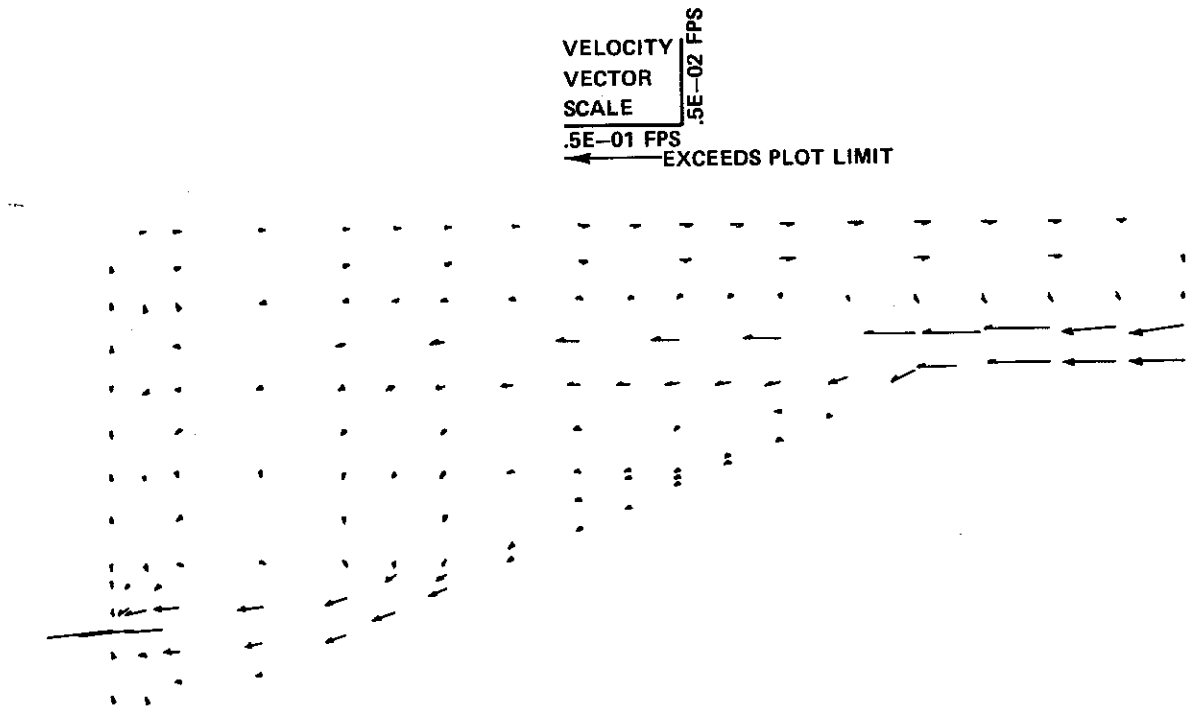

Figure 43. Velocities computed by RMA-7 at T = 6 min

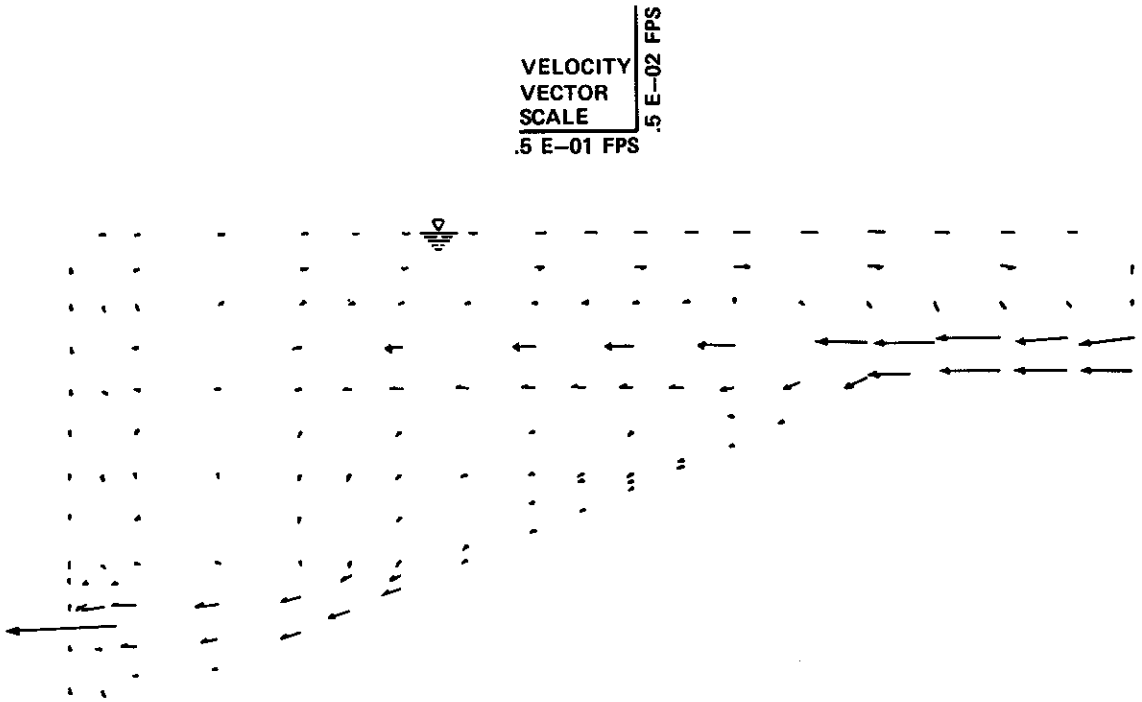

Figure 44. Velocities computed by RMA-7 at T = 9 min

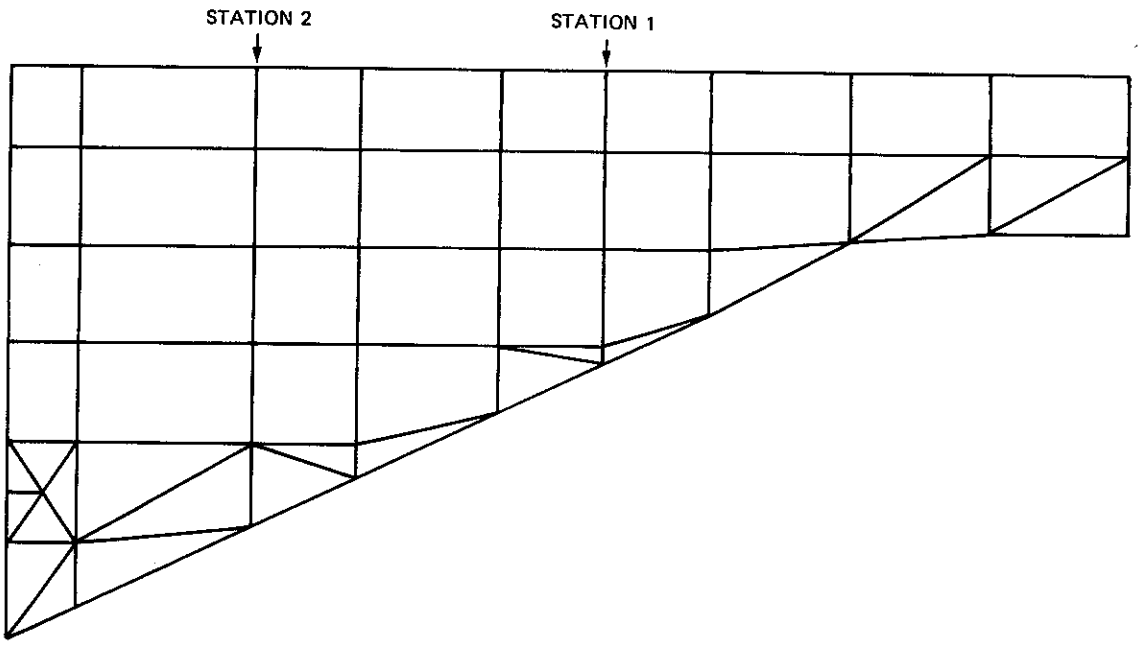

Figure 45. Finite element network for GRH flume applications

coldwater plume to reach the outlet were usually about 18 to 20 min from the time of initial inflow. However, outlet temperatures were several degrees (°F) greater than the temperatures measured in the physical model tests. In addition, the thickness of the plume and temperatures within the bottom flow plume were greater than observed. This indicates more vertical mixing is occurring in the numerical simulation than was occurring in the GRH flume, which MacArthur attributes to the choice of the vertical mixing coefficients.

240. An inspection of the two-dimensional velocity field presented after times of 3, 6, and 9 min in Figures 42, 43, and 44, respectively, reveals that the classical density underflow phenomenon has not fully developed in the computed results. At the point where the flume bottom begins sloping, the flow seems to be projected across in a horizontal plane. One reason for this may be the large values assumed for some of the eddy coefficients, e.g., the diagonal component in the x-direction $\varepsilon_{XX} = 0.48\ m^2/sec$. MacArthur has indicated that the stability of the model is extremely sensitive to the values used for these coefficients. Therefore, such large values were required to obtain stable solutions.

241. The computer time on a CDC 7600 to simulate the results presented here required 42 sec of execution time to compute 18 min of flow time. This compares with the approximately 5 sec required by LARM to compute 30 min of flow time and 46 sec required by the Waldrop explicit model to also simulate 30 min of flow time.

242. After these initial runs, MacArthur made some comparative runs, using the GRH flume geometry, for homogeneous flow conditions and additional thermally stratified flow conditions. In each case, flows of $0.00063\ m^3/sec$ were introduced with a linear velocity distribution in the bottom element at the upstream end of the flume. Figure 45 presents the finite element network used for the simulations. The homogeneous case was run isothermally at a temperature of 50.5°F, while the nonhomogeneous case was started with an initial temperature of 50.5°F throughout and an inflowing water temperature of 41.0°F.

243. Velocity distributions produced by these comparative runs

are presented in Figure 46 for three different time steps (after 3, 9, and 18 min) at the two sampling stations indicated on Figure 45. The effects of flow stratification are quite evident and appear to be qualitatively reasonable.

Application of
Eraslan's Discrete Element Model

244. After the initial writing of this report, Eraslan provided results from applications of his model called FLOWER.* FLOWER is a computer code for simulating fast-transient three-dimensional coupled hydrodynamic, thermal and salinity conditions in the intake and discharge zones of power plants operating on rivers, lakes, estuaries and coastal regions. The general 3-D model contains an automatic 2-D laterally averaged version, which was used in the GRH flume simulations.

245. Eraslan indicates that the turbulent transport model of FLOWER is completely closed; i.e., it utilizes the same turbulent (and laminar) transport model for all time and spatial scales in applications to vastly different problems, including the scales of physical models as well as the scales of prototype conditions. Therefore, the user never specifies any friction or turbulent diffusion coefficients.

246. Two separate simulations were made with the flume discretized as shown in Figure 47. One was a coldwater inflow, while the other was a hotwater input. The coldwater inflow simulation was the same as previously discussed, with the exception that the outflow was 0.00109 m^3/sec and the inflow temperature was 54.14°F. Therefore, the water surface dropped slightly during the simulation. Figures 48-55 present "snap shots" at 200-sec intervals of the velocity field with no exaggeration of the vertical component for 1600 sec after initiation of the inflow. From an inspection of Figure 52, it can be seen that the computed travel time required to traverse the flume is 16-17 min, which compares reasonably well with a recorded time of approximately 15 min for these input conditions. Eraslan indicates that if the inflow had been

* Personal communication, March 1980, Arsev Eraslan, Chief Scientist, Hennington, Durham, and Richardson, Knoxville, Tenn.

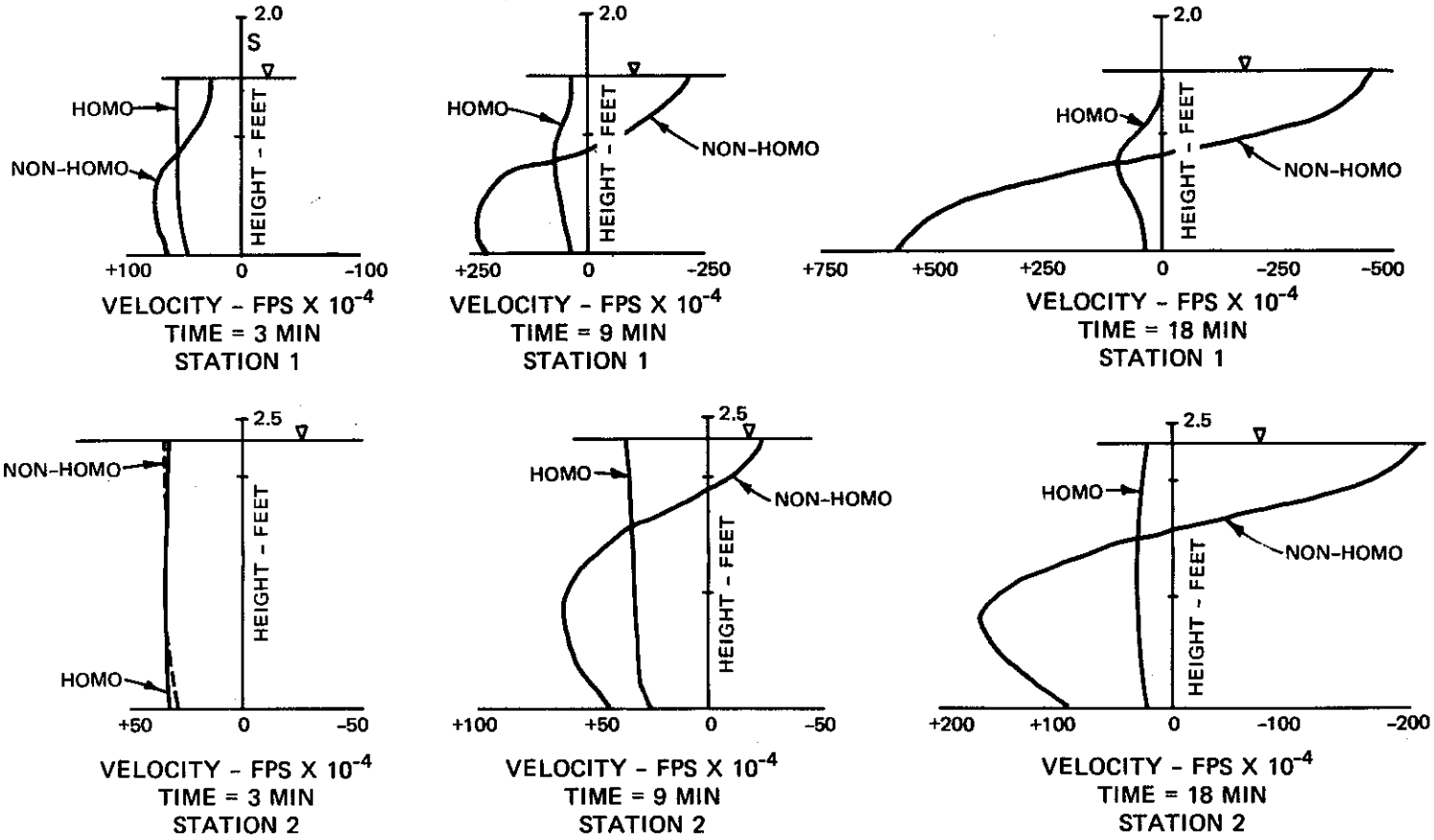

Figure 46. Comparison of homogeneous and nonhomogeneous simulated velocity distributions

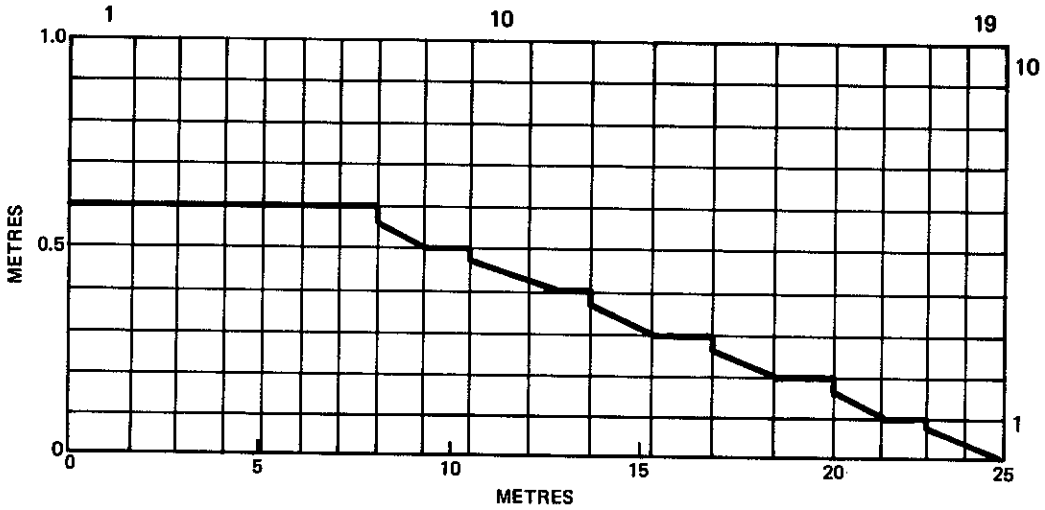

Figure 47. Schematization of GRH flume in Eraslan's application

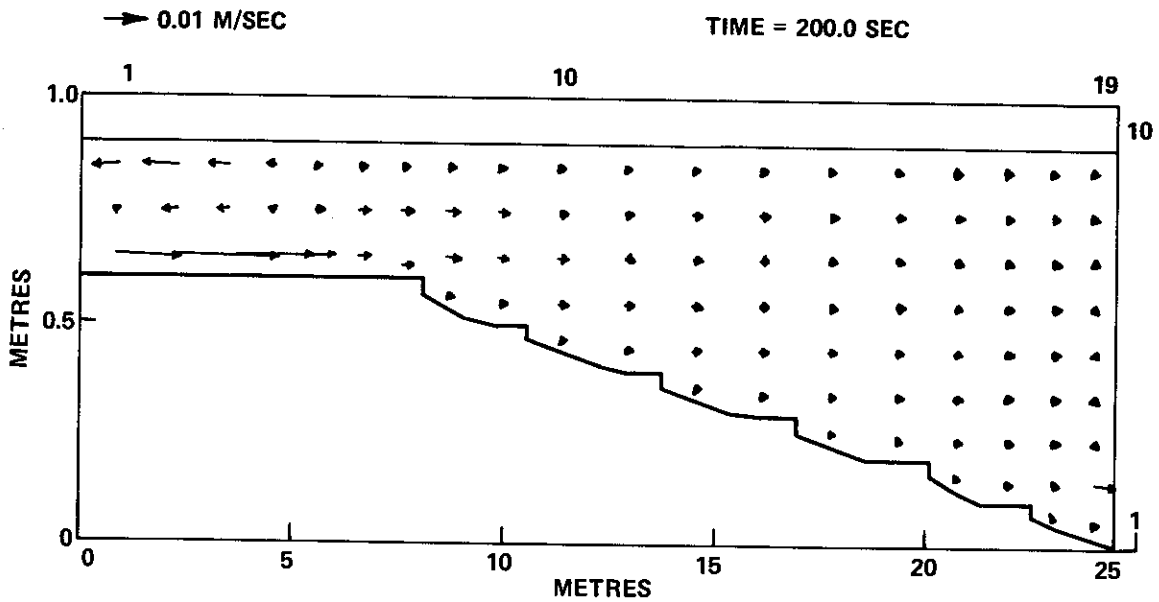

Figure 48. Velocities computed by Eraslan's Model at T = 200 sec, coldwater inflow

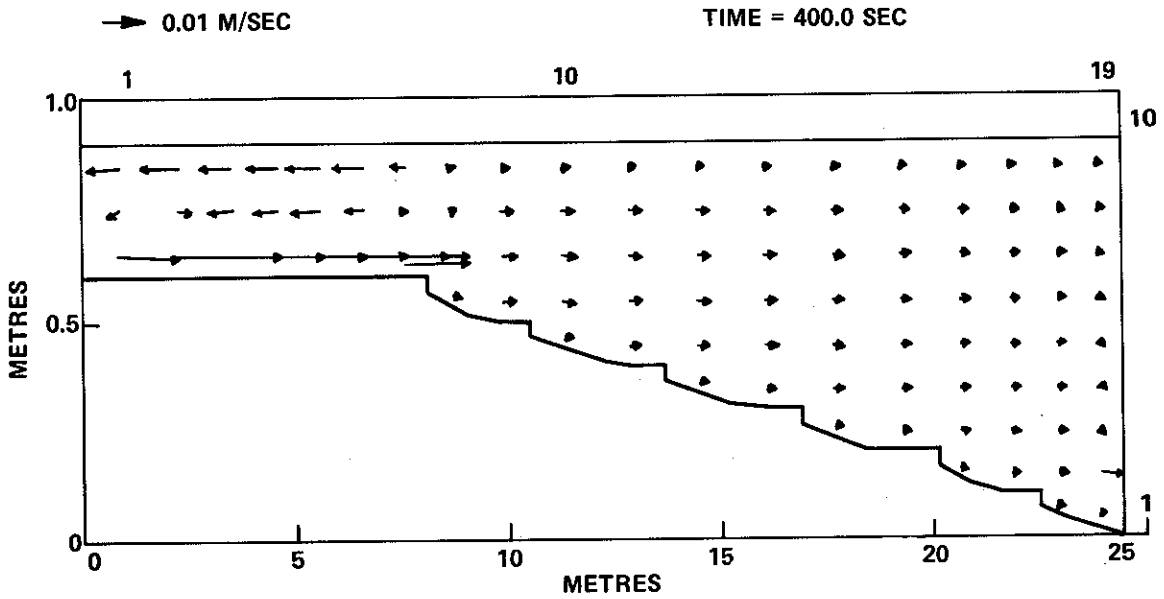

Figure 49. Velocities computed by Eraslan's Model at T = 400 sec, coldwater inflow

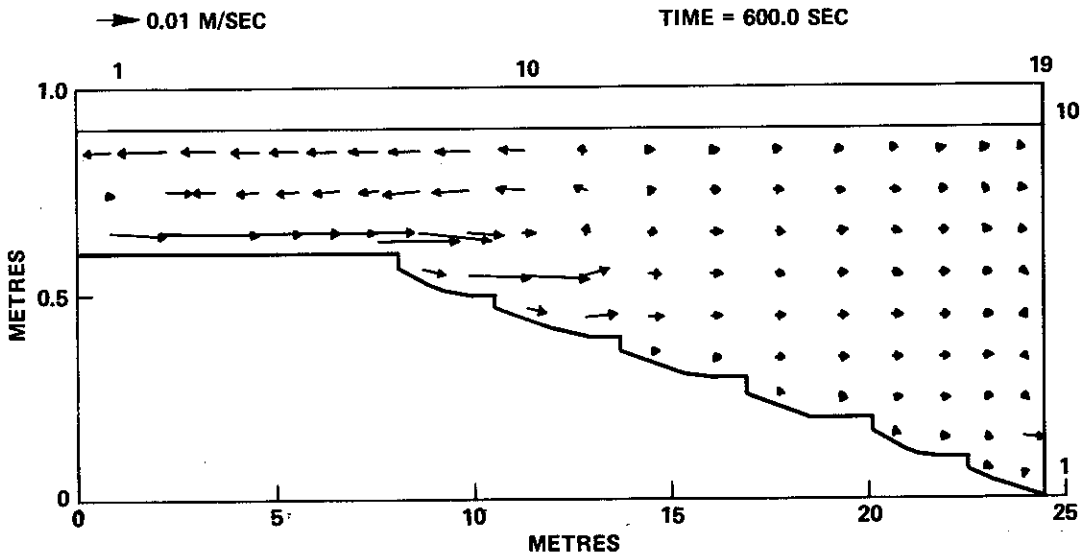

Figure 50. Velocities computed by Eraslan's Model at T = 600 sec, coldwater inflow

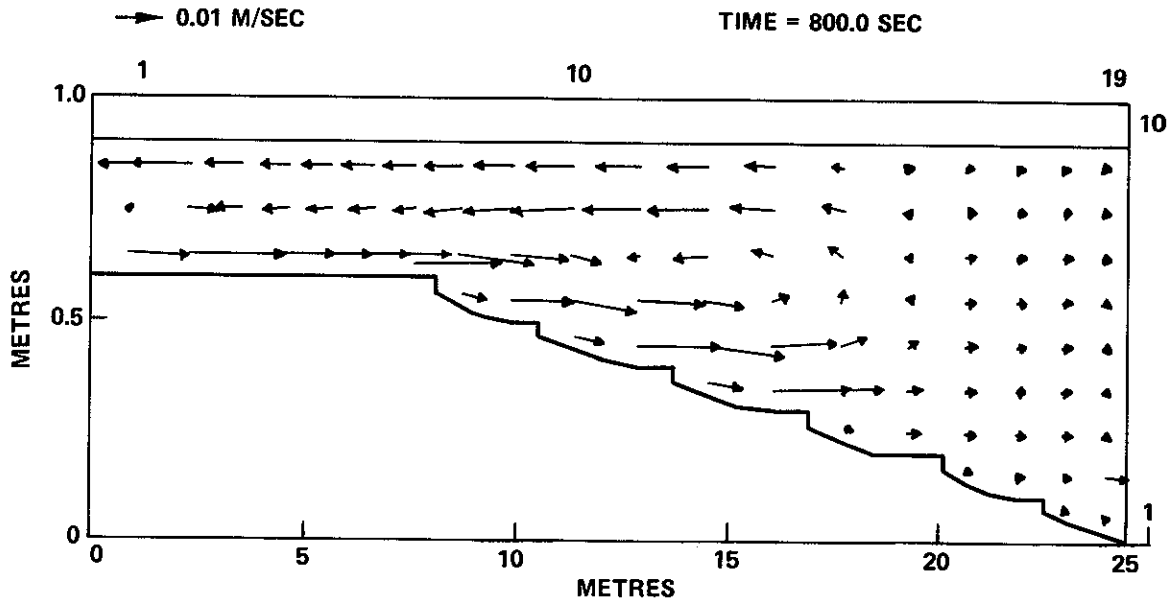

Figure 51. Velocities computed by Eraslan's Model at T = 800 sec, coldwater inflow

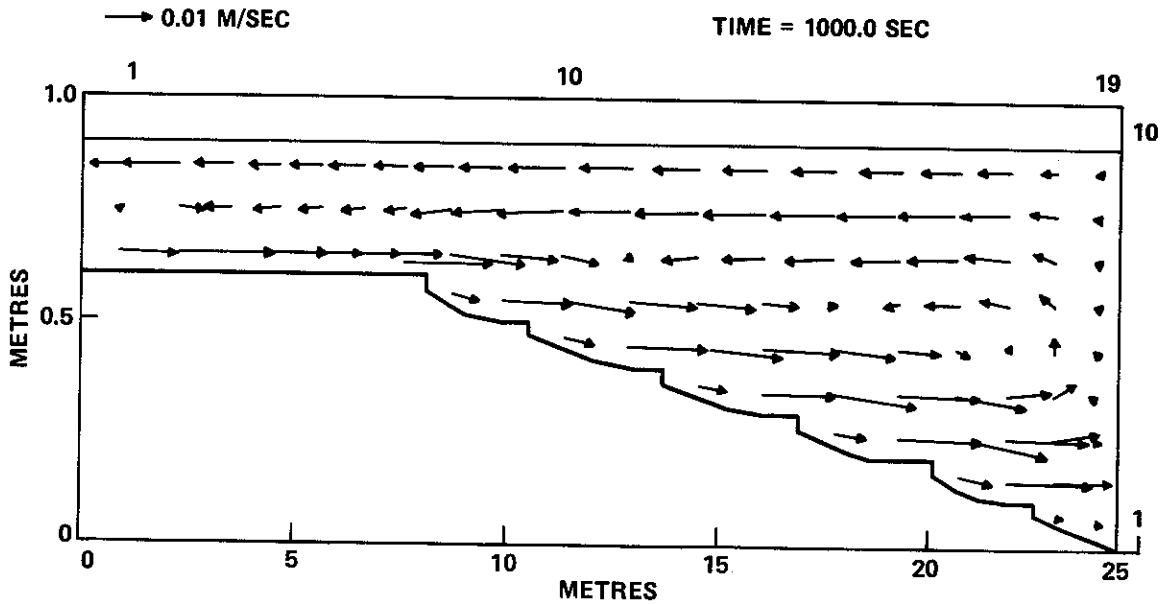

Figure 52. Velocities computed by Eraslan's Model at T = 1000 sec, coldwater inflow

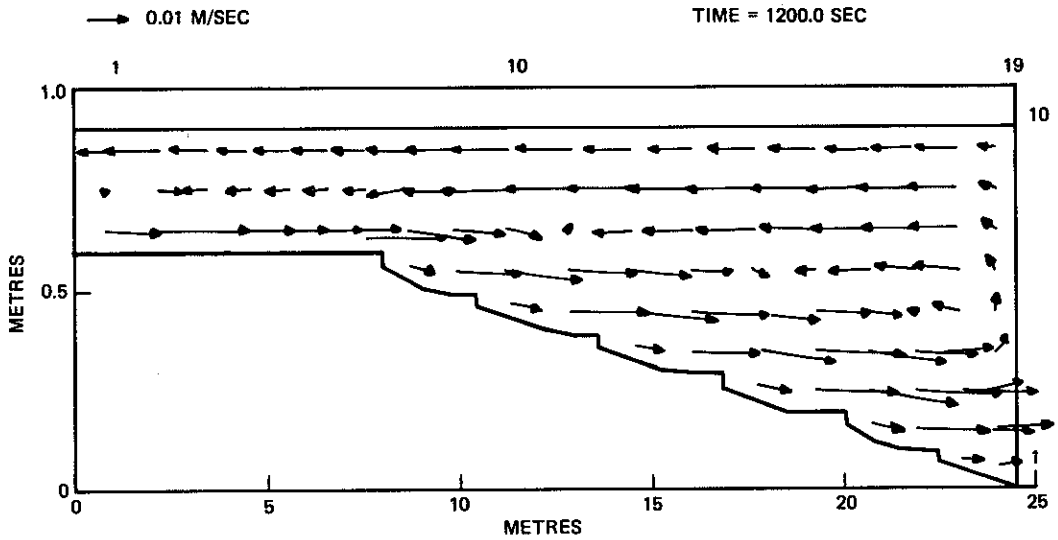

Figure 53. Velocities computed by Eraslan's Model at T = 1200 sec, coldwater inflow

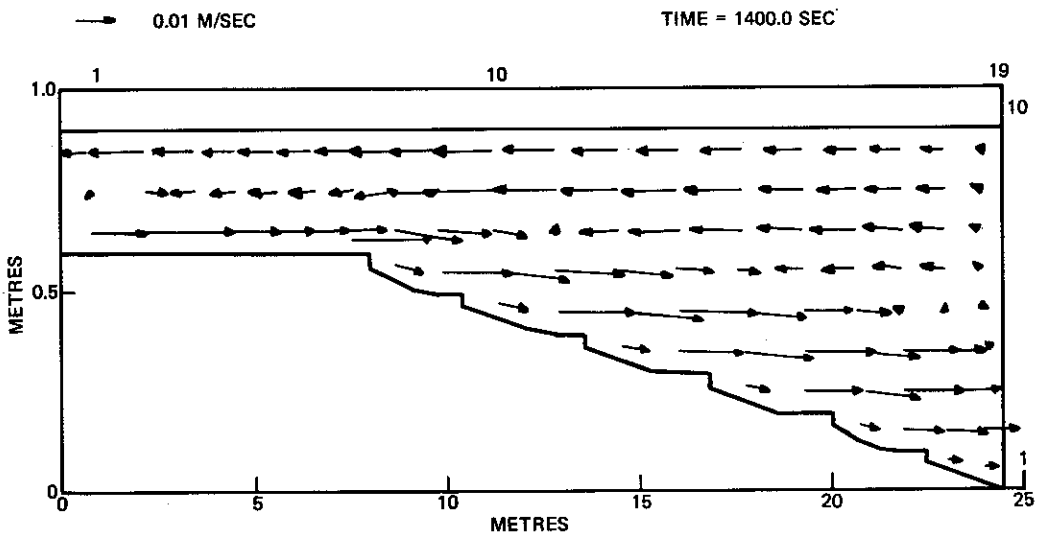

Figure 54. Velocities computed by Eraslan's Model at T = 1400 sec, coldwater inflow

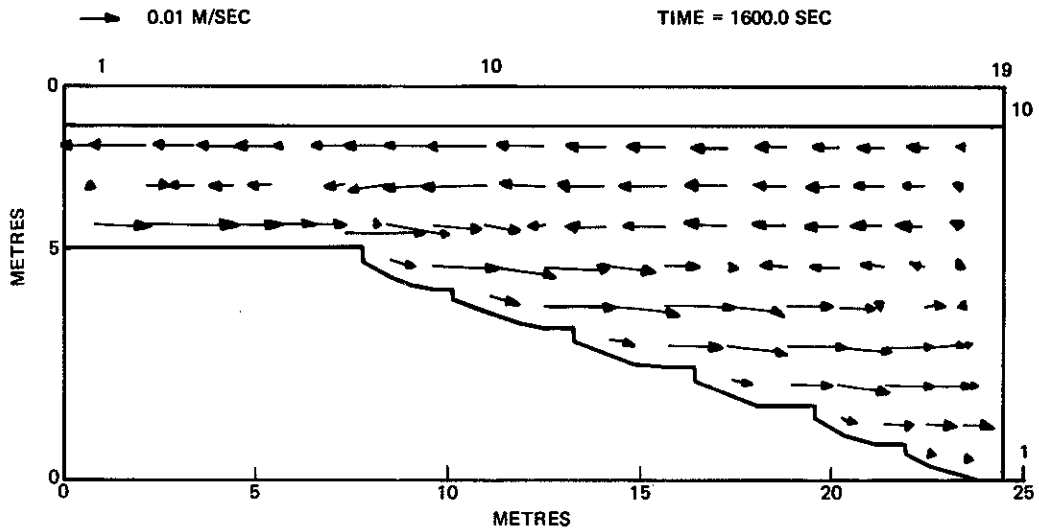

Figure 55. Velocities computed by Eraslan's Model at T = 1600 sec, coldwater inflow

specified over only the bottom half of the cross section rather than the complete section, a faster and less thick underflow current would have resulted.

247. As noted above, an additional simulation was made in which warm water at 70.6°F was input uniformly over the upstream end with the water in the flume initially being stationary and homogeneous at a temperature of 54.14°F. Figures 56-65 present "snap shots" at 200-sec intervals of the resulting 2-D flow field for 2000 sec after initiation of the inflow.

248. Since FLOWER is an explicit model, the time step is restricted by the gravity wave stability criterion based upon the deepest part of the flume. The results presented were obtained by Eraslan from running FLOWER on a PDP-10 computer.

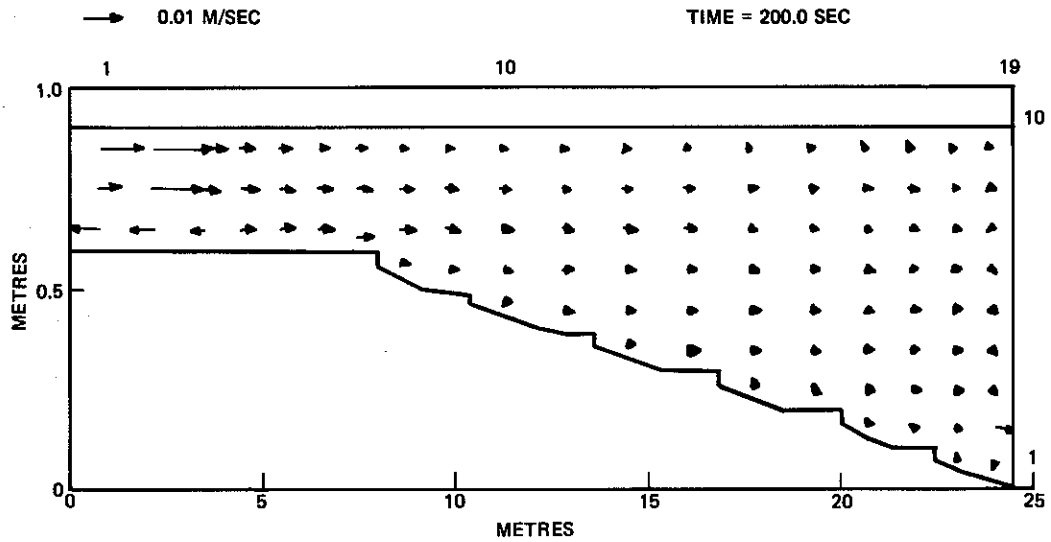

Figure 56. Velocities computed by Eraslan's Model at T = 200 sec, warmwater inflow

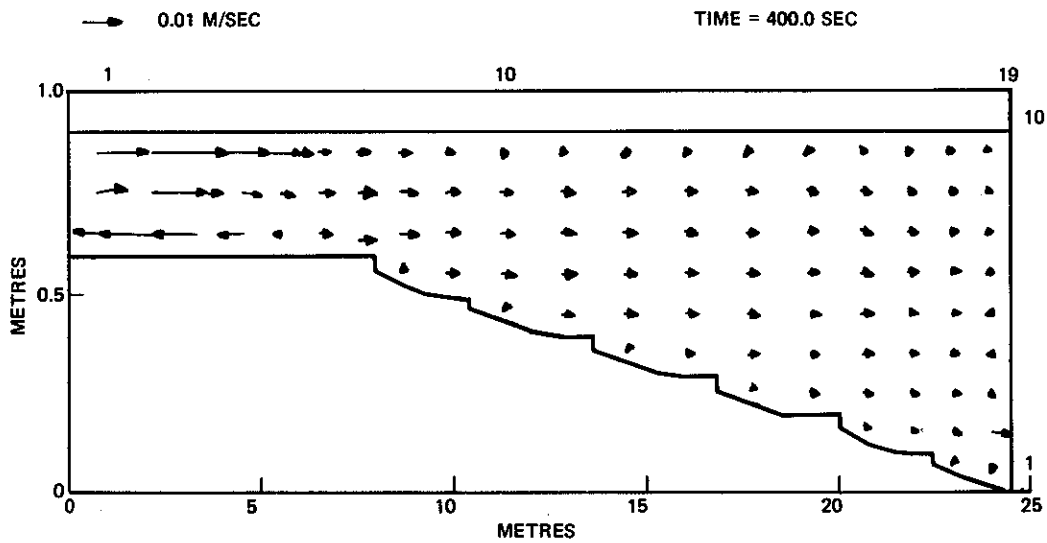

Figure 57. Velocities computed by Eraslan's Model at T = 400 sec, warmwater inflow

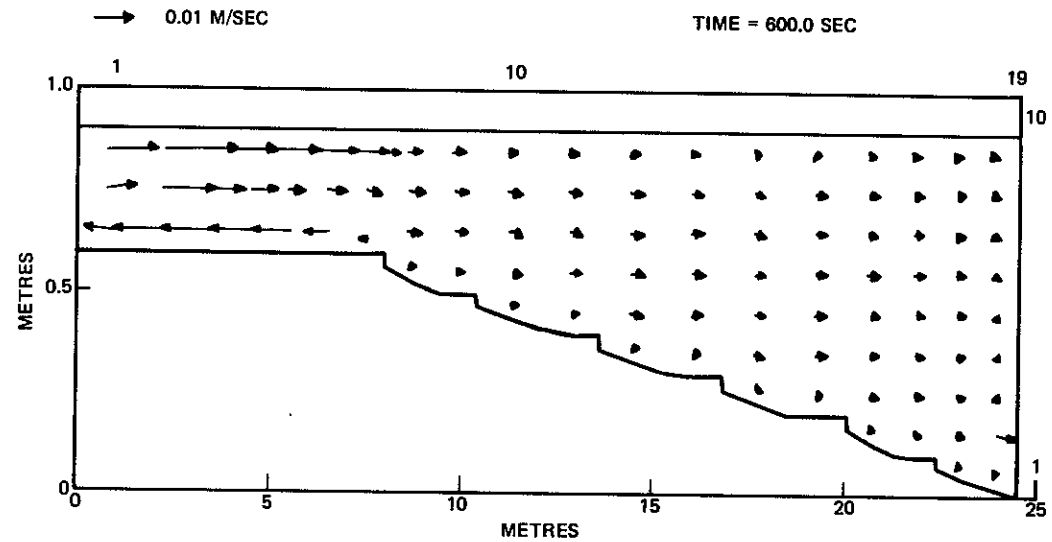

Figure 58. Velocities computed by Eraslan's model at T = 600 sec, warmwater inflow

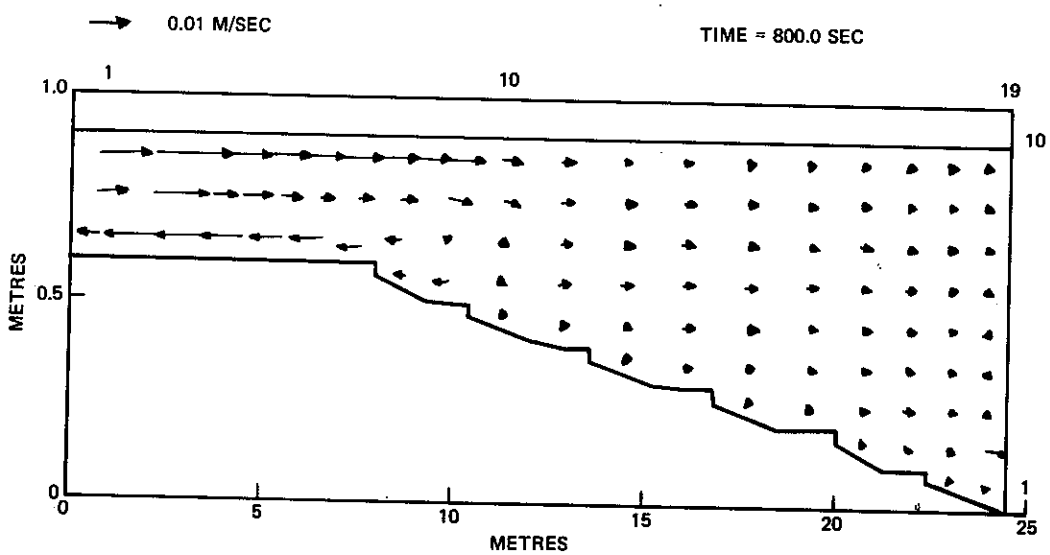

Figure 59. Velocities computed by Eraslan's model at T = 800 sec, warmwater inflow

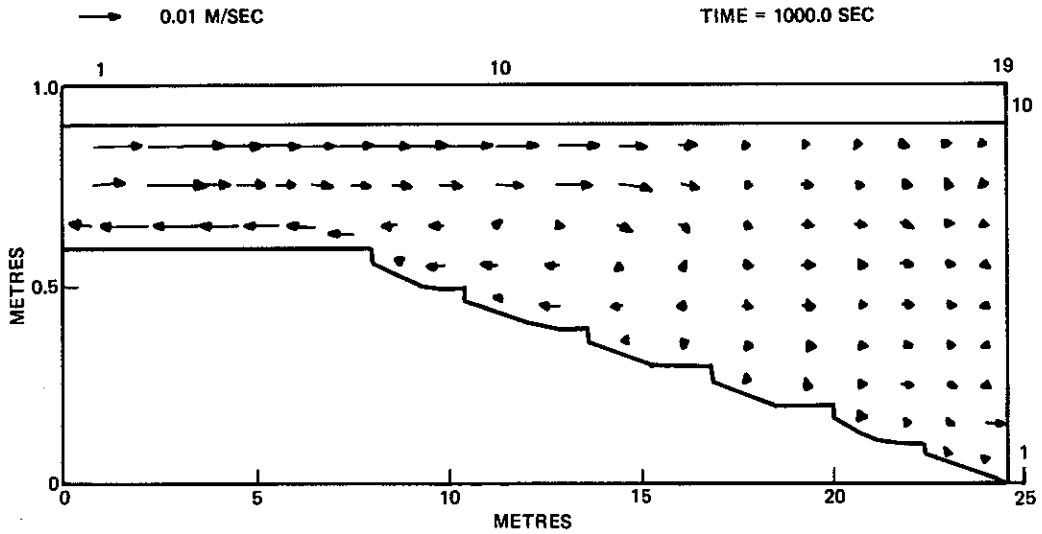

Figure 60. Velocities computed by Eraslan's Model at T = 1000 sec, warmwater inflow

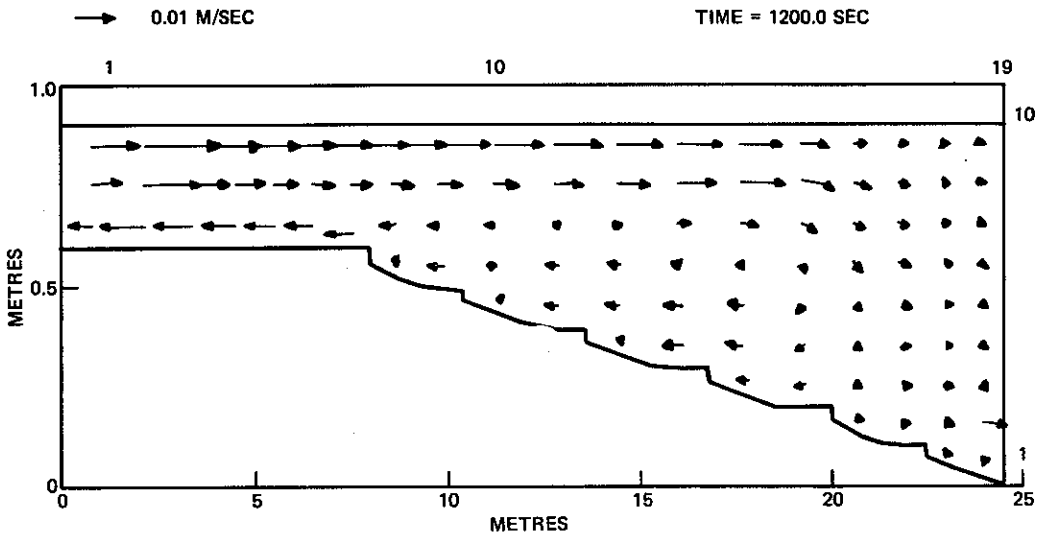

Figure 61. Velocities computed by Eraslan's Model at T = 1200 sec, warmwater inflow

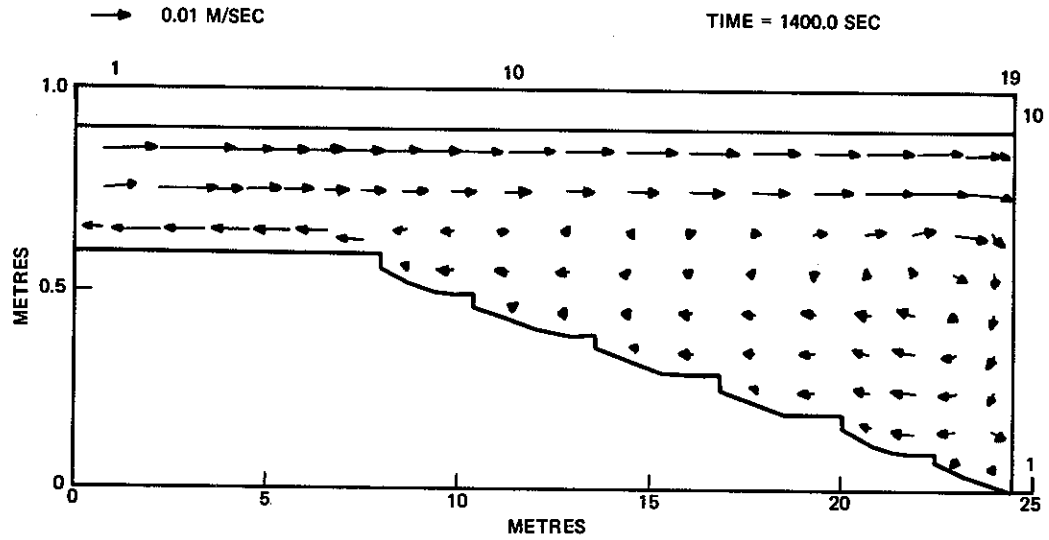

Figure 62. Velocities computed by Eraslan's Model at T = 1400 sec, warmwater inflow

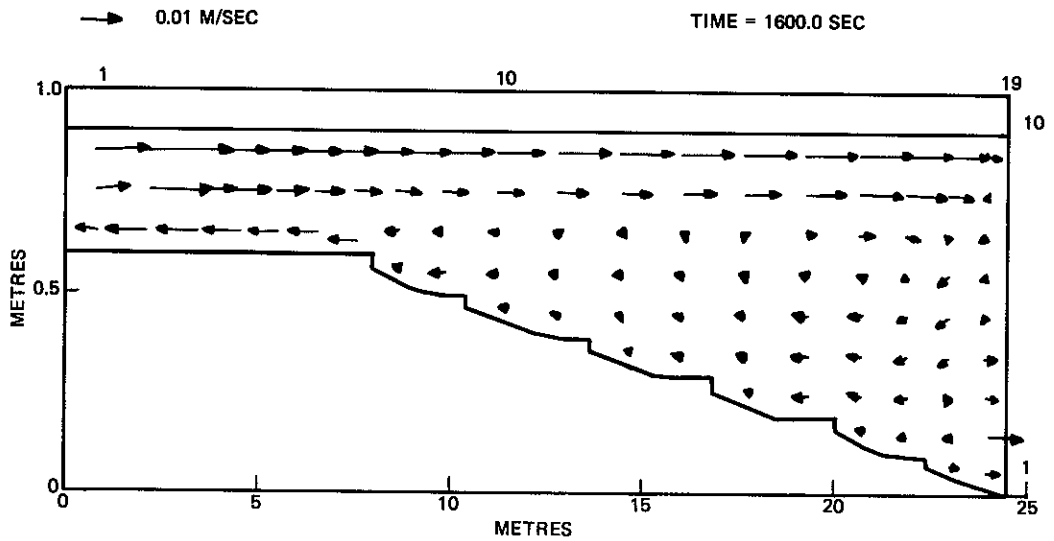

Figure 63. Velocities computed by Eraslan's Model at T = 1600 sec, warmwater inflow

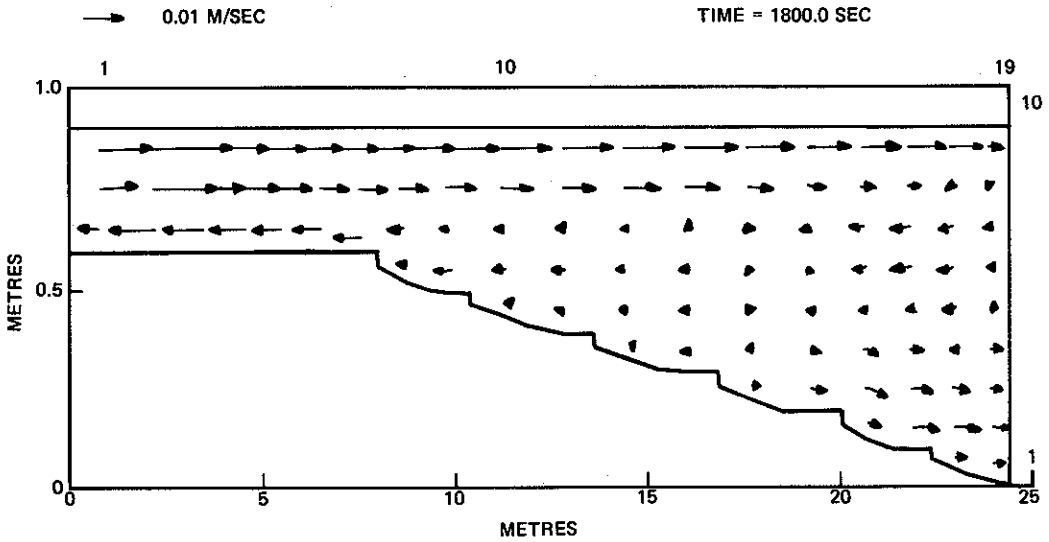

Figure 64. Velocities computed by Eraslan's Model at T = 1800 sec, warmwater inflow

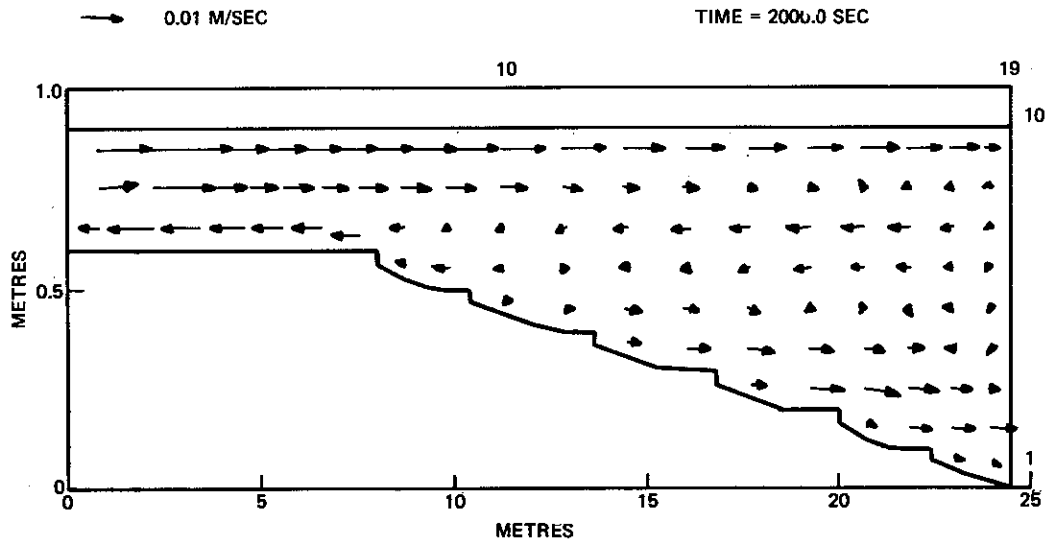

Figure 65. Velocities computed by Eraslan's Model at T = 2000 sec, warmwater inflow

PART VII: CONCLUSIONS AND RECOMMENDATIONS

249. Many different types of numerical hydrodynamic models exist. These range from steady to unsteady models with the physical problem area represented by one, two, or three spatial dimensions. In addition, some models consider the effect of temperature and/or salinity on the density of the water; whereas, others treat the water body as being homogeneous. Most numerical hydrodynamic models invoke the Boussinesq approximation as well as the hydrostatic pressure assumption; however, there are models that do neither and are thus able to convectively model buoyancy effects. Some models allow for the movement of a free surface and its subsequent effect on the internal flow; whereas, others impose a mathematical rigid-lid approximation to enable larger time steps to be employed in the numerical solution technique. A vast majority of the hydrodynamic models employ the finite difference method to develop numerical solutions, although there are existing models that employ the finite element method for the spatial integration of the governing fluid dynamic equations. The vast majority of numerical hydrodynamic models handle the exchange of energy from the large-scale circulation patterns to the small-scale unresolvable eddies through the use of eddy viscosity and diffusivity coefficients. However, there are substantial differences in the expressions used to relate these eddy coefficients to properties of the mean flow field.

250. One-dimensional models are often applied to reservoirs where the principal variation of flow characteristics is in the vertical direction. The primary advantage of such models is their ability to resolve long-term or seasonal temperature profiles economically. Such models, however, are not applicable for predicting multidimensional flow fields within stratified reservoirs for quality predictions. Therefore, only two- and three-dimensional models have been investigated in this study.

Conclusions on Two-Dimensional Modeling

251. In order for a numerical hydrodynamic model to be applicable

to the prediction of flow fields in stratified reservoirs, it must first of all be at least a two-dimensional (vertical-longitudinal) model and preferably one that is laterally averaged to account for width changes along the axis of the reservoir as well as with depth. The model must be dynamic, i.e., time-dependent, and must be a heat-conducting model that can handle unstable stratifications. In other words, surface heat exchange and a subsequent modeling of the temperature field and its coupling with the flow field through its influence on the water density must be handled. In addition, since the model will be applied over natural stratification cycles, during which significant flooding can occur, a free surface must be allowed as opposed to the rigid-lid approximation. These are necessary criteria. Considerations of accuracy and economy must naturally be taken into account also when selecting a model for widespread use throughout the Corps.

252. Of the various two-dimensional models investigated, six models come close to meeting the required criteria outlined above. These are the models of Edinger and Buchak; Waldrop; Thompson; Norton, King, and Orlob; Roberts and Street; and Slotta et al.'s NUMAC. The criteria satisfied by these models are summarized in Table 4. In addition, although an in-depth investigation has not been made due to a lack of published material as well as publication deadlines to be met, results from Eraslan's 2-D simulations imply that it also meets these criteria.

253. Thompson's laterally averaged model is being developed primarily for near field selective withdrawal studies. The governing equations are solved implicitly using an iterative technique. Thus, although the model will be a completely general, fully convective model that will accurately handle general boundaries through the use of boundary-fitted coordinates, the computing costs for long-term simulations will probably prohibit its use over natural stratification cycles in reservoirs.

254. The Roberts and Street model assumes a hydrostatic pressure but does handle unstable densities by allowing for a large diffusion of heat within the unstable water column. Of the six 2-D models that satisfy the necessary criteria, this model and NUMAC are the only

Table 4

Comparisons of Different Models

Model	Criteria						
	Dimensionality (3-D-LA 2-D)	Unsteady	Variable Density	Heat Conducting	Free Surface	Unstable Stratification	Economical for Long Simulation
Simons	x	x	x	x	x	x	--
Leendertse	x	x	x	--	x	x	--
Lick	x	x	x	x	--	x	--
Waldrop-Tatom	x	x	x	x	x	x	--
Spraggs-Street	x	x	x	x	x	x	--
Hamilton	?	x	x	--	x	x	--
Blumberg	x	x	x	--	x	x	--
Numac	--	x	x	?	?	x	--
Norton-King-Orlob	x	x	x	x	?	x	--
Thompson	x	x	x	x	?	x	--
Roberts-Street	--	x	x	x	x	x	--
Waldrop-Harper	x	x	x	x	x	x	--
Edinger-Buchak	x	x	x	x	x	x	x

pure 2-D models. The other four solve the laterally averaged equations. The major disadvantage of the Roberts and Street model lies in its use of a numerical solution technique that restricts the time step to be smaller than the time required for the surface gravity wave to traverse a computational cell. Such a restriction can result in excessive computer costs for applications extending over several months.

255. The Norton, King, and Orlob model is similar to the Thompson model in that the complete vertical momentum equation is solved. However, the Norton, King, and Orlob model uses the finite element method to perform the spatial integration of the governing equations. With the use of the finite element method, boundary geometry can be accurately handled but computing costs may become excessive for long-term simulations. Another disadvantage is that although a free surface is allowed, modifications would probably be required to allow for large fluctuations that might occur over a stratification cycle. With the complicated coding of finite element models, it appears that significant modifications can often become major tasks.

256. The NUMAC model is based upon the MAC work of Welch et al. and as such, like the Thompson and Norton, King, and Orlob models, is a completely convective model. Once again, however, the computing costs for long-term simulations would be excessive. Not only is a two-dimensional Poisson equation solved, but the basic computations utilize an explicit solution technique with the maximum time step restricted by the speed of the surface gravity wave.

257. The 2-D Waldrop model appears to be a well developed laterally averaged hydrostatic model that can be directly applied in its present form to predict stratified reservoir hydrodynamics. The manner in which the bottom boundary condition on the velocity is prescribed would seem to allow for a more accurate modeling of flow near the bottom. However, the bottom is still in essence represented in a stair-step fashion, which results in excessive mixing of density underflows. This can be seen from the results of the application to the GRH flume. The major disadvantage of the Waldrop model (and Eraslan's discrete element model) is the gravity wave restriction on

the time step as a result of the explicit finite difference scheme employed. As Waldrop has noted, if the boundary conditions are varying rapidly enough to require input at time intervals on the order of the maximum time step allowable by the Courant condition, explicit models can often be shown to be more economical than implicit ones due to their less complicated coding. However, if an extremely general model is desired for use in long-term reservoir simulations during which boundary input may or may not be rapidly varying, it appears difficult to justify the selection of a model with the time step restricted by the Courant condition.

258. The Edinger and Buchak model (LARM) is a laterally averaged, hydrostatic model that employs a unique method for removing the Courant condition as a stability criterion. This is accomplished through a coupling of the water surface computations and the internal flow such that the water surface is computed implicitly, while the internal computations are performed explicitly. Unstable stratifications are indirectly handled by forcing the maximum diffusion allowed by the stability criterion into adjacent cells. Results from applications of both the Edinger and Buchak and the Waldrop 2-D models to the GRH flume are encouraging. In addition, the results from the 2-D version of Eraslan's 3-D code agreed quite well with the flow phenomena observed in the flume for his input conditions.

259. There are several areas of the Edinger and Buchak model that should be investigated for possible further development. With its modular programming, significant modification of the model should not be unduly difficult. These areas are discussed later. Because the Edinger and Buchak model satisfies the necessary criteria--namely, time-dependent, free surface, 2-D laterally averaged, variable density and heat-conducting--and allows for unstable stratification and the solution technique allows for economical long-term simulations, it is the most logical 2-D model to select for further development to provide the Corps with an accurate and economical predictive capability in the area of reservoir hydrodynamics.

Conclusions on Three-Dimensional Modeling

260. The state of the art is such that it does not appear any of the three-dimensional models investigated can be economically applied for long-term reservoir simulations. However, since most reservoirs actually exhibit a three-dimensional nature, undoubtedly the need within the Corps for a three-dimensional predictive capability will increase over the next few years. To satisfy this need in a practical sense, new solution techniques as well as increased computing power must be realized. In addition, one should consider making the hydrostatic pressure assumption to remove the computing cost of solving for a nonhydrostatic pressure.

261. Neither of the 3-D models applied to the GRH flume yielded very encouraging results. Spraggs was not able to simulate more than 600 sec with THERMAC due to the extremely long computing times required. The nonhydrostatic version of the Waldrop-Tatom model was run with the free surface frozen, which allowed a large time step to be used. However, the density underflow was not properly computed. After 33 min, the model computed a travel of only approximately 10.06 m; whereas, only 18 min was required in actuality for the underflow to traverse the complete length of the flume (23.93 m). Tatom feels that the problem is related in some manner to the dynamic pressure computations. Therefore, if time and funds had permitted, it would have been interesting to apply the hydrostatic version to the same density underflow problem.

Recommendations for Two-Dimensional Modeling

262. As noted above, it is believed that the Edinger and Buchak 2-D laterally averaged model offers the most promise in the area of multidimensional stratified reservoir hydrodynamic modeling in the near future. However, additional developmental work and modifications are needed to make the model more flexible and accurate; therefore, it is recommended that the following items be investigated during the next year for possible further development and incorporation into LARM:

a. The application to the density underflow in the GRH flume demonstrates the mixing effect of a stair-stepped bottom. It is believed that a transformation of the vertical coordinate, as is performed in Lick's model, offers one solution to this problem. Particular attention should be directed toward the neglection of the cross-derivative terms resulting from the non-orthogonal transformation.

b. LARM presently allows for the vertical eddy coefficients to be functions of the Richardson number; however, the horizontal coefficients are assumed to be constant. It is recommended that an eddy coefficient model similar to that of Spraggs or perhaps the simpler model employed by Waldrop and Harper (or perhaps Eraslan's closed turbulence model) be incorporated into LARM. This should be relatively easy to accomplish, since the computer code was initially programmed with such an addition in mind.

c. LARM presently employs either windward or centered differences to represent the advective terms in both the momentum and the temperature transport equations along with a forward time difference. Such a first order transport scheme is adequate for continuous distributions. However, if instead of an essentially continuous distribution, a slug of some quality constituent is to be traced through the reservoir, large errors can result from the use of such first order schemes. Therefore, it is recommended that higher order transport schemes such as those employed by DHI or perhaps the 2-point scheme of Holly and Preissman be investigated for use in the modeling of quality constituents, rather than the scheme LARM presently uses for temperature.

d. It would seem that Waldrop's method of setting the bottom boundary condition on velocity by matching a logarithmic profile is quite realistic. It is recommended that the use of such a boundary condition in LARM be investigated. The layer-averaged approach taken in LARM may make this difficult.

e. The horizontal grid spacing in LARM is constant. A variable grid spacing would be useful to provide greater flexibility in the resolution of a quality constituent in a particular area. The difficulty in allowing this and the subsequent errors that might occur should be determined. Obviously, the linear averaging now employed to provide values of variables at points where they are not defined would have to be changed to reflect a weighted average. Also, as discussed by Brown and Pandolfo (1979), a nonuniform spatial grid can influence

the numerical stability of the transport equation. Recall also the deterioration of the truncation error associated with variable grids.

f. LARM models a single reach, i.e., the reach following the major axis of the reservoir. A desirable flexibility is the ability to simultaneously model the main body of the reservoir as well as its major arms or tributaries, i.e., to allow for a tree structure or branched network. The possibility of making LARM a multijunction model should be considered.

g. The applicability of LARM at the downstream end of a reservoir near the dam is questionable due to the hydrostatic pressure assumption as well as the inaccurate modeling of the momentum flux through the outlet. The hydrostatic pressure assumption is probably acceptable, except in the immediate vicinity of the outlet; whereas, the inaccurate modeling of the momentum flux as a result of the model being less than three-dimensional might extend for several dam widths. The use of a momentum correction factor to better model the momentum flux near the dam should be investigated. In addition, the coupling with LARM of a model that is more applicable near the vicinity of an outlet, e.g., Bohan and Grace (1969), to provide the downstream boundary condition for LARM might be considered.

h. LARM has been developed such that the user has to "hard wire," i.e., physically change code statements, the model for each application, although the version being run by WES personnel has been modified to provide a slightly more general model. It is not believed that the current approach of forcing a user to change code statements for each application is acceptable in a model to be made available to all Corps Division and District offices. Therefore, LARM should be made sufficiently general so that it can be applied to a wide range of problems strictly through a change of input data only.

i. In the modeling of real reservoirs, one often encounters side embayments that contribute essentially nothing to the momentum of the flow field, but must still be accounted for as storage areas in the conservation of mass. More accurate computations would be realized if LARM allowed for the specification of two widths. One for the total width that is currently input, which would continue to be used in the continuity equation. The other would be a width corresponding to the actual flow area for use in the momentum equation.

j. In the use of numerical hydrodynamic models, the initial state of the system as well as time-varying boundary conditions must be prescribed as input. The nature of the hyperbolic equations being solved is such that after a sufficient length of time, the effect of the initial conditions becomes negligible. The time simulated to remove initial condition effects is commonly referred to as the "start-up time." One way to handle this problem is to compute a steady state before imposing the time variation of the boundary conditions. LARM presently can only compute a steady state as the asymptotic convergence of a time-varying solution computed by holding the boundary conditions constant. The possibility of incorporating into LARM the capability of solving the steady-state equations, as allowed by the Norton, King, and Orlob FEM, should be investigated. After the above modifications are made, in particular Lick's transformation to allow for better representation of the bottom, LARM should again be applied to the density underflow problem in the GRH flume. In addition, hopefully a good set of field data will be available by then through EWQOS. Assuming an eddy coefficient model similar to that of Spraggs and Street (1975) has been incorporated, these two applications should provide information on whether a single scaling parameter can be used for a wide range of problems.

Recommendations for Three-Dimensional Modeling

263. Unlike the two-dimensional models, there are no three-dimensional models that can economically be applied for long-term reservoir simulations. This is because all of the models are explicit, and thus excessive computing time is required. Imposing the rigid-lid approximation removes the Courant condition on the time step, but results in a Poisson equation for the pressure that must be solved, which can be costly in itself. Making the hydrostatic pressure assumption helps in that only a 2-D Poisson equation rather than a full 3-D Poisson equation must be solved. However, it is not believed that the rigid-lid approximation is appropriate for models to be used over flooding cycles; therefore, new solution techniques that allow for a free surface but remove the speed of a gravity wave from the stability criteria must be devised.

264. The Spraggs and Street (1975) model currently solves for the free surface implicitly, but does not implicitly couple the internal flow to these computations. It is recommended that a coupling similar to that in Edinger and Buchak's (1979) work, but now in two dimensions, be investigated during the next year. If this can be accomplished in an efficient manner, long-term three-dimensional free surface hydrodynamic modeling will have taken a giant step forward.

REFERENCES

Abbott, M. B. 1979. Computational Hydraulics, Pitman Publishing Limited, London.

Adams, Charles W., Associates, Inc. 1967. "Computer Characteristics Table," Digital Computer User's Handbook, Melvin Klerer and Gramino Korn, editors, McGraw-Hill, New York.

Blumberg, A. F. 1975. "A Numerical Investigation into the Dynamics of Estuarine Circulation," TR-91, Chesapeake Bay Institute, John Hopkins University.

Blumberg, A. F. and Mellor, G. L. 1979. "A Whole Basin Model of the Gulf of Mexico," submitted to "Sixth OTEC Conference Ocean Energy for the 80's," Department of Energy, Washington, D. C.

Bohan, J. P. and Grace, J. L. 1969. "Mechanics of Flow from Stratified Reservoirs in the Interest of Water Quality," Technical Report H-69-10, U. S. Army Engineer Waterways Experiment Station, Vicksburg, Miss.

Bonham-Carter, G. et al. 1973. "A Numerical Model of Steady Wind-Driven Currents in Lake Ontario and the Rochester Embayment Based on Shallow-Lake Theory," University of Rochester, Rochester, N.Y.

Boris, J. P. and Book, D. L. 1973. "Flux-Corrected Transport. I: SHASTA, A Fluid Transport Algorithm that Works," Journal of Computational Physics 11, pp 38-69.

Brown, P. S. and Pandolfo, J. P. 1979. "Numerical Stability of the Combined Advection-Diffusion Equation with Nonuniform Spatial Grid," Monthly Weather Review, Vol 107, No. 8.

Chan, R. K.-C and Street, R. L. 1970. "SUMMAC-A Numerical Model for Water Waves," TR-135, Department of Civil Engineering, Stanford University.

Deardorff, J. W. 1970. "A Numerical Study of Three-Dimensional Turbulent Channel Flow at Large Reynolds Numbers," Journal, Fluid Mechanics, Vol 41, Part 2.

Edinger, J. R. and Buchak, E. M. 1979. "A Hydrodynamic Two-Dimensional Reservoir Model: Development and Test Application to Sutton Reservoir, Elk River, West Virginia," prepared for U. S. Army Engineer Division, Ohio River.

Fix, G. J. 1975. "A Survey of Numerical Methods for Selected Problems in Continuum Mechanics," Numerical Models of Ocean Circulation, National Academy of Science, Washington, D. C.

Gedney, R. T. and Lick, W. 1970. "Numerical Calculations of the Steady State, Wind Driven Currents in Lake Erie," Proceedings, Thirteenth Conference on Great Lakes Research, International Association for Great Lakes Research, pp 829-838.

Hamilton, P. 1975. "A Numerical Model of the Vertical Circulation of Tidal Estuaries and Its Application to the Rotterdam Waterway," Geophys. J. R. Astr. Soc., Vol 40, pp 1-21.

Harleman, D. R. F. 1966. "Stratified Flow," Proceedings of the Boston Society of Civil Engineers, Vol 53, No. 1.

Hinstrup, P. et al. 1977. "A High Accuracy Two-Dimensional Transport-Dispersion Model for Environmental Applications," Proceedings, Seventeenth Congress of the International Association for Hydraulic Research, Vol 3, pp 129-138.

Holley, E. R. 1969. "Unified View of Diffusion and Dispersion," Journal of the Hydraulics Division, Proceedings, ASCE, Vol 95, No. HY2.

Holly, F. M. and Preissman, A. 1977. "Accurate Calculation of Transport in Two Dimensions," Journal of Hydraulics Division, ASCE, Vol 103, No. HY11.

Johnson, B. H. and Thompson, J. F. 1978. "A Discussion of Boundary-Fitted Coordinate Systems and Their Applicability to the Numerical Modeling of Hydraulic Problems," Miscellaneous Paper H-78-9, U. S. Army Engineer Waterways Experiment Station, Vicksburg, Miss.

Kreiss, H. O. 1975. "A Comparison of Numerical Methods Used in Atmospheric and Oceanographic Applications," Numerical Models of Ocean Circulation, National Academy of Sciences, Washington, D. C.

Leendertse, J. J. 1967. "Aspects of a Computational Model for Long-Period Water-Wave Propagation," RM-5294-PR, The Rand Corporation, Santa Monica, Calif.

Leendertse, J. J. et al. 1973. "A Three-Dimensional Modél for Estuaries and Coastal Seas: Vol 1, Principles of Computation," R-1417-OWRR, Rand Corporation, Santa Monica, Calif.

Leith, C. E. 1975. "Future Computing Machine Configurations and Numerical Models," Numerical Models of Ocean Circulation, National Academy of Sciences, Washington, D. C.

Lick, Wilbert. 1976. "Numerical Models of Lake Currents," EPA-600/3-76-020, U. S. Environmental Protection Agency, Office of Research and Development, Environmental Research Laboratory, Duluth, Minn.

Liggett, J. A. 1970. "Cell Method for Computing Lake Circulation," Journal of the Hydraulics Division, ASCE.

MacArthur, R. C. 1979. "Application and Evaluation of Two Multidimensional Reservoir Models; LARM and RMA-7," Research Report, the Hydrologic Engineering Center.

Masch, F. D. et al. 1969. "A Numerical Model for the Simulation of Tidal Hydrodynamic in Shallow Irregular Estuaries," TR-HYD-12-6901, Hydraulics Engineering Laboratory, University of Texas, Austin, Tex.

Mellor, G. L. and Yamada, T. 1977. "A Turbulence Model Applied to Geophysical Fluid Problems," Proceedings: Symposium on Turbulent Shear Flows, Pennsylvania State University, University Park, Penn.

Norton, W. R., King, I. P., and Orlob, G. T. 1973. "A Finite Element Model for Lower Granite Reservoir," prepared for Walla Walla District, U. S. Army Corps of Engineers.

Orianski, I. 1976. "A Simple Boundary Condition for Unbounded Hyperbolic Flows," Journal of Computational Physics, Vol 21.

Parker, F. L. et al. 1975. "Evaluation of Mathematical Models for Temperature Prediction in Deep Reservoirs," EPA-660/3-75-038, National Environmental Research Center, Office of Research and Development, U. S. Environmental Protection Agency, Corvallis, Oreg.

Phillips, N. A. 1959. "An Example of Non-Linear Computational Instability," The Atmosphere and the Sea in Motion, Rockfeller Institute Press in association with Oxford University Press, New York, pp 501-504.

Reid, R. O. and Bodine, B. R. 1968. "Numerical Model for Storm Surges in Galveston Bay," Journal Waterways of Harbors Division, Proceedings, ASCE, Vol 94, No. WW1.

Roache, P. J. 1972. Computational Fluid Mechanics, Hermosa Publishers, Albuquerque, N. Mex.

Roberts, B. R. and Street, R. L. 1975. "Two-Dimensional Hydrostatic Simulation of Thermally-Influenced Hydrodynamic Flows," TR-194, Department of Civil Engineering, Stanford University.

Simons, T. J. 1973. "Development of Three-Dimensional Numerical Models of the Great Lakes," Scientific Series No. 12, Canada Center for Inland Waters, Burlington, Ontario.

Slotta, L. S. et al. 1969. "Stratified Reservoir Currents," Bulletin No. 44, Engineering Experiment Station, Oregon State University, Corvallis, Oreg.

Spraggs, L. D. and Street, R. L. 1975. "Three-Dimensional Simulation of Thermally-Influenced Hydrodynamic Flows," TR-190, Department of Civil Engineering, Stanford University.

Tatom, F. B. and Smith, S. R. 1978. "Near-Field Model for Brine Diffusion at West Hackberry," prepared for Department of Energy, Strategic Petroleum Reserve Program.

_____. 1979a. "Three-Dimensional Computer Simulation of Cold Water Inflow," prepared for U. S. Army Engineer Waterways Experiment Station, Vicksburg, Miss.

_____. 1979b. "Vectorization of 3-D PLUME for the Advanced Scientific Computer," prepared for U. S. Army Engineer Waterways Experiment Station, Vicksburg, Miss.

Thompson, J. F. et al. 1974. "Automatic Numerical Generation of Body-Fitted Curvilinear Coordinate System for Field Containing Any Number of Arbitrary Two-Dimensional Bodies," Journal of Computational Physics, Vol 15, No. 3.

Waldrop, W. R. and Farmer, R. C. 1976. "A Computer Simulation of Density Currents in a Flowing Stream," International Symposium on Unsteady Flow in Open Channels.

Waldrop, W. R. and Tatom, F. B. 1976. "Analysis of the Thermal Effluent from the Gallatin Steam Plant During Low River Flows," Report No. 33-30, Tennessee Valley Authority.

Ward, G. H. and Espey, W. H. 1971. "Estuarine Modeling: An Assessment," TRACOR, Inc., Austin, Tex., for the Water Quality Office, Environmental Protection Agency.

Welch, J. E. et al. 1966. "The MAC Method," Los Alamos Scientific Laboratory, University of California.

APPENDIX A: NUMERICAL RESULTS FROM APPLICATION OF 3-D PLUME TO GRH FLUME

1. The nonhydrostatic version of the Waldrop-Tatom (1976)* model was used to generate a numerical solution to the density underflow problem in the GRH flume. Values of various input parameters are presented in Table A1. In an effort to increase the computational time step, and thereby reduce the number of steps required, the free surface was initially assigned zero slope and was "frozen" for all subsequent computations.

2. With a time step of 0.5 sec, the numerical solution was marched forward for 4000 time steps corresponding to 2000 sec of real time in the flume. Outputs of velocity, in terms of the u, v, and w components, and temperature, as taken from Tatom and Smith (1979a), are presented at 0, 1000, and 2000 sec in Tables A2 through A13.

* References used in the appendixes of this report are listed in the References section at the end of the main text.

Table A1

3-D Flume Input

Parameter	Value
Inlet volumetric flow rate	0.02228 ft^3/sec
Exit volumetric flow rate	0.02228 ft^3/sec
Inlet area	0.5 ft^2
Outlet area	0.25 ft^2
Inlet velocity	0.04456 ft/sec
Outlet velocity	0.08912 ft/sec
Initial ambient velocity	0 ft/sec
Inlet temperature	61.97°F
Initial ambient temperature	70.79°F
Inlet density	62.358 lbm/ft^3
Initial ambient density	62.298 lbm/ft^3
Inlet equivalent diameter	0.67 ft
Inlet kinematic viscosity	$1.19 \cdot 10^{-5}$ ft^2/sec
Inlet Reynolds number	2496
Chezy coefficient	13.75 $ft^{1/2}/sec$
Fanning friction factor	0.00497
Water depth at inlet	1 ft
Water depth at outlet	3 ft

Table A2

Region 1 Predicted Velocity and Temperature Distribution in Vertical Plane (I = 2) at Time = 0 sec

X-VELOCITY COMPONENT, U (FT/SEC)

J=	1	2	3
K=13	-0.0000	0.0000	0.0000
K=12	-0.0000	0.0000	0.0000
K=11	0.0000	0.0000	0.0000
K=10	0.0000	0.0000	0.0000
K= 9	**********	**********	**********
K= 8	**********	**********	**********
K= 7	**********	**********	**********
K= 6	**********	**********	**********
K= 5	**********	**********	**********
K= 4	**********	**********	**********
K= 3	**********	**********	**********
K= 2	**********	**********	**********
K= 1	**********	**********	**********

Y-VELOCITY COMPONENT, V (FT/SEC)

J=	1	2	3
K=13	0.0000	0.0000	0.0000
K=12	0.0000	0.0000	0.0000
K=11	0.0000	0.0000	0.0000
K=10	0.0000	0.0000	0.0000
K= 9	**********	**********	**********
K= 8	**********	**********	**********
K= 7	**********	**********	**********
K= 6	**********	**********	**********
K= 5	**********	**********	**********
K= 4	**********	**********	**********
K= 3	**********	**********	**********
K= 2	**********	**********	**********
K= 1	**********	**********	**********

Z-VELOCITY COMPONENT, W (FT/SEC)

J=	1	2	3
K=13	0.0000	0.0000	0.0000
K=12	0.0000	0.0000	0.0000
K=11	0.0000	0.0000	0.0000
K=10	0.0000	0.0000	0.0000
K= 9	**********	**********	**********
K= 8	**********	**********	**********
K= 7	**********	**********	**********
K= 6	**********	**********	**********
K= 5	**********	**********	**********
K= 4	**********	**********	**********
K= 3	**********	**********	**********
K= 2	**********	**********	**********
K= 1	**********	**********	**********

TEMPERATURE (^{o}F)

J=	1	2	3
K=13	70.8	70.8	70.8
K=12	70.8	70.8	70.8
K=11	62.0	70.8	70.8
K=10	62.0	70.8	70.8
K= 9	**********	**********	**********
K= 8	**********	**********	**********
K= 7	**********	**********	**********
K= 6	**********	**********	**********
K= 5	**********	**********	**********
K= 4	**********	**********	**********
K= 3	**********	**********	**********
K= 2	**********	**********	**********
K= 1	**********	**********	**********

Table A3

Region 2 Predicted Velocity and Temperature Distribution in Vertical Plane (I = 2) at Time = 0 sec

X-VELOCITY COMPONENT, U (FT/SEC)

J=	1	2	3	4
K=13	0.0000	0.0000	0.0000	0.0000
K=12	0.0000	0.0000	0.0000	0.0000
K=11	0.0000	0.0000	0.0000	0.0000
K=10	0.0000	0.0000	0.0000	0.0000
K= 9	**********	**********	**********	**********
K= 8	**********	**********	**********	**********
K= 7	**********	**********	**********	**********
K= 6	**********	**********	**********	**********
K= 5	**********	**********	**********	**********
K= 4	**********	**********	**********	**********
K= 3	**********	**********	**********	**********
K= 2	**********	**********	**********	**********
K= 1	**********	**********	**********	**********

Y-VELOCITY COMPONENT, V (FT/SEC)

J=	1	2	3	4
K=13	0.0000	0.0000	0.0000	0.0000
K=12	0.0000	0.0000	0.0000	0.0000
K=11	0.0000	0.0000	0.0000	0.0000
K=10	0.0000	0.0000	0.0000	0.0000
K= 9	**********	**********	**********	**********
K= 8	**********	**********	**********	**********
K= 7	**********	**********	**********	**********
K= 6	**********	**********	**********	**********
K= 5	**********	**********	**********	**********
K= 4	**********	**********	**********	**********
K= 3	**********	**********	**********	**********
K= 2	**********	**********	**********	**********
K= 1	**********	**********	**********	**********

Z-VELOCITY COMPONENT, W (FT/SEC)

J=	1	2	3	4
K=13	0.0000	0.0000	0.0000	0.0000
K=12	0.0000	0.0000	0.0000	0.0000
K=11	0.0000	0.0000	0.0000	0.0000
K=10	0.0000	0.0000	0.0000	0.0000
K= 9	**********	**********	**********	**********
K= 8	**********	**********	**********	**********
K= 7	**********	**********	**********	**********
K= 6	**********	**********	**********	**********
K= 5	**********	**********	**********	**********
K= 4	**********	**********	**********	**********
K= 3	**********	**********	**********	**********
K= 2	**********	**********	**********	**********
K= 1	**********	**********	**********	**********

TEMPERATURE (^{o}F)

J=	1	2	3	4
K=13	70.8	70.8	70.8	70.8
K=12	70.8	70.8	70.8	70.8
K=11	70.8	70.8	70.8	70.8
K=10	70.8	70.8	70.8	70.8
K= 9	**********	**********	**********	**********
K= 8	**********	**********	**********	**********
K= 7	**********	**********	**********	**********
K= 6	**********	**********	**********	**********
K= 5	**********	**********	**********	**********
K= 4	**********	**********	**********	**********
K= 3	**********	**********	**********	**********
K= 2	**********	**********	**********	**********
K= 1	**********	**********	**********	**********

Table A4

Region 3 Predicted Velocity and Temperature Distribution in Vertical Plane (I = 2) at Time = 0 sec, Components u and v

X-VELOCITY COMPONENT, U (FT/SEC)

J=	1	2	3	4	5	6	7	8	9	10	11	12	13	14	15
K=13	0.0000	0.0000	0.0000	0.0000	0.0000	0.0000	0.0000	0.0000	0.0000	0.0000	0.0000	0.0000	0.0000	0.0000	0.0000
K=12	0.0000	0.0000	0.0000	0.0000	0.0000	0.0000	0.0000	0.0000	0.0000	0.0000	0.0000	0.0000	0.0000	0.0000	0.0000
K=11	0.0000	0.0000	0.0000	0.0000	0.0000	0.0000	0.0000	0.0000	0.0000	0.0000	0.0000	0.0000	0.0000	0.0000	0.0000
K=10	0.0000	0.0000	0.0000	0.0000	0.0000	0.0000	0.0000	0.0000	0.0000	0.0000	0.0000	0.0000	0.0000	0.0000	0.0000
K= 9	**********	**********	0.0000	0.0000	0.0000	0.0000	0.0000	0.0000	0.0000	0.0000	0.0000	0.0000	0.0000	0.0000	0.0000
K= 8	**********	**********	0.0000	0.0000	0.0000	0.0000	0.0000	0.0000	0.0000	0.0000	0.0000	0.0000	0.0000	0.0000	0.0000
K= 7	**********	**********	**********	**********	0.0000	0.0000	0.0000	0.0000	0.0000	0.0000	0.0000	0.0000	0.0000	0.0000	0.0000
K= 6	**********	**********	**********	**********	**********	**********	0.0000	0.0000	0.0000	0.0000	0.0000	0.0000	0.0000	0.0000	0.0000
K= 5	**********	**********	**********	**********	**********	**********	**********	**********	0.0000	0.0000	0.0000	0.0000	0.0000	0.0000	0.0000
K= 4	**********	**********	**********	**********	**********	**********	**********	**********	**********	**********	0.0000	0.0000	0.0000	0.0000	0.0000
K= 3	**********	**********	**********	**********	**********	**********	**********	**********	**********	**********	**********	**********	0.0000	0.0000	0.0000
K= 2	**********	**********	**********	**********	**********	**********	**********	**********	**********	**********	**********	**********	**********	**********	0.0000
K= 1	**********	**********	**********	**********	**********	**********	**********	**********	**********	**********	**********	**********	**********	**********	**********

Y-VELOCITY COMPONENT, V (FT/SEC)

J=	1	2	3	4	5	6	7	8	9	10	11	12	13	14	15
K=13	0.0000	0.0000	0.0000	0.0000	0.0000	0.0000	0.0000	0.0000	0.0000	0.0000	0.0000	0.0000	0.0000	0.0000	0.0000
K=12	0.0000	0.0000	0.0000	0.0000	0.0000	0.0000	0.0000	0.0000	0.0000	0.0000	0.0000	0.0000	0.0000	0.0000	0.0000
K=11	0.0000	0.0000	0.0000	0.0000	0.0000	0.0000	0.0000	0.0000	0.0000	0.0000	0.0000	0.0000	0.0000	0.0000	0.0000
K=10	0.0000	0.0000	0.0000	0.0000	0.0000	0.0000	0.0000	0.0000	0.0000	0.0000	0.0000	0.0000	0.0000	0.0000	0.0000
K= 9	**********	**********	0.0000	0.0000	0.0000	0.0000	0.0000	0.0000	0.0000	0.0000	0.0000	0.0000	0.0000	0.0000	0.0000
K= 8	**********	**********	**********	0.0000	0.0000	0.0000	0.0000	0.0000	0.0000	0.0000	0.0000	0.0000	0.0000	0.0000	0.0000
K= 7	**********	**********	**********	**********	**********	0.0000	0.0000	0.0000	0.0000	0.0000	0.0000	0.0000	0.0000	0.0000	0.0000
K= 6	**********	**********	**********	**********	**********	**********	**********	0.0000	0.0000	0.0000	0.0000	0.0000	0.0000	0.0000	0.0000
K= 5	**********	**********	**********	**********	**********	**********	**********	**********	**********	0.0000	0.0000	0.0000	0.0000	0.0000	0.0000
K= 4	**********	**********	**********	**********	**********	**********	**********	**********	**********	**********	**********	0.0000	0.0000	0.0000	0.0000
K= 3	**********	**********	**********	**********	**********	**********	**********	**********	**********	**********	**********	**********	0.0000	0.0000	0.0000
K= 2	**********	**********	**********	**********	**********	**********	**********	**********	**********	**********	**********	**********	**********	**********	0.0000
K= 1	**********	**********	**********	**********	**********	**********	**********	**********	**********	**********	**********	**********	**********	**********	**********

Table A5

Region 3 Predicted Velocity and Temperature Distribution in Vertical Plane (I = 2) at Time = 0 sec, Components w and T

Z-VELOCITY COMPONENT, W (FT/SEC)

J=	1	2	3	4	5	6	7	8	9	10	11	12	13	14	15
K=13	0.0000	0.0000	0.0000	0.0000	0.0000	0.0000	0.0000	0.0000	0.0000	0.0000	0.0000	0.0000	0.0000	0.0000	0.0000
K=12	0.0000	0.0000	0.0000	0.0000	0.0000	0.0000	0.0000	0.0000	0.0000	0.0000	0.0000	0.0000	0.0000	0.0000	0.0000
K=11	0.0000	0.0000	0.0000	0.0000	0.0000	0.0000	0.0000	0.0000	0.0000	0.0000	0.0000	0.0000	0.0000	0.0000	0.0000
K=10	0.0000	0.0000	0.0000	0.0000	0.0000	0.0000	0.0000	0.0000	0.0000	0.0000	0.0000	0.0000	0.0000	0.0000	0.0000
K= 9	**********	**********	**********	0.0000	0.0000	0.0000	0.0000	0.0000	0.0000	0.0000	0.0000	0.0000	0.0000	0.0000	0.0000
K= 8	**********	**********	**********	**********	0.0000	0.0000	0.0000	0.0000	0.0000	0.0000	0.0000	0.0000	0.0000	0.0000	0.0000
K= 7	**********	**********	**********	**********	**********	0.0000	0.0000	0.0000	0.0000	0.0000	0.0000	0.0000	0.0000	0.0000	0.0000
K= 6	**********	**********	**********	**********	**********	**********	0.0000	0.0000	0.0000	0.0000	0.0000	0.0000	0.0000	0.0000	0.0000
K= 5	**********	**********	**********	**********	**********	**********	**********	0.0000	0.0000	0.0000	0.0000	0.0000	0.0000	0.0000	0.0000
K= 4	**********	**********	**********	**********	**********	**********	**********	**********	0.0000	0.0000	0.0000	0.0000	0.0000	0.0000	0.0000
K= 3	**********	**********	**********	**********	**********	**********	**********	**********	**********	**********	**********	**********	0.0000	0.0000	0.0000
K= 2	**********	**********	**********	**********	**********	**********	**********	**********	**********	**********	**********	**********	**********	0.0000	********
K= 1	**********	**********	**********	**********	**********	**********	**********	**********	**********	**********	**********	**********	**********	**********	**********

TEMPERATURE, T (^{o}F)

J=	1	2	3	4	5	6	7	8	9	10	11	12	13	14	15
K=13	70.8	70.8	70.8	70.8	70.8	70.8	70.8	70.8	70.8	70.8	70.8	70.8	70.8	70.8	70.8
K=12	70.8	70.8	70.8	70.8	70.8	70.8	70.8	70.8	70.8	70.8	70.8	70.8	70.8	70.8	70.8
K=11	70.8	70.8	70.8	70.8	70.8	70.8	70.8	70.8	70.8	70.8	70.8	70.8	70.8	70.8	70.8
K=10	70.8	70.8	70.8	70.8	70.8	70.8	70.8	70.8	70.8	70.8	70.8	70.8	70.8	70.8	70.8
K= 9	**********	**********	**********	70.8	70.8	70.8	70.8	70.8	70.8	70.8	70.8	70.8	70.8	70.8	70.8
K= 8	**********	**********	**********	**********	70.8	70.8	70.8	70.8	70.8	70.8	70.8	70.8	70.8	70.8	70.8
K= 7	**********	**********	**********	**********	**********	70.8	70.8	70.8	70.8	70.8	70.8	70.8	70.8	70.8	70.8
K= 6	**********	**********	**********	**********	**********	**********	70.8	70.8	70.8	70.8	70.8	70.8	70.8	70.8	70.8
K= 5	**********	**********	**********	**********	**********	**********	**********	70.8	70.8	70.8	70.8	70.8	70.8	70.8	70.8
K= 4	**********	**********	**********	**********	**********	**********	**********	**********	70.8	70.8	70.8	70.8	70.8	70.8	70.8
K= 3	**********	**********	**********	**********	**********	**********	**********	**********	**********	**********	**********	**********	70.8	70.8	0.0
K= 2	**********	**********	**********	**********	**********	**********	**********	**********	**********	**********	**********	**********	**********	70.8	********
K= 1	**********	**********	**********	**********	**********	**********	**********	**********	**********	**********	**********	**********	**********	**********	**********

Table A6

Region 1 Predicted Velocity and Temperature Distribution in Vertical Plane (I = 2) at Time = 1000 sec

X-VELOCITY COMPONENT, U (FT/SEC)

J=	1	2	3
K=13	-0,0004	0,0004	-0,0001
K=12	-0,0367	0,0367	0,0112
K=11	0,0446	0,0423	0,0203
K=10	0,0446	0,0657	0,0228
K= 9	**********	**********	**********
K= 8	**********	**********	**********
K= 7	**********	**********	**********
K= 6	**********	**********	**********
K= 5	**********	**********	**********
K= 4	**********	**********	**********
K= 3	**********	**********	**********
K= 2	**********	**********	**********
K= 1	**********	**********	**********

Y-VELOCITY COMPONENT, V (FT/SEC)

J=	1	2	3
K=13	-0,0001	-0,0001	-0,0021
K=12	-0,0002	-0,0002	-0,0033
K=11	0,0000	-0,0002	0,0037
K=10	0,0000	-0,0003	0,0185
K= 9	**********	**********	**********
K= 8	**********	**********	**********
K= 7	**********	**********	**********
K= 6	**********	**********	**********
K= 5	**********	**********	**********
K= 4	**********	**********	**********
K= 3	**********	**********	**********
K= 2	**********	**********	**********
K= 1	**********	**********	**********

Z-VELOCITY COMPONENT, W (FT/SEC)

J=	1	2	3
K=13	-0,0011	-0,0011	-0,0076
K=12	0,0009	0,0009	-0,0097
K=11	0,0000	0,0012	-0,0087
K=10	0,0000	-0,0003	-0,0045
K= 9	**********	**********	**********
K= 8	**********	**********	**********
K= 7	**********	**********	**********
K= 6	**********	**********	**********
K= 5	**********	**********	**********
K= 4	**********	**********	**********
K= 3	**********	**********	**********
K= 2	**********	**********	**********
K= 1	**********	**********	**********

TEMPERATURE (^{O}F)

J=	1	2	3
K=13	70,8	70,8	70,8
K=12	69,4	69,4	70,4
K=11	62,0	65,6	69,8
K=10	62,0	67,3	70,0
K= 9	**********	**********	**********
K= 8	**********	**********	**********
K= 7	**********	**********	**********
K= 6	**********	**********	**********
K= 5	**********	**********	**********
K= 4	**********	**********	**********
K= 3	**********	**********	**********
K= 2	**********	**********	**********
K= 1	**********	**********	**********

Table A7

Region 2 Predicted Velocity and Temperature Distribution in Vertical Plane (I = 2) at Time = 1000 sec

X-VELOCITY COMPONENT, U (FT/SEC)

J=	1	2	3	4
K=13	0,0004	-0,0001	0,0029	0,0011
K=12	0,0367	0,0112	0,0035	0,0021
K=11	0,0423	0,0203	0,0125	0,0062
K=10	0,0637	0,0228	0,0120	0,0061
K= 9	**********	**********	**********	**********
K= 8	**********	**********	**********	**********
K= 7	**********	**********	**********	**********
K= 6	**********	**********	**********	**********
K= 5	**********	**********	**********	**********
K= 4	**********	**********	**********	**********
K= 3	**********	**********	**********	**********
K= 2	**********	**********	**********	**********
K= 1	**********	**********	**********	**********

Y-VELOCITY COMPONENT, V (FT/SEC)

J=	1	2	3	4
K=13	-0,0001	-0,0021	-0,0030	-0,0018
K=12	-0,0002	-0,0033	-0,0046	-0,0021
K=11	-0,0002	0,0037	-0,0012	-0,0005
K=10	-0,0003	0,0185	0,0066	0,0038
K= 9	**********	**********	**********	**********
K= 8	**********	**********	**********	**********
K= 7	**********	**********	**********	**********
K= 6	**********	**********	**********	**********
K= 5	**********	**********	**********	**********
K= 4	**********	**********	**********	**********
K= 3	**********	**********	**********	**********
K= 2	**********	**********	**********	**********
K= 1	**********	**********	**********	**********

Z-VELOCITY COMPONENT, W (FT/SEC)

J=	1	2	3	4
K=13	-0,0011	-0,0076	-0,0012	-0,0005
K=12	0,0009	-0,0097	-0,0025	-0,0015
K=11	0,0012	-0,0087	-0,0041	-0,0026
K=10	-0,0003	-0,0045	-0,0021	-0,0013
K= 9	**********	**********	**********	**********
K= 8	**********	**********	**********	**********
K= 7	**********	**********	**********	**********
K= 6	**********	**********	**********	**********
K= 5	**********	**********	**********	**********
K= 4	**********	**********	**********	**********
K= 3	**********	**********	**********	**********
K= 2	**********	**********	**********	**********
K= 1	**********	**********	**********	**********

TEMPERATURE, T (^{o}F)

J=	1	2	3	4
K=13	70,8	70,8	70,8	70,8
K=12	69,4	70,4	70,7	70,8
K=11	65,6	69,8	70,5	70,7
K=10	67,3	70,0	70,5	70,7
K= 9	**********	**********	**********	**********
K= 8	**********	**********	**********	**********
K= 7	**********	**********	**********	**********
K= 6	**********	**********	**********	**********
K= 5	**********	**********	**********	**********
K= 4	**********	**********	**********	**********
K= 3	**********	**********	**********	**********
K= 2	**********	**********	**********	**********
K= 1	**********	**********	**********	**********

Table A8

Region 3 Predicted Velocity and Temperature Distribution in Vertical Plane (I = 2) at Time = 1000 sec, Components u and v

X-VELOCITY COMPONENT, U (FT/SEC)

J=	1	2	3	4	5	6	7	8	9	10	11	12	13	14	15
K=13	0.0029	0.0011	0.0002	0.0002	0.0000	0.0000	0.0000	0.0000	0.0000	-0.0000	-0.0000	0.0000	0.0000	-0.0000	0.0000
K=12	0.0035	0.0021	0.0005	0.0005	0.0000	0.0001	0.0001	0.0001	-0.0000	-0.0000	-0.0000	0.0000	0.0001	0.0000	-0.0000
K=11	0.0125	0.0062	0.0054	0.0013	0.0000	0.0001	0.0001	0.0001	-0.0000	-0.0000	-0.0001	0.0000	0.0001	0.0001	-0.0001
K=10	0.0120	0.0061	0.0085	0.0021	-0.0000	0.0000	0.0001	0.0001	-0.0000	-0.0001	0.0000	0.0000	0.0001	0.0001	-0.0001
K= 9	**********	**********	**********	-0.0011	0.0000	0.0001	0.0001	0.0000	-0.0001	-0.0001	-0.0000	0.0000	0.0000	0.0002	-0.0002
K= 8	**********	**********	**********	**********	0.0001	0.0001	0.0001	0.0000	-0.0001	-0.0001	-0.0000	0.0000	0.0000	0.0002	-0.0002
K= 7	**********	**********	**********	**********	**********	0.0000	-0.0000	-0.0001	-0.0001	-0.0001	-0.0000	0.0001	-0.0004	0.0002	-0.0002
K= 6	**********	**********	**********	**********	**********	**********	-0.0000	-0.0001	-0.0001	-0.0001	0.0001	-0.0004	-0.0043	0.0002	-0.0002
K= 5	**********	**********	**********	**********	**********	**********	**********	-0.0000	0.0005	-0.0009	-0.0073	0.0006	-0.0006		
K= 4	**********	**********	**********	**********	**********	**********	**********	**********	0.0020	-0.0015	-0.0117	0.0103	-0.0103		
K= 3	**********	**********	**********	**********	**********	**********	**********	**********	**********	-0.0170	0.0398	0.0891			
K= 2	**********	**********	**********	**********	**********	**********	**********	**********	**********	**********	0.0301	********			
K= 1	**********	**********	**********	**********	**********	**********	**********	**********	**********	**********	**********	**********	**********	**********	**********

Y-VELOCITY COMPONENT, V (FT/SEC)

J=	1	2	3	4	5	6	7	8	9	10	11	12	13	14	15
K=13	-0.0030	-0.0018	-0.0004	-0.0005	-0.0002	-0.0000	-0.0000	-0.0000	0.0000	0.0000	-0.0002	-0.0002	-0.0004	-0.0000	-0.0000
K=12	-0.0046	-0.0021	-0.0009	-0.0006	-0.0007	-0.0008	-0.0006	-0.0003	0.0000	0.0001	-0.0003	-0.0003	-0.0008	0.0000	0.0000
K=11	-0.0012	-0.0005	-0.0005	-0.0008	-0.0007	-0.0010	-0.0007	-0.0003	0.0000	-0.0002	-0.0005	-0.0003	-0.0010	-0.0004	-0.0004
K=10	0.0066	0.0038	0.0002	-0.0012	-0.0009	-0.0010	-0.0008	-0.0004	-0.0000	-0.0004	-0.0007	-0.0004	-0.0009	-0.0006	-0.0006
K= 9	**********	**********	**********	-0.0015	-0.0012	-0.0010	-0.0007	-0.0000	-0.0004	-0.0007	-0.0008	-0.0005	-0.0011	-0.0009	-0.0009
K= 8	**********	**********	**********	**********	-0.0012	-0.0010	-0.0007	0.0000	-0.0005	-0.0008	-0.0010	-0.0005	-0.0008	-0.0009	-0.0009
K= 7	**********	**********	**********	**********	**********	0.0001	0.0000	-0.0005	-0.0010	-0.0011	-0.0004	-0.0005	-0.0013	-0.0013	
K= 6	**********	**********	**********	**********	**********	**********	0.0000	-0.0006	-0.0011	-0.0013	-0.0006	-0.0003	-0.0011	-0.0011	
K= 5	**********	**********	**********	**********	**********	**********	**********	-0.0011	-0.0014	-0.0007	-0.0004	-0.0022	-0.0022		
K= 4	**********	**********	**********	**********	**********	**********	**********	**********	-0.0017	-0.0011	-0.0009	-0.0023	-0.0023		
K= 3	**********	**********	**********	**********	**********	**********	**********	**********	**********	-0.0030	0.0022	0.0000			
K= 2	**********	**********	**********	**********	**********	**********	**********	**********	**********	**********	0.0080	********			
K= 1	**********	**********	**********	**********	**********	**********	**********	**********	**********	**********	**********	**********	**********	**********	**********

Table A9

Region 3 Predicted Velocity and Temperature Distribution in Vertical Plane (l = 2) at Time = 1000 sec, Components w and T

Z-VELOCITY COMPONENT, W (FT/SEC)

J=	1	2	3	4	5	6	7	8	9	10	11	12	13	14	15
K=13	-0,0012	-0,0005	0,0002	0,0013	0,0004	0,0002	0,0001	0,0000	0,0000	0,0001	0,0009	0,0011	0,0006	-0,0013	-0,0013
K=12	-0;0025	-0;0015	-0,0000	0,0014	0;0003	0,0001	0,0001	0,0000	0,0000	0,0002	0;0009	0,0011	0;0005	-0;0014	-0;0014
K=11	-0,0041	-0,0026	-0,0004	0,0013	0,0003	0,0001	0,0000	0,0000	0,0000	0,0003	0,0008	0,0010	0,0003	-0,0012	-0,0012
K=10	-0,0021	-0,0013	-0,0002	0,0011	0,0002	0,0001	0,0000	-0,0000	0,0000	0,0003	0,0007	0,0010	0,0001	-0,0015	-0,0015
K= 9	**********	**********	0;0003	-0,0001	0,0000	-0;0000	-0;0000	0;0001	0;0003	0;0006	0;0010	0,0000	-0;0013	-0;0013	
K= 8	**********	**********	0,0002	0,0000	-0,0000	-0,0000	0,0000	0,0003	0,0005	0,0010	-0,0001	-0,0018	-0,0018		
K= 7	**********	**********	**********	-0,0000	-0,0000	0,0000	0,0002	0,0004	0,0010	-0,0001	-0,0016	-0,0016			
K= 6	**********	**********	**********	**********	-0,0000	0,0000	0;0002	0,0002	0,0008	-0,0001	-0,0024	-0,0024			
K= 5	**********	**********	**********	**********	**********	0,0000	0,0001	0,0007	-0,0002	-0,0020	-0,0020				
K= 4	**********	**********	**********	**********	**********	**********	-0,0000	0,0004	-0,0002	-0,0038	-0,0038				
K= 3	**********	**********	**********	**********	**********	**********	**********	-0;0002	-0;0051	0;0000					
K= 2	**********	**********	**********	**********	**********	**********	**********	**********	0,0014	*******					
K= 1	**********	**********	**********	**********	**********	**********	**********	**********	**********	**********	**********	**********	**********	**********	**********

TEMPERATURE, T (^{0}F)

J=	1	2	3	4	5	6	7	8	9	10	11	12	13	14	15
K=13	70,8	70,8	70,8	70,8	70,8	70,8	70,8	70,8	70,8	70,8	70,8	70,8	70,8	70,8	70,8
K=12	70,7	70,8	70,8	70,8	70,8	70,8	70,8	70,8	70,8	70,8	70,8	70,8	70,8	70,8	70,8
K=11	70,5	70,7	70,8	70,8	70,8	70,8	70,8	70,8	70,8	70,8	70,8	70,8	70,8	70,8	70,8
K=10	70,5	70,7	70,7	70,8	70,8	70,8	70,8	70,8	70,8	70,8	70,8	70,8	70,8	70,8	70,8
K= 9	**********	**********	70,8	70,8	70,8	70,8	70,8	70,8	70,8	70,8	70,8	70,8	70,8	70,8	70,8
K= 8	**********	**********	70;8	70;8	70;8	70;8	70;8	70;8	70;8	70;8	70;8	70;8	70;8	70;8	70;8
K= 7	**********	**********	**********	**********	70,8	70,8	70,8	70,8	70,8	70,8	70,8	70,8	70,8	70,8	70,8
K= 6	**********	**********	**********	**********	**********	70,8	70,8	70,8	70,8	70,8	70,8	70,8	70,8	70,8	70,8
K= 5	**********	**********	**********	**********	**********	**********	70,8	70,8	70,8	70,8	70,8	70,8	70,7	70,7	
K= 4	**********	**********	**********	**********	**********	**********	**********	70,8	70,8	70,8	70,2	70,2			
K= 3	**********	**********	**********	**********	**********	**********	**********	**********	70,8	69,0	0,0				
K= 2	**********	**********	**********	**********	**********	**********	**********	**********	**********	65;3	*******				
K= 1	**********	**********	**********	**********	**********	**********	**********	**********	**********	**********	**********	**********	**********	**********	**********

Table A10

Region 1 Predicted Velocity and Temperature Distribution in Vertical Plane (I = 2) at Time = 2000 sec

X-VELOCITY COMPONENT, U (FT/SEC)

J=	1	2	3
K=13	-0,0000	0,0000	-0,0001
K=12	-0,0359	0,0359	0,0109
K=11	0,0446	0,0427	0,0202
K=10	0,0446	0,0638	0,0227
K= 9	**********	**********	**********
K= 8	**********	**********	**********
K= 7	**********	**********	**********
K= 6	**********	**********	**********
K= 5	**********	**********	**********
K= 4	**********	**********	**********
K= 3	**********	**********	**********
K= 2	**********	**********	**********
K= 1	**********	**********	**********

Y-VELOCITY COMPONENT, V (FT/SEC)

J=	1	2	3
K=13	-0,0001	-0,0001	-0,0021
K=12	-0,0002	-0,0002	-0,0033
K=11	0,0000	-0,0002	0,0037
K=10	0,0000	-0,0003	0,0185
K= 9	**********	**********	**********
K= 8	**********	**********	**********
K= 7	**********	**********	**********
K= 6	**********	**********	**********
K= 5	**********	**********	**********
K= 4	**********	**********	**********
K= 3	**********	**********	**********
K= 2	**********	**********	**********
K= 1	**********	**********	**********

Z-VELOCITY COMPONENT, W (FT/SEC)

J=	1	2	3
K=13	-0,0010	-0,0010	-0,0077
K=12	0,0009	0,0009	-0,0097
K=11	0,0000	0,0012	-0,0087
K=10	0,0000	-0,0003	-0,0045
K= 9	**********	**********	**********
K= 8	**********	**********	**********
K= 7	**********	**********	**********
K= 6	**********	**********	**********
K= 5	**********	**********	**********
K= 4	**********	**********	**********
K= 3	**********	**********	**********
K= 2	**********	**********	**********
K= 1	**********	**********	**********

TEMPERATURE (^{O}F)

J=	1	2	3
K=13	70,8	70,8	70,8
K=12	69,4	69,4	70,4
K=11	62,0	65,7	69,8
K=10	62,0	67,2	70,0
K= 9	**********	**********	**********
K= 8	**********	**********	**********
K= 7	**********	**********	**********
K= 6	**********	**********	**********
K= 5	**********	**********	**********
K= 4	**********	**********	**********
K= 3	**********	**********	**********
K= 2	**********	**********	**********
K= 1	**********	**********	**********

Table A11

Region 2 Predicted Velocity and Temperature Distribution in Vertical Plane (I = 2) at Time = 2000 sec

X-VELOCITY COMPONENT, U (FT/SEC)

J=	1	2	3	4
K=13	0,0000	-0,0001	0,0027	-0,0001
K=12	0,0359	0,0109	0,0034	0,0002
K=11	0,0427	0,0202	0,0124	0,0067
K=10	0,0638	0,0227	0,0120	0,0068
K= 9	**********	**********	**********	**********
K= 8	**********	**********	**********	**********
K= 7	**********	**********	**********	**********
K= 6	**********	**********	**********	**********
K= 5	**********	**********	**********	**********
K= 4	**********	**********	**********	**********
K= 3	**********	**********	**********	**********
K= 2	**********	**********	**********	**********
K= 1	**********	**********	**********	**********

Y-VELOCITY COMPONENT, V (FT/SEC)

J=	1	2	3	4
K=13	-0,0001	-0,0021	-0,0030	-0,0010
K=12	-0,0002	-0,0033	-0,0045	-0,0022
K=11	-0,0002	0,0037	-0,0012	-0,0011
K=10	-0,0003	0,0185	0,0064	0,0038
K= 9	**********	**********	**********	**********
K= 8	**********	**********	**********	**********
K= 7	**********	**********	**********	**********
K= 6	**********	**********	**********	**********
K= 5	**********	**********	**********	**********
K= 4	**********	**********	**********	**********
K= 3	**********	**********	**********	**********
K= 2	**********	**********	**********	**********
K= 1	**********	**********	**********	**********

Z-VELOCITY COMPONENT, W (FT/SEC)

J=	1	2	3	4
K=13	-0,0010	-0,0077	-0,0011	-0,0012
K=12	0,0009	-0,0097	-0,0024	-0,0018
K=11	0,0012	-0,0087	-0,0040	-0,0028
K=10	-0,0003	-0,0045	-0,0020	-0,0013
K= 9	**********	**********	**********	**********
K= 8	**********	**********	**********	**********
K= 7	**********	**********	**********	**********
K= 6	**********	**********	**********	**********
K= 5	**********	**********	**********	**********
K= 4	**********	**********	**********	**********
K= 3	**********	**********	**********	**********
K= 2	**********	**********	**********	**********
K= 1	**********	**********	**********	**********

TEMPERATURE (^{o}F)

J=	1	2	3	4
K=13	70,8	70,8	70,8	70,8
K=12	69,4	70,4	70,7	70,8
K=11	65,7	69,8	70,5	70,7
K=10	67,2	70,0	70,5	70,7
K= 9	**********	**********	**********	**********
K= 8	**********	**********	**********	**********
K= 7	**********	**********	**********	**********
K= 6	**********	**********	**********	**********
K= 5	**********	**********	**********	**********
K= 4	**********	**********	**********	**********
K= 3	**********	**********	**********	**********
K= 2	**********	**********	**********	**********
K= 1	**********	**********	**********	**********

Table A12

Region 3 Predicted Velocity and Temperature Distribution in Vertical Plane (I = 2) at Time = 2000 sec, Components u and v

X-VELOCITY COMPONENT, U (FT/SEC)

J=	1	2	3	4	5	6	7	8	9	10	11	12	13	14	15
K=13	0,0027	-0,0001	0,0046	0,0022	0,0005	-0,0001	0,0000	0,0000	-0,0000	0,0000	0,0000	-0,0002	0,0000	0,0000	-0,0000
K=12	0,0034	0,0002	0,0024	0,0015	0,0003	-0,0004	0,0000	0,0000	0,0000	0,0001	0,0000	-0,0003	-0,0000	0,0000	-0,0000
K=11	0,0124	0,0067	0,0059	0,0020	0,0005	-0,0010	-0,0002	0,0000	0,0000	0,0002	0,0002	-0,0004	-0,0004	0,0001	-0,0001
K=10	0,0120	0,0068	0,0071	0,0024	0,0011	-0,0024	-0,0004	0,0000	0,0001	0,0004	0,0002	-0,0007	-0,0010	0,0001	-0,0001
K= 9	**********	**********	0,0016	0,0011	-0,0009	-0,0001	0,0000	0,0002	0,0006	0,0001	-0,0010	-0,0018	0,0001	-0,0001	
K= 8	**********	**********	**********	-0,0022	-0,0010	0,0000	0,0000	0,0005	0,0007	-0,0000	-0,0012	-0,0027	0,0001	-0,0001	
K= 7	**********	**********	**********	**********	0,0000	0,0002	0,0010	0,0009	-0,0000	-0,0009	-0,0036	0,0001	-0,0001		
K= 6	**********	**********	**********	**********	**********	-0,0000	0,0034	0,0024	0,0006	0,0002	-0,0048	-0,0000	0,0000		
K= 5	**********	**********	**********	**********	**********	**********	0,0071	0,0028	0,0023	-0,0065	-0,0003	0,0003			
K= 4	**********	**********	**********	**********	**********	**********	**********	0,0074	0,0068	-0,0090	0,0031	-0,0031			
K= 3	**********	**********	**********	**********	**********	**********	**********	**********	**********	-0,0118	0,0312	0,0891			
K= 2	**********	**********	**********	**********	**********	**********	**********	**********	**********	**********	0,0173	**********			
K= 1	**********	**********	**********	**********	**********	**********	**********	**********	**********	**********	**********	**********			

Y-VELOCITY COMPONENT, V (FT/SEC)

J=	1	2	3	4	5	6	7	8	9	10	11	12	13	14	15
K=13	-0,0030	-0,0010	-0,0010	-0,0008	-0,0007	-0,0005	-0,0003	-0,0001	-0,0005	-0,0006	-0,0006	-0,0007	-0,0005	-0,0000	-0,0000
K=12	-0,0045	-0,0022	-0,0009	-0,0007	-0,0010	-0,0010	-0,0005	-0,0005	-0,0006	-0,0010	-0,0005	-0,0009	-0,0003	-0,0001	-0,0001
K=11	-0,0012	-0,0011	-0,0003	-0,0009	-0,0006	-0,0010	-0,0010	-0,0008	-0,0010	-0,0010	-0,0007	-0,0010	-0,0007	-0,0004	-0,0004
K=10	0,0064	0,0038	0,0008	-0,0015	-0,0009	-0,0013	-0,0014	-0,0003	-0,0011	-0,0008	-0,0006	-0,0008	-0,0005	-0,0006	-0,0006
K= 9	**********	**********	-0,0034	-0,0014	-0,0014	-0,0014	-0,0002	-0,0010	-0,0006	-0,0004	-0,0005	-0,0003	-0,0007	-0,0007	
K= 8	**********	**********	**********	-0,0017	-0,0013	-0,0005	-0,0004	-0,0011	-0,0006	-0,0002	-0,0003	-0,0001	-0,0007	-0,0007	
K= 7	**********	**********	**********	**********	0,0001	-0,0014	-0,0012	-0,0006	-0,0001	-0,0001	0,0002	-0,0009	-0,0009		
K= 6	**********	**********	**********	**********	**********	-0,0006	-0,0014	-0,0007	-0,0004	-0,0000	0,0004	-0,0004	-0,0004		
K= 5	**********	**********	**********	**********	**********	**********	-0,0009	-0,0005	-0,0002	0,0003	-0,0015	-0,0015			
K= 4	**********	**********	**********	**********	**********	**********	**********	-0,0011	-0,0008	-0,0005	-0,0009	-0,0009			
K= 3	**********	**********	**********	**********	**********	**********	**********	**********	**********	-0,0042	0,0023	0,0000			
K= 2	**********	**********	**********	**********	**********	**********	**********	**********	**********	**********	-0,0009	**********			
K= 1	**********	**********	**********	**********	**********	**********	**********	**********	**********	**********	**********	**********			

Table A13

Region 3 Predicted Velocity and Temperature Distribution in Vertical Plane (I = 2) at Time = 2000 sec, Components w and T

Z-VELOCITY COMPONENT, W (FT/SEC)

J=	1	2	3	4	5	6	7	8	9	10	11	12	13	14	15
K=13	-0,0011	-0,0012	0,0000	0,0025	0,0019	0,0008	0,0003	0,0002	0,0005	0,0004	0,0007	0,0017	0,0005	-0,0012	-0,0012
K=12	-0,0024	-0,0018	-0,0002	0,0023	0,0014	0,0005	0,0003	0,0001	0,0004	0,0003	0,0007	0,0016	0,0006	-0,0013	-0,0013
K=11	-0,0040	-0,0028	-0,0007	0,0019	0,0012	0,0004	0,0001	0,0000	0,0004	0,0002	0,0006	0,0015	0,0004	-0,0011	-0,0011
K=10	-0,0020	-0,0013	-0,0003	0,0017	0,0009	0,0002	0,0002	0,0001	0,0003	0,0002	0,0005	0,0013	0,0004	-0,0013	-0,0013
K= 9	**********	**********	**********	0,0006	0,0004	0,0000	0,0001	0,0001	0,0003	0,0002	0,0004	0,0012	0,0004	-0,0010	-0,0010
K= 8	**********	**********	**********	**********	-0,0001	-0,0003	-0,0001	0,0001	0,0003	0,0002	0,0004	0,0011	0,0005	-0,0010	-0,0010
K= 7	**********	**********	**********	**********	**********	**********	-0,0000	0,0000	0,0001	0,0001	0,0003	0,0010	0,0006	-0,0004	-0,0004
K= 6	**********	**********	**********	**********	**********	**********	**********	-0,0003	-0,0001	-0,0000	0,0003	0,0009	0,0008	-0,0005	-0,0005
K= 5	**********	**********	**********	**********	**********	**********	**********	**********	-0,0002	0,0001	0,0007	0,0009	0,0012	0,0012	
K= 4	**********	**********	**********	**********	**********	**********	**********	**********	**********	-0,0002	0,0004	0,0008	0,0006	0,0006	
K= 3	**********	**********	**********	**********	**********	**********	**********	**********	**********	**********	**********	0,0003	0,0019	0,0000	
K= 2	**********	**********	**********	**********	**********	**********	**********	**********	**********	**********	**********	**********	0,0048	********	
K= 1	**********	**********	**********	**********	**********	**********	**********	**********	**********	**********	**********	**********	**********	**********	**********

TEMPERATURE (^{O}F)

J=	1	2	3	4	5	6	7	8	9	10	11	12	13	14	15
K=13	70,8	70,8	70,8	70,8	70,8	70,8	70,8	70,8	70,8	70,8	70,8	70,8	70,8	70,8	70,8
K=12	70,7	70,8	70,8	70,8	70,8	70,8	70,8	70,8	70,8	70,8	70,8	70,8	70,8	70,8	70,8
K=11	70,5	70,7	70,7	70,8	70,8	70,8	70,8	70,8	70,8	70,8	70,8	70,8	70,8	70,8	70,8
K=10	70,5	70,7	70,7	70,8	70,8	70,8	70,8	70,8	70,8	70,8	70,8	70,8	70,8	70,8	70,8
K= 9	**********	**********	**********	70,8	70,8	70,8	70,8	70,8	70,8	70,8	70,8	70,8	70,8	70,8	70,8
K= 8	**********	**********	**********	**********	70,8	70,8	70,8	70,8	70,8	70,8	70,8	70,8	70,8	70,8	70,8
K= 7	**********	**********	**********	**********	**********	**********	70,8	70,8	70,8	70,8	70,8	70,8	70,8	70,8	70,8
K= 6	**********	**********	**********	**********	**********	**********	**********	70,8	70,8	70,8	70,8	70,8	70,8	70,8	70,8
K= 5	**********	**********	**********	**********	**********	**********	**********	**********	**********	70,8	70,8	70,8	70,8	70,7	70,7
K= 4	**********	**********	**********	**********	**********	**********	**********	**********	**********	**********	70,8	70,8	70,8	70,4	70,4
K= 3	**********	**********	**********	**********	**********	**********	**********	**********	**********	**********	**********	**********	70,8	69,8	0,0
K= 2	**********	**********	**********	**********	**********	**********	**********	**********	**********	**********	**********	**********	**********	68,3	********
K= 1	**********	**********	**********	**********	**********	**********	**********	**********	**********	**********	**********	**********	**********	**********	**********

APPENDIX B: RESULTS OF VECTORIZATION OF 3-D PLUME

1. A series of benchmark runs were carried out to compare the performance of the scalar and vector versions of 3-D PLUME (Tatom and Smith 1979b). Such runs were all carried out with the K-Compiler on the WES ASC Computer and consisted of two types: (a) numerical consistency and (b) computational speed.

Numerical Consistency Results

2. Benchmark runs concerned with numerical consistency between the scalar and vector programs were relatively short and included printouts of variables not included in the normal output of either program. Such printouts initially revealed a series of minor discrepancies in the vector version of the program and also one previously undetected discrepancy in the scalar version. After such discrepancies were corrected, numerical consistency within one percent was achieved.

Computational Speed Results

3. Two types of timing runs were carried out with both the vector and scalar versions of the program. The first type consisted of only the initialization computations plus one time step computation and was designed to provide a measure of initialization time. The second type of run extended for 2000 time steps and was designed to provide a measure of the computation time associated with each time step. The results of these timing runs (including compilation time) are summarized in Table B1.

4. As indicated in Table B1, the compilation time for the vector version of the program was approximately three times the scalar compilation time, as would be expected because of the additional optimization procedures involved in vector compilation. The initialization times were essentially equal. The time required for 2000 time steps with the vector version was approximately 44 percent of the corresponding time

with the scalar version. It is important to note that in carrying out the timing comparison the amount of central memory (versus extended memory), as shown in Table B1, was not the same for all runs. For the 2000-time step vector run, no central memory was used; while for the corresponding scalar run central memory comprised 11 percent of the total memory. Because fetch times associated with central memory are smaller than the fetch times with extended memory by a factor of approximately 6, the actual improvement in performance of the vector version over the scalar version is somewhat greater than the 56-percent reduction in computation time noted. With an equal portion of central memory, the vector version should be approximately three times as fast as the scalar version. For a production run consisting of 4000 time steps, the computation time would thus be reduced from 2400 sec to 800 sec.

Table B1

Comparison of Computation Time*

Item	Scalar			Vector		
	Central Memory words	Extended Memory words	Time sec	Central Memory words	Extended Memory words	Time sec
Compilation	0	184,320	576.63	0	184,320	1,799.89
Initialization and 1 step	4,096	106,496	3.74	4,096	131,072	3.26
Computation for 2000 steps	12,288	98,304	1,200.59	0	143,360	530.14

* Tatom and Smith 1979b.

APPENDIX C: NOTATION

a,b,c	Constants in expression for surface heat flux
A_{cv}	Area of discrete element
A_H	Horizontal eddy diffusivity
A_i	Cross-sectional area
A_{ij}	Eddy diffusivity tensor from time averaging
A'_{ij}	Eddy diffusivity tensor from spatial averaging
A_v	Vertical eddy diffusivity
B	Width
B_i	Surface width
B_o	Width of opening at the dam
C	Chezy coefficient; constant in expression for surface wind stress; phase velocity
C^*	Constant in expression for surface wind stress
C_{ij}	Sum of eddy diffusivities due to time- and spatial-averaging
CSHE	Coefficient of surface heat exchange
C_v	Discrete element volume
dv_o	Volume of a discrete element
D_{ij}	Diffusivity tensor
ET	Equilibrium temperature
f	Nondimensional friction factor
$\vec{f}$	Force vector
F,f	Arbitrary variables
F_s	Smoothed solution in leapfrog scheme
g,g_i	Acceleration due to gravity
G	Volumetric flow rate

h	Water depth
h_{DF}	Height of density underflow
h_n	Rate of surface heat exchange
H	Height of opening at the dam; water depth
H_i	Surface elevation
$\hat{i},\hat{j},\hat{k}$	Unit vectors
J	Boundary point
k	Coefficient in expression for bottom friction; diameter of average bottom roughness
k_1	Constant = 0.10
L_x,L_y	Length scales
L_z	Reference depth; length scale
$\hat{n}$	Unit normal vector to the surface
n_x,n_z	Components of outward unit normal vector to the surface
P	Pressure; function to control coordinate spacing
$\overline{P}$	Time-averaged pressure
$\tilde{\tilde{P}}$	Time-averaged and spatially averaged press
P_a	Atmospheric pressure
P_h	Hydrostatic pressure
P_R	Reduced pressure
P_s	Surface pressure
q_s	Surface heat flux
Q	Function to control coordinate spacing; discharge through the dam
R_e	Reynolds number
R_i	Richardson number
R_{i_c}	Critical Richardson number

S	Salinity; slope of reservoir bottom
S_{ij}, S_{mn}	Rate of strain tensor
t	Time
$\vec{t}$	Stress force vector
T	Temperature
T'	Deviation between instantaneous and time-averaged temperature
$\overline{T}$	Time-averaged temperature
$\overline{T}'$	Difference between time-averaged temperature and time- and space-averaged temperature
$\tilde{\overline{T}}$	Time-averaged and spatially averaged temperature
T_s	Surface temperature
u,v,w	Velocity components
u_i	Tensor notation for velocity
$\overline{u}_i$	Time-averaged velocity
u_i'	Deviation between instantaneous velocity and time-averaged velocity
$\tilde{\overline{u}}_i$	Time- and space-averaged velocity
$\overline{u}_i'$	Deviation between time-averaged velocity and time- and space-averaged velocity
$\overline{U}$	Average velocity of density underflow
U_o	Outlet velocity
U_{WIND}	Velocity of the wind
$\vec{v}$	Velocity vector
w_a	Wind speed
x,y,z	Cartesian coordinates
x_i	Tensor notation of spatial coordinates
z_B	Elevation of reservoir bottom

α	Arbitrary variable; constant in an expression for vertical eddy coefficient dissipative coefficient
α_p	Turbulent Prandtl number
β	Momentum correction factor; constant in an expression for vertical eddy coefficient
$\Gamma_{k,\ell}$	Sum of $\varepsilon_{k\ell}$, $\varepsilon'_{k,\ell}$, and μ
$\Delta\rho$	Change in water density
$\Delta t, \Delta x_i$	Time and spatial steps
Δt_c	Time step restricted by Courant condition
δ_{ij}	Kronecker delta
ε_H	Horizontal eddy viscosity
ε_{ij}	Eddy viscosity tensor as a result of time averaging
ε'_{ij}	Eddy viscosity tensor as a result of space averaging
ε_{ijk}	Cyclic tensor
ε_v	Vertical eddy viscosity
ζ	Water surface elevation; vorticity
μ	Molecular eddy viscosity
ξ, η	Nonorthogonal curvilinear coordinates
ρ	Water density
$\overline{\rho}$	Time-averaged water density
$\tilde{\overline{\rho}}$	Time-averaged and spatially averaged water density
ρ_a	Air density
ρ_o, ρ_r	Reference water density
σ	Transformed vertical coordinate
τ, τ_o	Bottom shear stress
$\tau_{ij}, \overleftrightarrow{\tau}$	Laminar stress tensor
τ_n	Normal internal stress at the surface

T_t	Tangential internal stress at the surface
T_w, T_{WIND}	Wind shear stress
ϕ	Arbitrary variable; angle of wind with reservoir axis
Ω	Scaling parameter in an expression for the eddy viscosity tensor
Ω_j	Coriolis parameter
$\vec{\omega}$	Vorticity
∇	$\partial/\partial x\, \hat{i} + \partial/\partial y \hat{j} + \partial/\partial z \hat{k}$

In accordance with letter from DAEN-RDC, DAEN-ASI dated 22 July 1977, Subject: Facsimile Catalog Cards for Laboratory Technical Publications, a facsimile catalog card in Library of Congress MARC format is reproduced below.

Johnson, Billy H
A review of numerical reservoir hydrodynamic modeling / by Billy H. Johnson. (Hydraulics Laboratory. U.S. Army Engineer Waterways Experiment Station) ; prepared for Office, Chief of Engineers, U.S. Army, under EWQOS Work Unit No. IA.4 -- Vicksburg, Miss. : U.S. Army Engineer Waterways Experiment Station ; Springfield, Va. : available from NTIS, 1981.
160, [22] p. : ill. 27 cm. -- (Technical report / U.S. Army Engineer Waterways Experiment Station ; E-81-2)
Cover title.
"February 1981."
References: p. 157-160.
1. Hydrodynamics. 2. Mathematical models. 3. Reservoir stratification. 4. Stratified flow. 5. Water quality models. I. United States. Army. Corps of Engineers. Office of the Chief of Engineers. II. United States. Army Engineer Waterways Experiment Station. Hydraulics Laboratory. III. Title. IV. Series: Technical report (United States. Army Engineer Waterways Experiment Station) ; E-81-2.
TA7.W34 no.E-81-2